



National Library
of Canada

Bibliothèque nationale
du Canada

Canadian Theses Service Service des thèses canadiennes

Ottawa, Canada
K1A 0N4

NOTICE

The quality of this microform is heavily dependent upon the quality of the original thesis submitted for microfilming. Every effort has been made to ensure the highest quality of reproduction possible.

If pages are missing, contact the university which granted the degree.

Some pages may have indistinct print especially if the original pages were typed with a poor typewriter ribbon or if the university sent us an inferior photocopy.

Reproduction in full or in part of this microform is governed by the Canadian Copyright Act, R.S.C. 1970, c. C-30, and subsequent amendments.

AVIS

La qualité de cette microforme dépend grandement de la qualité de la thèse soumise au microfilmage. Nous avons tout fait pour assurer une qualité supérieure de reproduction.

S'il manque des pages, veuillez communiquer avec l'université qui a conféré le grade.

La qualité d'impression de certaines pages peut laisser à désirer, surtout si les pages originales ont été dactylographiées à l'aide d'un ruban usé ou si l'université nous a fait parvenir une photocopie de qualité inférieure.

La reproduction, même partielle, de cette microforme est soumise à la Loi canadienne sur le droit d'auteur, SRC 1970, c. C-30, et ses amendements subséquents.



National Library
of Canada

Bibliothèque nationale
du Canada

Canadian Theses Service

Service des thèses canadiennes

Ottawa, Canada
K1A 0N4

The author has granted an irrevocable non-exclusive licence allowing the National Library of Canada to reproduce, loan, distribute or sell copies of his/her thesis by any means and in any form or format, making this thesis available to interested persons.

The author retains ownership of the copyright in his/her thesis. Neither the thesis nor substantial extracts from it may be printed or otherwise reproduced without his/her permission.

L'auteur a accordé une licence irrévocable et non exclusive permettant à la Bibliothèque nationale du Canada de reproduire, prêter, distribuer ou vendre des copies de sa thèse de quelque manière et sous quelque forme que ce soit pour mettre des exemplaires de cette thèse à la disposition des personnes intéressées.

L'auteur conserve la propriété du droit d'auteur qui protège sa thèse. Ni la thèse ni des extraits substantiels de celle-ci ne doivent être imprimés ou autrement reproduits sans son autorisation.

ISBN 0-315-53211-4

Sputter-deposition of epitaxial CdTe and PbTe layers:
Plasma emission spectroscopy of the discharge
and
Photoluminescence spectroscopy of the layers

By

MOHAMED-SAMIR AOUADI

Thesis submitted to the School of Graduate
Studies of the University of Ottawa
in partial fulfillment of the requirements
for the degree of Master of Science
in Physics

DEPARTMENT OF PHYSICS
FACULTY OF SCIENCE
UNIVERSITY OF OTTAWA
Ottawa, Ontario, CANADA
1989

Mohamed-Samir Aouadi, Ottawa, Canada, 1989



UNIVERSITÉ D'OTTAWA
UNIVERSITY OF OTTAWA

TO MY PARENTS



ACKNOWLEDGEMENTS

First of all, I would like to express my sincere gratitude to my thesis supervisor Dr. S. R. Das for his guidance, advice, encouragement and help during the course of this work.

The work reported in this thesis was carried out in the Chemical Physics Section of the Microstructural Sciences Laboratory at the Division of Physics, National Research Council (N.R.C.) and thanks are due to the Director of the Division of Physics for permitting me to work at the Laboratory as a guest worker. I especially would like to thank Dr. J. G. Cook, Dr. N. L. Rowell and Mr. H. Moeller of the N.R.C. for their cooperation and assistance at all times during this thesis work.

Acknowledgement is also extended to all my friends at Department of Physics, Ottawa University, especially Mostefa Golea who helped me with the computer facilities, Ms. Lorraine Johnston for her typing and Mrs. Rhoda Diebel for English language training.

Finally, the financial assistance provided by the government of Algeria is gratefully acknowledged.

ABSTRACT

This thesis reports (i) a plasma emission spectroscopy study of an rf magnetron discharge used to sputter-deposit PbTe in Ar and (ii) a photoluminescence (PL) spectroscopy study of epitaxial (100) CdTe layers sputter-deposited onto (100) KBr substrates.

Previously, emission spectra had been measured for an rf magnetron discharge used to deposit CdTe in Ar. In this work, a study of the discharge used to deposit PbTe has been carried out to prepare for co-deposition and/or sequential deposition of CdTe and PbTe in a multi-gun magnetron system, using emission spectroscopy as a probe for process control and analysis. The principal lines for Pb, Te, and Ar are identified; almost all are neutral lines, while at the lowest pressures, just before extinction, a number of Ar-ion lines are observed close to the target. The Pb, Te, and Ar line intensities, for both the negative glow and positive column at pressures near 0.5 Pa, vary with power (W) as W^n , with n near 1.4 for Pb and Te, and $n \approx 0.4$ for Ar. Thus, the Ar-normalized Pb and Te intensities vary approximately linearly with power, as does the deposition rate. From this, together with an observed insensitivity of the value of n to the energy of the excited Pb and Te levels, it may be concluded that the electron temperature is not sensitive to power, and that the Ar-normalized intensity varies with power as the sputtered atom density.

As the Ar gas pressure is varied, the electron temperature is not constant so that Ar-normalized Pb intensities are not simply related to the

Pb densities. Application of a substrate bias voltage has a large effect on the emission spectra which is not well understood.

PL spectra were measured for sputter-deposited epitaxial (100) CdTe layers of varying thicknesses up to $\approx 14\mu\text{m}$. The layers were structurally characterized by x-ray diffraction prior to PL studies. Three PL emission bands at 0.80 eV, 1.00 eV, and 1.42 eV are observed. This is the first observation of PL lines at 0.80 eV and 1.00 eV in epitaxial CdTe layers. The 1.42 eV line has been reported previously by many workers. The spectrum, injection level dependence, and temperature dependence of the 1.42 eV luminescence in our films do not differ greatly from the results of corresponding measurements by other workers. The 0.80 eV line is tentatively proposed to be a donor-acceptor transition while the 1.00 eV line is proposed to be a transition from a band to a defect level or vice-versa. From comparison of the PL spectra of the films with those of several single crystal and polycrystalline CdTe bulk samples, the 1.42 eV band is correlated to structural defects. The 0.80 eV and 1.00 eV bands are proposed to originate due to deviation from stoichiometry.

Contents

ACKNOWLEDGEMENTS	ii
ABSTRACT	iii
LIST OF CHAPTERS	v
LIST of FIGURES	ix
LIST of TABLES	xiv
1 Introduction	1
1.1 Aim of the project	1
1.2 Processes involved in sputtering	6

1.3	RF sputtering	13
1.4	Planar magnetron sputtering	14
1.5	Film growth	15
1.6	Optical emission from a glow discharge	19
1.7	Radiative transitions in a semiconductor	23
1.7.1	Exciton recombination	24
1.7.2	Conduction band to Valence band transition	25
1.7.3	Transition between a band and an impurity level	26
1.7.4	Donor-Acceptor transitions	27
1.8	General properties of CdTe	28
1.9	General properties of PbTe	28
2	Apparatus and Experimental procedure	31
2.1	Sputtering apparatus	31
2.2	Deposition of CdTe and PbTe	34
2.3	Plasma emission spectroscopy	37

2.4	Structural characterization of CdTe	39
2.5	Photoluminescence spectroscopy	42
3	Emission spectroscopy results and discussion	47
3.1	Introduction	47
3.2	Results	50
3.3	Discussion	64
3.4	Summary	69
4	Photoluminescence spectroscopy of epitaxial CdTe films	72
4.1	Photoluminescence in CdTe	72
4.2	Results	76
4.2.1	Structural properties of CdTe	76
4.2.2	PL spectra	80
4.2.3	Variation of PL with thickness	86
4.2.4	Variation of PL with laser power	90

4.2.5	Variation of PL with temperature	90
4.3	Discussion	94
4.4	Conclusion	104
5	Scope of future work	106

List of Figures

1.1	Schematic of (a) a glow discharge and (b) a planar magnetron discharge.	7
2.1	Schematic of the sputtering apparatus.	32
2.2	Schematic of a magnetron cathode.	35
2.3	Schematic of the emission spectroscopy arrangement.	38
2.4	Schematic diagram of the x-ray diffractometer.	40
2.5	Components of a Fourier transform photoluminescence apparatus.	43
3.1	The power dependence of some Pb, Ar, and Ar ⁺ emission intensities at a gas pressure of 0.068 Pa.	52

3.2	The power dependence of intense Pb and Ar lines at a pressure of 5.3 Pa.	53
3.3	The intensity of strong Cd and Te atomic lines for the negative glow, in relative units, as a function of rf power. The pressure was 0.5 Pa.	55
3.4	The intensity of some Ar and Xe atomic lines for the negative glow as a function of rf power; the total pressure was 0.5 Pa.	56
3.5	Part of the spectrum observed near the target at 50 W, 0.068 Pa. The smaller peaks are largely noise.	57
3.6	Part of the spectrum measured near the target at 50 W, 0.5 Pa. The intensities are in relative units, which differ from those of fig. 3.5.	58
3.7	Pb and Te emission intensities as a function of gas pressure at 50 W rf power.	59
3.8	Emission intensities for neutral and singly-ionized Ar as a function of gas pressure at 50 W.	60
3.9	Intensities for some Cd and Te lines observed in the negative glow as a function of the total gas pressure. For the sake of clarity, data points are not shown. The rf power level was 100 W.	62

3.10	The variation of strong Ar and Xe lines in the negative glow with the total gas pressure. The rf power was 100 W.	63
3.11	Some emission intensities near the substrate for varying self-bias voltage on the substrate. The target self-bias voltage was -90 V, and the gas pressure was 0.5 Pa. The power W required to achieve these conditions is given normalised on its value at $V'_{SB} = 0V$ (left axis).	65
4.1	X-ray diffractometer scan of (200) and (400) reflections for (100)-oriented CdTe films grown on (100)-oriented KBr substrates. The corresponding reflections from the KBr substrate are also shown for comparison.	77
4.2	Deconvolution of the experimental (400) x-ray reflection peak for CdTe (sample HM29) grown on KBr (100) into two Gaussian peaks corresponding to $K\alpha_1$ and $K\alpha_2$ reflections.	78
4.3	Thickness dependence of the FWHM of the (400) $K\alpha_1$ x-ray reflection for CdTe sputter-deposited layers.	79
4.4	PL spectra at 4.2 K for a (100) oriented CdTe epilayer (HM32). The laser power was 100 mW.	81
4.5	PL spectra at 4.2 K for a CdTe bulk single crystal from II-VI Inc.. The laser power was 100 mW.	82

4.6	PL spectra at 4.2 K for a bulk polycrystalline CdTe wafer from II-VI Inc.. The laser power was 100 mW.	83
4.7	PL spectra at 4.2 K for the hot-pressed CdTe sputtering target. The laser power was 100 mW.	84
4.8	PL spectra at 4.2 K for a bulk single crystal CdTe wafer from Cominco. The laser power was 100 mW.	85
4.9	PL spectra at 4.2 K for a CdTe bulk single crystal from II-VI Inc. after mechanical polishing. The laser power was 100 mW.	87
4.10	Thickness dependence of the FWHM of the 1.42 eV line for CdTe sputter-deposited layers.	88
4.11	FWHM of the 1.42 eV PL line for CdTe sputter-deposited samples as a function of the corresponding FWHM of the (400) x-ray diffraction peak.	89
4.12	Injection level dependence of the PL band emission intensities for CdTe (sample HM32) at 4.2 K.	91
4.13	Injection level dependence of the peak position of the different PL bands for CdTe (sample HM32) at 4.2 K.	92
4.14	Injection level dependence of the FWHM of the different PL bands for CdTe (sample HM32) at 4.2 K.	93

4.15	Temperature dependence of the PL band emission intensities for CdTe (sample HM32) at 100 mW.	95
4.16	Temperature dependence of the peak position of the different PL bands for CdTe (sample HM32) at 100mW.	96
4.17	Temperature dependence of the FWHM of the different PL bands for CdTe (sample HM32) at 100 mW.	97
4.18	Peak intensity of the 1.0 eV line as a function of the peak intensity of the 0.8 eV line at different temperatures and laser power for CdTe (sample HM32).	98

List of Tables

1.1	Species present in a sputtering discharge	16
1.2	General properties of CdTe and PbTe.	29
3.1	The function W^n , where W is the rf power, was fit to the data for emission intensities and deposition rate versus power. The error limits for the intensity n values represent the scatter in the separate values for the various Pb and Ar emission lines. The uncertainty limits for the rate are due to the scatter in the original data.	54

Chapter 1

Introduction

1.1 Aim of the project

The widespread utilisation of opto-electronic effects in semiconductors in such diverse applications as photon detectors, vidicon displays, electroluminescent devices, solar cells, infrared devices and semiconductor lasers, and the advent of optical communication and integrated optics has provided the impetus for intensive research and development in the field of materials engineering.

Semiconductors are characterized by an electrical conductivity (associated with the motion of electrons or holes or both) which on one hand is considerably smaller than that of metals, and on the other hand, is much larger than that of insulators. It is an insulator at absolute-zero. Its con-

ductivity increases with temperature, in contrast with the behaviour of metals.

Electrons in crystals are localized in energy bands [1,2,3] separated by energy domains for which no electron energy states are allowed. The topmost filled band is called the valence band (VB) and the next higher band is called the conduction band (CB). The gap between the top of the VB and the bottom of the CB is called forbidden gap and is characteristic of the semiconductor. The energy band diagram can be calculated by various theoretical techniques [2,3]. There are two types of forbidden gaps: direct and indirect. In a direct-gap, the bottom of the CB and the top of the VB (in an E-k diagram) are at the same point in k space whereas in an indirect gap semiconductor, the extrema are at different points in k space [1]. We must distinguish two processes of conduction: (i) Intrinsic conduction in which equal numbers of electrons in the CB and holes in the VB are created by thermal excitation of electrons across the forbidden gap, and (ii) extrinsic conduction, giving rise to n-type conduction in which electrons are excited to the CB from donor levels or p-type conduction in which holes are produced by excitation of electrons from the VB to acceptor levels. In a metal, the number of carriers is large and constant with temperature, whereas in a semiconductor it is smaller and variable. This characteristic suggests that in a semiconductor, the conductivity may be controlled.

Semiconductors with different bandgaps can be alloyed to synthesize new semiconductors with electrical and optical properties tailored to specific applications. Novel semiconductor structures such as superlattices and variable composition alloys are examples of materials engineering. In

particular, variable composition alloys such as $Cd_xHg_{1-x}Te$ have been successfully utilised to fabricate photon detectors with composition dependent responses covering a wide spectral range. The concept of graded bandgap structures had been proposed many years earlier and has been revived more recently in relation to photovoltaic devices. The central theme of this concept is to grow a semiconductor alloy with a spatially varying composition along the thickness of the layer leading to a position dependent bandgap which varies continuously and smoothly from a high value E_{g1} at the bottom to a low value E_{g2} at the top or vice versa.

Although graded bandgap structures have been fabricated in the past, mostly for photovoltaic applications [4,5], there has been no systematic study of the properties of such structures, particularly on the effect of the composition and bandgap gradient on the structural, electrical, optical and opto-electronic characteristics. Therefore, our group in the Chemical Physics Section of the Division of Physics at the National Research Council has undertaken a systematic investigation of graded bandgap structures based on the CdTe-PbTe semiconductor alloy system deposited by rf magnetron sputtering. CdTe and PbTe are very well lattice matched and it should be possible to grow graded CdTe-PbTe structures without strain-induced structural defects. This deposition process has been chosen for several reasons, the most prominent ones being

- It is a relatively inexpensive technique.
- It is a clean, reproducible and well controlled process.

- There are a large number of independently controllable deposition parameters which facilitate the modification and control of layer growth, properties, crystallinity, and composition.
- It offers the possibility of co-sputtering for growing alloys as well as sequential sputtering for multilayer structures.
- CdTe and PbTe high purity targets are available.

The first step of this project consists of growing epitaxial single-crystal CdTe and PbTe films. The former has received considerable attention due to promising applications in optoelectronics, integrated optics, and solar cells whereas the latter is one of the basic infrared detectors.

Epitaxial growth of the films is one of the main goals of this project. The films are structurally characterized by means of electron microscopy and diffraction, x-ray diffraction, and scanning electron microscopy and electron channeling. The compositional analysis is done by energy dispersive x-ray analysis (EDX) and chemical analysis. The effect of sputtering parameters, substrate quality and film thickness are investigated. The electrical characterization of the films is carried out by means of Hall measurements, photoconductivity, and current-voltage characteristics measurements. From these measurements, carrier type, resistivity, carrier concentration and mobility are determined as a function of crystallinity, temperature, stoichiometry (doping), and composition (alloying). The optical characterization involves reflectance and transmittance measurements, Raman spectroscopy, and photoluminescence. These measurements permit

the determination of the refractive index, the optical band gap as well as the defect and impurity levels in the gap. Finally, emission spectroscopy of the sputter discharge is carried out to study the emission lines of the species present in the sputtering chamber as a function of the deposition parameters. This would permit one to fine-tune the Cd/Pb ratio during deposition of the alloy films. In previous publications, our group has reported [6,7] the uniphase epitaxial growth of thin CdTe films on single-crystal KBr substrates by planar rf magnetron sputtering in all the crystallographic forms (cubic, hexagonal and tetragonal). References 3 and 4 are the first reports of sputter deposited epitaxial CdTe layers and the only observation of the epitaxial growth of tetragonal CdTe by any form of deposition. Epitaxial PbTe has never been obtained by sputtering. Recently, our group has succeeded in preparing epitaxial layers of PbTe on BaF_2 by rf magnetron sputtering [8].

This thesis reports the results of an investigation on the use of plasma emission spectroscopy for providing fundamental information on the complex processes controlling the sputter discharge used to deposit epitaxial films of CdTe and PbTe and the results of optical characterization of epitaxial CdTe layers by means of PL (photoluminescence) spectroscopy.

An outline of glow discharge sputtering and the use of optical spectroscopy for sputtering diagnostics, radiative recombination processes occurring in a semiconductor, and general properties of CdTe and PbTe is presented in this chapter. Chapter 2 describes the experimental procedures and equipment used in this investigation. The two following chapters contain experimental results and discussions. Chapter 3 deals with emis-

sion spectroscopy while chapter 4 is on photoluminescence spectroscopy. Finally, chapter 5 discusses the scope of future work.

1.2 Processes involved in sputtering

In this section we describe some of the processes involved in a discharge by considering the sputtering process, the parameters that control the state of the glow discharge as well as the deposition mechanisms.

Sputtering is a process where some energetic particles bombard a target leading to the ejection of the sputtered particles. This is usually achieved in a glow discharge. A gas (in our case Argon) is injected in a stainless sputtering chamber which is under vacuum and a glow discharge is initiated by providing a high-voltage to the cathode. The detailed description of the apparatus is given in the next chapter. Fig. 1.1 shows a schematic of the discharge. First, in front of the cathode (target), one can see a very weak luminous region called *cathode dark space* (cds). Next to it is a region of bright luminosity called negative glow. In literature are also mentioned the Faraday dark space and the positive glow region. However, these regions occur only at very high pressures and large target/anode distances.

The negative glow is composed of the same number of ions and electrons, or, in other words, is neutral. Consequently, it is a true plasma and no applied potential is dropped there. The potential appears across the cds and exhibits a linear increase with distance from the target.

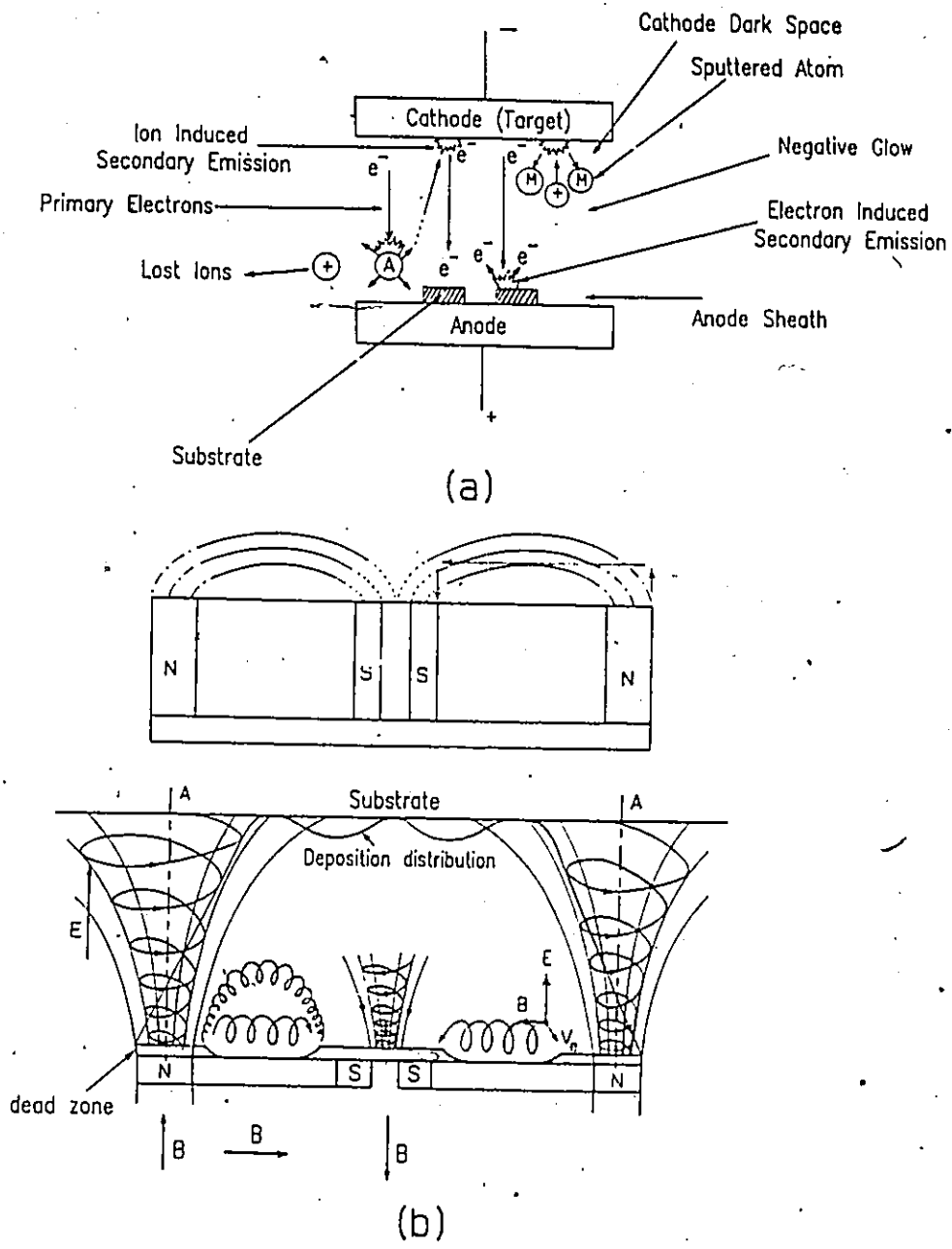


Figure 1.1: Schematic of (a) a glow discharge and (b) a planar magnetron discharge.

The electrons which are released from the target are accelerated by the field next to it. These electrons suffer collisions with Ar-atoms. The mean free path (mfp) is given by

$$l_e^{-1} = 0.025p \frac{\pi\sigma^2}{4} \text{cm}^{-1} \quad (1.1)$$

where p is the pressure in Pascals and $\frac{\pi\sigma^2}{4}$ is the cross-sectional area of the gas molecule in \AA^2 , which is 6.46\AA^2 for Ar, and 0.025 is in $10^{-8}Pa^{-1}\text{\AA}^{-3}$. The collision of an electron with an Ar atom can be elastic or inelastic. The latter case leads to the formation of an Ar ion and a new electron; both electrons will be accelerated as far as the electric field is present and undergo more collisions. Because of this proliferation of electrons the discharge is sustained. The distance L from the target to the edge of the cds is almost equal to the average distance an electron travels from the target before its first collision with an Ar atom. It is given by Aston's empirical relation [9]

$$L = \frac{A}{p} + \frac{B}{\sqrt{J}} \quad (1.2)$$

where J is the current density and A, B are constants whose values depend on the target material and the gas.

Larsen et al. [10] used a Langmuir probe in order to determine the shape of the dark space boundary near the edge of the target. It shows a circular arc centered on the edge of the target.

Two main groups of electrons enter the glow discharge: those created near the cathode which are quite fast even if they suffer some collisions and those created in the cds which do not carry as much energy as the former. However, the latter have enough energy to excite the atoms present there.

The fast ones however, penetrate farther and lose their energy in ionization as well as in excitation.

The ions at the edge of the cds are accelerated towards the target because of the field and suffer collisions with Ar atoms as well. The mfp of a gas A in a gas B is given by [11]

$$l^{-1} = \sqrt{2\pi}N_A\sigma_A^2 + \pi N_B\left(\frac{1}{2}(\sigma_A + \sigma_B)\right)^2\left(1 + \frac{m_A}{m_B}\right)^{\frac{1}{2}} \quad (1.3)$$

where N_A , N_B are the number densities of the two molecules, m_A , m_B are their masses and σ_A , σ_B are their diameters. If A and B both represent Argon (Ar) atoms, (1.3) is simplified to the following expression

$$l^{-1} = 2\sqrt{2\pi}N_B\sigma_B^2 = 0.235p\sigma_B^2 \text{ cm}^{-1} \quad (1.4)$$

where p is in pascals and σ in Å. In our case however, A and B are slightly different and represent both Ar ions and atoms. Moreover, there is a possibility that a charge interchange occurs. Therefore, the ion loses most of its energy and is again accelerated by the same field but from a different starting point.

The collision diameter of Ar ions in Ar atoms is 8Å [12] while the Ar atom diameter is about 2.9Å. Consequently, and assuming that the density of Ar^+ is very small compared to Ar, (1.4) becomes

$$l(Ar^+) = (3.5p)^{-1} \text{ cm} \quad (1.5)$$

As an illustration, at 3 Pa, the mfp of Ar^+ in Ar is about 0.9 mm. As a result, Ar^+ ions suffer many collisions before reaching the target and lose energy. Collision dynamics calculations [13] show that 45 % of the Ar^+

reaching the target have energies less than 10 % of the applied voltage.

Davis and Vanderslice [13] measured the ~~energy~~ spectrum of the ions reaching the target in a glow discharge. Even if they performed their experiments at higher pressures and lower voltages than in usual sputtering, their results were consistent with the theory assuming that all the ions are generated at the edge of cds and that they lose their energy mainly because of symmetric charge transfer. In other words, a collision between an energetic ion and a neutral atom leads to an energetic neutral and an ion carrying only a thermal velocity.

The ions produced at the edge of the cds strike the target and cause a transfer of energy to the target atoms. This transfer of energy depends on the geometry of the collision and the relative masses of the ions and target atoms. The transfer of energy causes a collision cascade in the target. Some of the target atoms escape and become sputtered atoms. The sputtering yield S is defined as the number of atoms ejected per incident ion. It is a very important parameter which depends on the energy spectrum, number and nature of the ions as well as on the crystallographic direction and nature of the target. Increasing the sputtering yield S (number of sputtered atoms per incident ions) and the current density J (number of ions incident per unit area of target) leads to high deposition rates. To increase S means to increase p or increase the mfp and thus to increase the average Ar^+ energy at the target.

There are many types of particles ejected from the target: atoms, dimers, trimers, their positive and negative ions plus electrons. These particles can be both in ground or excited state. However, excited atoms

constitute only 1 % of the sputtered flux [14] and can be seen spectroscopically as they return to ground state by emitting photons. On the other hand, ground state atoms can be seen by atomic absorption analysis. Kreye [15] used this method in order to measure the sputtering yield and found similar results as in excitation studies. It should be noted that some of the incident ions may be reflected almost without losing their energy.

The sputtered particles (atoms and negative ions) travel from the target to the substrate. The negative ions are first accelerated by the potential across the cds and suffer some collisions similar to Ar^+ but in a reversed direction. Then, in the negative glow, they are not accelerated anymore, and lose their energy in collisions. However, these ions are very few (less than 1 %).

The neutrals of course are not accelerated during their trip to the anode. Consequently, they lose their energy in successive collisions and have about the same mfp as $l(Ar)$. After each collision, a neutral atom retains an energy which depends on the ratio of the masses of the sputtered atoms and gas ions. The thermalization energy is about 0.025 eV. An obvious result is that all the sputtered atoms are thermalized before they reach the substrate, as the inter-electrode distance is usually greater or equal to 5 cm. Moreover, optical emission measurements for a cylindrical sputtering system showed that the diffusion equation controls the motion of the atoms present in the negative glow. This result also supports the hypothesis that the sputtered atoms are thermalized before reaching the substrate.

The measurements involved in determining the energies of sputtered neutrals are not direct but consist of looking at the excited [16] or ionized

[17] species after sputtering. The position of the peak energy for the spectrum of the sputtered neutrals is less than 10 eV and depends on incident ion energy.

On the other hand, Ar atoms can exist in a metastable state (Ar^m) as a result of a collision with an electron which does not carry enough energy to ionize it (15.7 eV). The metastable energies are 11.55 and 11.72 eV. Then, in a collision, this Argon atom (Ar^m) would transfer its energy to a sputtered atom and would ionize it as most of the possible sputtered species have ionization energies less than the Ar^m energies. This is called the Penning ionization. Using a mass spectrometer to sample ions reaching the anode, Coburn and Kay [18,19,20,21] have examined ions formed by Penning ionization of sputtered atoms and concluded that these neutrals consisted either of single atoms or dimers.

Finally, these are some residual gases which may be present in the negative glow. Coburn and Kay [21] detected a number of species such as H_2O^+ , H_3O^+ , ArH^+ because of the presence of residual water vapour. Furthermore, these ions are produced near the anode and could have an effect on the film growth. In an rf discharge, for instance, these ions may bombard the anode because they have higher energies than in a dc discharge. In the latter case, the anode is only a few volts negative in comparison to the plasma, while for the rf discharge, the difference is usually greater [22].

1.3 RF sputtering

Let us suppose that an ac voltage is applied between two electrodes of a sputtering system. At low frequencies, the discharge is switched from one electrode to the other. Nevertheless, at frequencies exceeding 50 KHz, the discharge can be operated at lower pressures. Indeed, the minimum pressure decreases with increasing frequency. The minimum pressure in a dc discharge depends on the need for sufficient ionization by the electrons.

In the rf case, we still have a dark space and the same voltage to accelerate the electrons. Thus, this decrease in the minimum pressure is proof that the electrons gain energy from the rf field. Secondary electrons from the electrodes are still accelerated across the dark space and cause ionization but less significantly than the rf driven electrons.

The mobility of the electrons is much greater than the mobility of the ions. Therefore, the number of electrons reaching an electrode in half a cycle when it is positive is greater than the number of ions reaching it in the other half cycle. This in turn results in the presence of a negative space charge in front of the electrode. The potential across this space charge region causes the Ar^+ to be accelerated to the electrodes with enough energy to cause sputtering. The ions do not respond to the rf field because of their much greater mass, but respond to the net dc levels.

To sputter the target and deposit on the substrate, one has to create an asymmetry. An easy way of doing this is by making the target small compared to the other electrode by connecting it to the walls of the

chambers. Since the number of electrons reaching each target is the same, the current density is higher at the smaller electrode, hence, at the target. Moreover, the target is essentially a capacitor in the circuit so that the dc voltage is higher at the target than at the *ground* electrode. This assymetry is then the cause of a larger dc dark space in front of the target. As in the dc case, the Ar^+ are accelerated across this dark space and give rise to sputtering at the target. An oscilloscope between the target electrode would display an rf waveform with a dc offset V_{dc} . The electron current flowing to the target when positive is equal to the ion current to the target in the rest of the cycle. The much higher electron mobility leads the target to the positive only for a small fraction of each cycle.

1.4 Planar magnetron sputtering

Magnetron systems attempt to trap electrons near the target so as to increase their ionization efficiency. This is achieved with electric and magnetic fields that are generally perpendicular.

The planar magnetron consists of a classic dc or rf sputtering arrangement (planar cathode surrounded by a dark space shield) with the essential addition of permanent magnets behind the flat target face. The planar magnetron principle is shown in fig. 1.1. The permanent magnets create magnetic field lines which leave and enter the target plane around an elongated track. The electric field is normal to the target and also to the magnetic field as shown in the figure. As a result, the electrons, which

are repelled by the target voltage and deflected by the magnetic field, hop around the track and create a high density plasma right above the target. Only the electron motion is influenced by magnetic fields of the strengths used in sputtering sources in the magnetron mode.

As an illustration, the discharge current is greater than 5 A and the effective ion current density is of the order of 20 mA/cm^2 compared with 0.5 mA/cm^2 for the dc diode configuration. As a result of the higher current density (which requires water cooling) and the lower operating pressures, the planar magnetron displays much higher sputtering rates. The lower operating pressures lead to purer films and confinement of the electrons at the target eliminates uncontrolled substrate heating due to electron bombardment as in non-magnetron sputtering.

However, the sputtering rate is not uniform. Indeed, the track may be eroded completely through the target, while the remainder is practically untouched. To improve this, one has to move the magnet assembly by shifting the track to different positions on the target.

1.5 Film growth

Usually, the substrate is within the negative glow. The particles that arrive on the substrate are of different kinds. There are gas atoms and ions, electrons, sputtered species from target and contaminants in their different states including dimers and ions. These species are summarized in table 1.1.

Species	Neutral	+	-
Sputtered atoms	X	X	X
Sputtered molecules	X	X	X
Gas atoms	X	X	
Gas molecules	X	X	
Residual gas molecules	X	X	
Hybrid molecules		X	
High energy electrons			X
Low energy electrons			X

Table 1.1: Species present in a sputtering discharge

As far as film thickness is concerned, it is very important to know the rate of deposition. This can be done by direct measurement using a quartz crystal microbalance or a rate monitor. From the theoretical point of view, the computation of the deposition rate and the uniformity of the film requires the knowledge of the sputtering rate and of the solution of the diffusion equation. However, this is a complex method. It should suffice to know that the geometrical arrangement of the anode and the substrate play an important role in the deposition rate and uniformity of the film since diffusion is the process which governs the transport of the sputtered material.

In many applications of thin film technology, it is very important to obtain a steady substrate temperature in order to control the structure and

composition of the film . The power dissipated in a glow discharge is of the order of 0.1 to 10.0 Wcm^{-2} . There is no doubt that a part of this power has a heating effect on the substrate which affects the film growth. The high energy secondary electrons accelerated through the cathode fall cause the initial temperature rise, while the equilibrium temperature depends on the radiation from the target. However, if the target is well-cooled, the heating at the substrate is mainly due to the high-energy electrons. In rf sputtering, Brodie et al. [22] found that high-energy electrons are the main source of heating at the substrate.

The process governing the nucleation and growth of films sputtered in a glow discharge is not well understood. There are several theories for nucleation and growth. However the most common three dimensional growth model consists of four stages [23]

- Growth to an observable size ($> 10\text{\AA}$) of the initial nuclei, which may contain a few atoms [24]. It appears as a three-dimensional island with a surface density of 10^{10} to $10^{12}cm^{-2}$.
- Coalescence of these islands because of their further growth and closeness due to the migration of the atoms from the target.
- Formation of an interconnected network structure because of large scale coalescence of the islands.
- Fill up of the empty channels in this network.

The mobility of the adatoms on the surface is an important coalescence factor; a high surface mobility results in considerable coalescence. The equilibrium of the growth conditions can be altered or does not even exist if the diffusion rate is less than the arrival rate of atoms, if electrostatic charges or adsorbed impurities are present or if the surface contains defects.

A film remains attached to the substrate as a result of two parameters involved in the deposition process: stress and adhesion. Usually, sputtered films are highly stressed. The total stress is composed of the intrinsic stress in the film and the thermal stress which is a consequence of the difference in thermal expansion coefficient between the film and the substrate.

Four mechanisms have been considered by Chapman [25] in the adhesion of thin films

- Simple interfacial adhesion due to Van der Waals forces.
- Interdiffusion between two materials since a graded junction appears between the substrate and the film [26] if two metals form solid solutions.
- Formation of intermediate layers where the bonding is a result of the presence of a compound between the two materials or between these materials and a residual gas in the system. As an illustration, for metals deposited on oxide surfaces (e.g. glass), the adhesion is proportional to the heat formation of the metal oxide.
- Mechanical adhesion where the roughness of the substrate surface improves the bonding.

A substrate ion sheath appears in front of the substrate if it is biased negatively with respect to the plasma. Therefore, ions are accelerated across this sheath and cause sputtering there depending on the ion energy. A necessary condition to net deposition of material is that the substrate voltage be less negative than the target voltage. This method of substrate bombardment cleans the film from adsorbed gases, so that one obtains higher purity or lower resistivity in bias-sputter deposited films, better adhesion, and the possibility of structural modification. Reviews of bias sputtering have been given by Seeman [27] and Christensen [28].

On the other hand, if the sum of the plasma potential and the negative applied bias potential is greater than a threshold energy, resputtering of deposited species occurs. However, the resputtering of the deposited target atoms is less significant than the resputtering of the adsorbed gas. This mechanism is consequently proposed to explain the decrease in resistivity of bias sputtering films.

1.6 Optical emission from a glow discharge

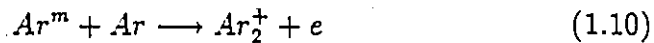
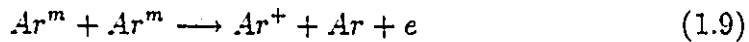
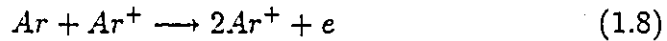
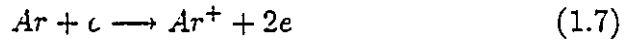
Excitation is the cause of radiation from a gas discharge. An electron in the discharge can excite an atom provided that it can supply the necessary energy between the electron levels. This excitation is in general due to an inelastic electron collision. The cross-section σ for a binary collision is

defined as

$$\frac{dN}{dt} = \sigma N_1 N_2 \bar{u} \quad (1.6)$$

where N_1 , N_2 are the concentrations of the colliding particles of both species, \bar{u} is their mean relative velocity, and $\frac{dN}{dt}$ is the rate of production of the altered state.

Three primary ionization processes are involved in a glow discharge: electron impact, ion impact and metastable-neutral interactions. These are summarized for an Ar discharge as follows



The first two processes require high energy electrons in contrast to the third one. The metastable species Ar^m are created by electron-neutral atom interactions where the metastable specie is a neutral atom in an electronically excited state [29]. However, the electron-neutral collision is the dominant collisional process [30]. This will also be demonstrated in this work.

Emission spectroscopy is the most widely used technique for glow discharge studies. It is based on the detection of emission from plasma species from their excited electronic states. Often, the excitation occurs as a result of a simple electron impact excitation. The advantage of this method is that it requires little sophisticated equipment. Even the small

percentage of optical emission from a glow discharge observable by eye provides useful, though non-quantitative, diagnostic information.

In 1926, Von Hippel [31] observed the first emission spectra of sputtered atoms. Then, Stuart and Wehner [32,33] showed that for low voltages, the sputtered atom emission intensity was proportional to the sputtering yield. Kreye [15,34] investigated the threshold sputtering energies for single crystal gold targets by means of emission spectroscopy.

Savatzky and Kay [35] used this method to monitor the sputtering yield over the energy range of 0.5-10 KeV for a polycrystalline copper target. Greene and Whelam [36] investigated trace elements as well as the profile of the impurities in thin films. Spectroscopy of sputtering discharges has been further developed by Greene and Sequeda-Osorio [37] to give spatial resolution within the discharge.

Harshbarger et al [38] have recently used emission spectroscopy to investigate reactive plasma etching, a technique which plays an important role in semiconductor technology for selective etching and pattern generation.

Assuming excitation due to inelastic electron collisions, the emission intensity at any position x in the discharge corresponding to the transition $i \rightarrow j$ is related to the number density of sputtered atoms $N(x)$ by

$$I(x) = N(x)P_i(x)T_{ij}g(\lambda) \quad (1.11)$$

where $P_i(x)$ is the probability of exciting an atom to state i , T_{ij} is the probability that the electron will decay back to state j through the radiative transition of interest, and $g(\lambda)$ is the fraction of emitted photons

corresponding to this transition which are collected. The total number of excitation collisions per second per atom is given by

$$P_i(x) = \int n_e(x, v_e) \sigma_{exc}(v_e) dv_e \quad (1.12)$$

where n_e is the electron population density and v_e is the electron velocity.

The equations (1.11) and (1.12) are obviously quite complicated relationships. However, optical emission can be used for monitoring the discharge by calibrating I for standard samples under known discharge conditions. Moreover, these equations can be simplified in some cases and direct relationships between I and N(x) obtained, which can provide quantitative results.

The emitting species, when identified, give qualitative information on the change in plasma properties as a function of the discharge parameters. Our concern in this work, for instance, is the power, pressure and substrate bias dependence of the emission lines. However, the majority of the species are in their ground state, and the relationship between the optical emission intensities and the electronic ground state species concentrations can be quite complicated. To overcome these complications, Coburn and Chen [39] developed a technique called actinometry. This method relies on estimating the ground state species X concentration from the ratios of the optical emission intensity of interest to the emission intensity from an inert gas A (the actinometer). This normalization corrects any change in emission intensities due to a change in excitation rate as a result of a change in energy distribution rather than species concentration.

Three major conditions need to be satisfied for the theory to be

valid

- The excited species X and A must be produced by an electron impact excitation of ground states.
- The excited states must decay exclusively by photon emission.
- The electron impact cross-section for X and A must have similar thresholds and shapes as a function of electron energy.

In practice, although the conditions listed above are violated, actinometry does hold over some range of plasma conditions. Coburn and Chen [39] used optical emission spectroscopy for the study of reactive plasmas. Their experiments were carried out using a $CF_4 : O_2 : Ar$ plasma. The emission intensity ratio $I_F(703.6nm)/I_{Ar}(705.4nm)$ was used to monitor ground state F atom concentration by means of actinometry. The authors concluded that *the ratio of intensities of the reactive particles to noble atom emission can be used to monitor the relative concentration of the reactive particles as plasma parameters are varied.*

1.7 Radiative transitions in a semiconductor

In a semiconductor, if an electron occupying a higher-state than in equilibrium makes a transition to a vacant lower energy state, it may emit the energy difference between these two levels as an electromagnetic radiation.

As a result, some kind of deviation from equilibrium is needed to create such transitions. This is achieved by means of excitation. The light emission is called luminescence. Moreover, if the excitation is accomplished by optical absorption, this process is then called photoluminescence.

Several excitation and recombination mechanisms are possible. These are discussed below.

1.7.1 Exciton recombination

If a semiconductor is sufficiently pure, the electrons and holes form excitons. The exciton may be considered as a neutral electron-hole pair which is bound by a Coulombic potential and is free to migrate through the lattice. It may be formed by exciting a valence electron to a state just below the conduction band by the absorption of a photon. The ionization energy of such a system is [40]

$$E_x(n) = (-m_i^* q^4 / 2h^2 \epsilon^2(0)) (1/n^2) \quad (1.13)$$

where q is the electronic charge, and n is an integer greater or equal to one, depending upon whether the exciton system is in the ground state or in an excited state and $\epsilon(0)$ is the static dielectric constant of the material. The term m_i^* is the reduced mass given by

$$(1/m_i^*) = (1/m_e^*) + (1/m_h^*) \quad (1.14)$$

where m_e^* and m_h^* are, respectively, the electron and hole effective masses. Hence, in a direct-gap semiconductor, the free exciton emission might con-

sist of a series of narrow lines due to the recombination of the pair and, starting at $E_g - E_x(1)$, and occurring at $E_g - (1/n^2)E_x(1)$. However, the intensity of the high order peaks decreases rapidly (as n^{-3}) and is therefore difficult to observe.

In an indirect gap semiconductor, a phonon is emitted to conserve the momentum. The energy of the emitted photon is, therefore,

$$h\nu = E_g - E_x(n) - mE_p \quad (1.15)$$

where E_p is the phonon energy and m is the number of optical phonons emitted per transition. Excitons may be bound to an impurity level in the gap. These are called bound excitons. Their recombination results in the emission of a photon at a lower energy than that of the free exciton.

1.7.2 Conduction band to Valence band transition

Excitons represent the lowest energy states of electron-hole pairs. However, if the temperature is such that $kT > E_x(n)$, or if the crystal is not that pure and perfect, the excitons are more likely to break up and form free carriers. This could be followed by a band to band radiative recombination.

Since the momentum is conserved in direct gap semiconductors, transitions occur for states having the same k -values. The low-energy threshold is therefore $h\nu = E_g$. With increasing either the excitation rate or the sample temperature, emission at higher photon energies occurs as deeper

states in the band become filled.

In an indirect-gap semiconductor, all the occupied upper states connect to all the empty lower states. But the transition must be mediated by an intermediate process. Phonon emission is the most likely intermediate process. An optical transition assisted by phonon emission occurs at lower photon energy than the gap energy, $h\nu_{min} = E_g - E_p$. Phonon absorption results in a higher photon energy of at least $E_g + E_p$, which can be more readily reabsorbed by the semiconductor.

1.7.3 Transition between a band and an impurity level

Shallow transitions could occur by emitting a radiation in the far infrared. However, a phonon emission process is more probable. Such a transition neutralizes ionized donors or acceptors. As an illustration for the donor case, the recombination consists of trapping an electron in an excited state of the donor which then cascades to lower-lying states.

A deep transition consists of either a conduction band to acceptor transition or a donor to valence band transition. For a direct transition, a photon $h\nu = E_g - E_i$ is emitted whereas for indirect transitions, it is phonon assisted and the energy of the emitted photon is $h\nu = E_g - E_i - E_p$.

In most direct gap semiconductors, E_a is greater than E_d because the effective mass of the electron is smaller than that of the hole. Thus, a conduction band to acceptor transition can be easily distinguished from a donor to valence band transition. This is true unless $E_a \simeq E_d$ in which case

the conductivity of the semiconductor and the emission intensity must be correlated with the impurity concentration. In indirect gap semiconductors however, donor states are associated with the lowest valley of the conduction band and phonons assist such kind of transition.

Deep levels in the energy gap are formed as a result of the presence of impurities with large ionization energies. Transitions between these states and the band edge emits radiation at $h\nu = E_g - E_i$.

1.7.4 Donor-Acceptor transitions

When both donor and acceptor impurities are present in a semiconductor, Coulomb interaction between them modifies the binding energies (compared to the isolated impurity case) such that the energy separating the paired donor and acceptor states is

$$h\nu = E_g - E_a - E_d + \frac{e^2}{kr} \quad (1.16)$$

where E_g is the energy gap, E_a is the acceptor binding energy, E_d is the donor binding energy and e^2/kr is the repulsive potential between the ionized acceptor and donor at a distance r .

1.8 General properties of CdTe

CdTe is a direct gap semiconductor with the smallest energy gap at the center of the Brillouin zone(Γ). The optical gap is 1.49 eV at room temperature. The zinc blende structure is the stable form for bulk single crystals of CdTe at atmospheric pressure. This structure belongs to the cubic space group $F\bar{4}3m$ (T_d^2) and consists of two interpenetrating face center cubic lattices offset from one another by one fourth of a body diagonal. The best value of the cubic lattice parameter at room temperature is 6.481 Å [41,42]. This value is subject to change due to deviation from stoichiometry. Table 1.2 summarizes the main properties of CdTe.

1.9 General properties of PbTe

PbTe is a IV-VI compound which belongs to the lead salt group and crystallizes in the rock-salt crystal structure. The fundamental space lattice (Bravais lattice) is face centered cubic. The customary lattice constant a is the edge distance between lead ions or between anions forming the unit cube and is approximately 6.4603 Å. There are four PbTe units in each unit cube of volume a^3 , and each ion has six nearest-neighbour ions of the opposite kind, giving a coordination number of six. Its spacegroup is O_h^5 or (Fm3m).

	E_G (0 K) eV	E_G (300 K) eV	Lowest conduction- band minimum,	$(\frac{dE_G}{dT})$ $\times 10^4$ (300 K) eV/K	$(\frac{dE_G}{dP})_T$ $\times 10^6$ eV/bar	Effective mass m_e^*	Effective mass m_h^*	Refractive index n	Static dielectric constant ϵ (300 K)	Lattice constant a \AA (300 K)
CdTe	1.60	1.49	dir 000	-5.35	1.5	0.11	0.35	2.75	10.2	6.486
PbTe	0.19	0.31	dir 111	+4.50	-9	m_t 0.24 m_t 0.02	m_t 0.3 m_t 0.02	3.80	414	6.462

Table 1.2: General properties of CdTe and PbTe.

PbTe is a narrow gap semiconductor ($E_g = 0.31\text{eV}$ at room temperature) with extrema of conduction and valence bands at the L points of the Brillouin zone. Lead salt semiconductors are very interesting semiconductors. The temperature coefficient (dE_g/dT) of their minimum gap E_g is positive. Moreover, their static dielectric constants are unusually large when compared with values observed for other semiconductors. Table 1.2 summarizes the most important properties of PbTe.

Chapter 2

Apparatus and Experimental procedure

2.1 Sputtering apparatus

The sputtering apparatus is shown schematically in fig. 2.1. The sputtering chamber (Materials research corporation 8667 model) provides three sputtering targets (1, 2 and 3) mounted 90 degrees apart on a 71 cm diameter stainless steel top-plate. The targets consist of hot-pressed 99.999 % PbTe and CdTe discs, 0.6 cm thick and of 16.5 cm diameter. Substrates are placed on a large annular table which can be either rotated continuously or stepped to discrete positions below the targets.

Four sputter modes are available: dc or rf conventional diode sput-

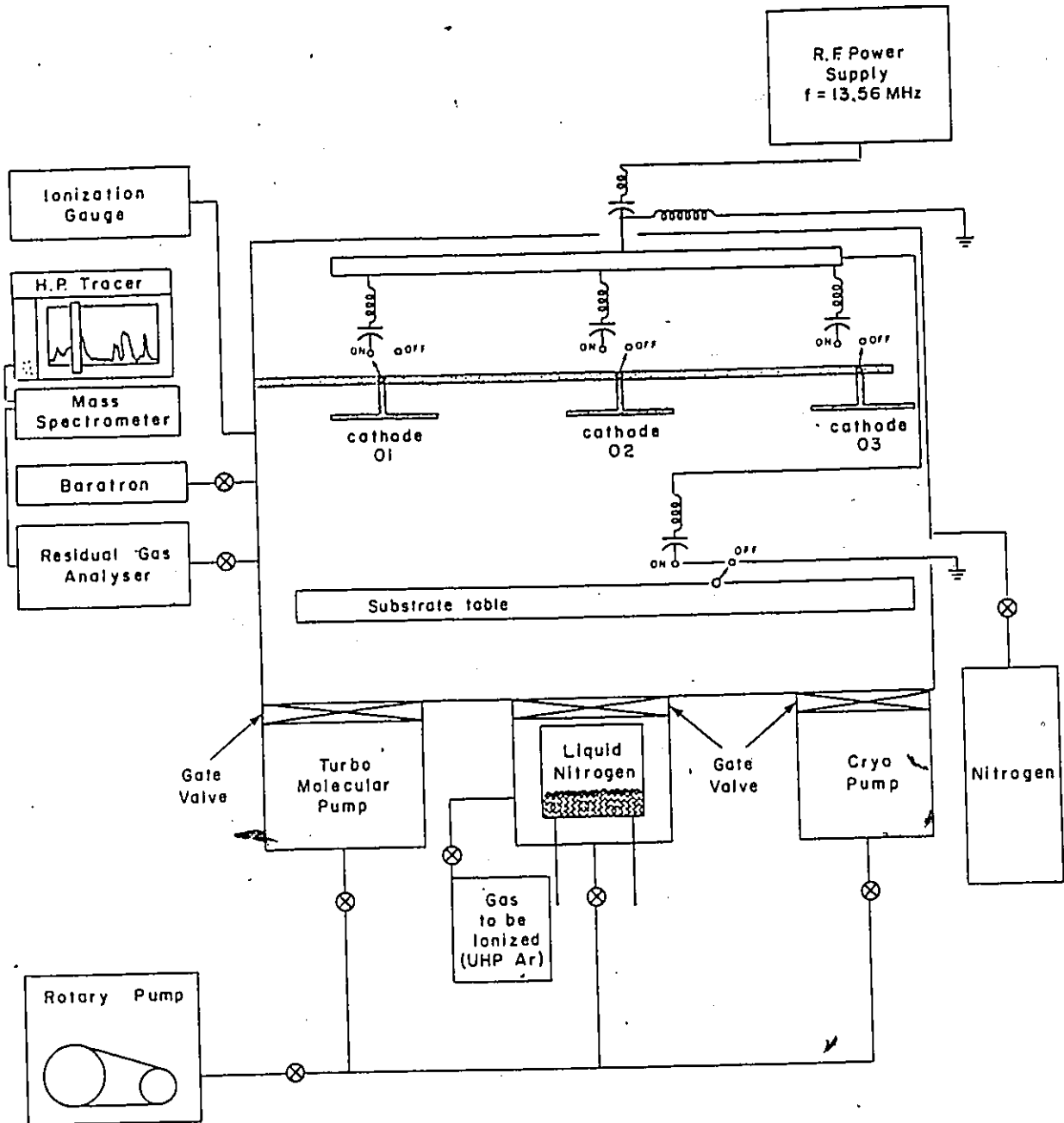


Figure 2.1: Schematic of the sputtering apparatus.

tering and dc or rf high rate magnetron sputtering. All our films were grown in the rf magnetron sputtering mode. By locating permanent magnets behind the flat target face, a magnetic field is generated that is orthogonal to the normal electric field associated with the cathode. Also, substrates can be heated or sputter etched prior to deposition and can be biased during deposition. In addition, our apparatus also provides

- Sequential deposition of up to three layers of different materials.
- Simultaneous deposition or co-deposition of different materials.

Up to four individual stainless steel shutters are provided. Each is individually positioned. Position indicators and position locks assure correct location. The aim of these shutters is to prevent the sputtered species to get to the substrate when pre-sputtering. Also, it is used for sequential deposition purposes in order to permit the deposition of each layer at a time.

The austenitic (non-magnetic) stainless steel chamber is a nominal 66 cm diameter by 25.4 cm high. The interior surface is polished to minimize the effective surface area. A 10 cm diameter viewport is provided with disposable windows. Four V4 flanges provide two spare positions. The annular water-cooled anode is 61 cm OD by 10 cm ID. It is constructed of aluminum and stainless steel. Rf and cooling lines are routed through a centre post and connect to the cathode inside a cavity which is at atmospheric pressure. The rf generator is an MRC model S3013 and its frequency is 13.56 MHz. Magnetron cathodes (fig. 2.2) are constructed of stainless steel

and copper with water flow concentrated over areas of high power density. This can be operated as diode cathodes by removing the magnets.

The sputtering chamber is pumped down using a roughing pump, a Varian V80 turbo pump, an NRC-made liquid nitrogen trap and a CTI CRYO-TORR \S cryogenic pump. The latter provides fast, clean pumping of all gases in the 10^{-3} to 10^{-10} torr range. It operates on the principle that gases can be condensed and held at extremely low vapour pressures, achieving high speeds and throughputs. A Varian 843 vacuum ionization gauge reads the pressures in the above range while a THERMOVAC TM 210 S reads higher pressures. A spectromass 100D (Spectrum Scientific Ltd.), which is a small partial pressure analyser of the quadrupole type, is used for residual gas analysis, vacuum problem solving, leak detection, process control and many other similar applications. Ultra high purity Ar is used as the sputter gas. The gas flow is controlled by an MKS electronic mass flow controller and the pressure during sputtering is read by an MKS Baratron capacitance manometer.

2.2 Deposition of CdTe and PbTe

The substrates (freshly cleaved (100) KBr for CdTe and freshly cleaved and polished (111) BaF_2 for PbTe), as well as some chemically cleaned glass slides were attached to the heater block using a dag or an In/Ga solution. The chamber was opened, and the substrates were loaded on the etch platform. The chamber was then closed and pumped down to the

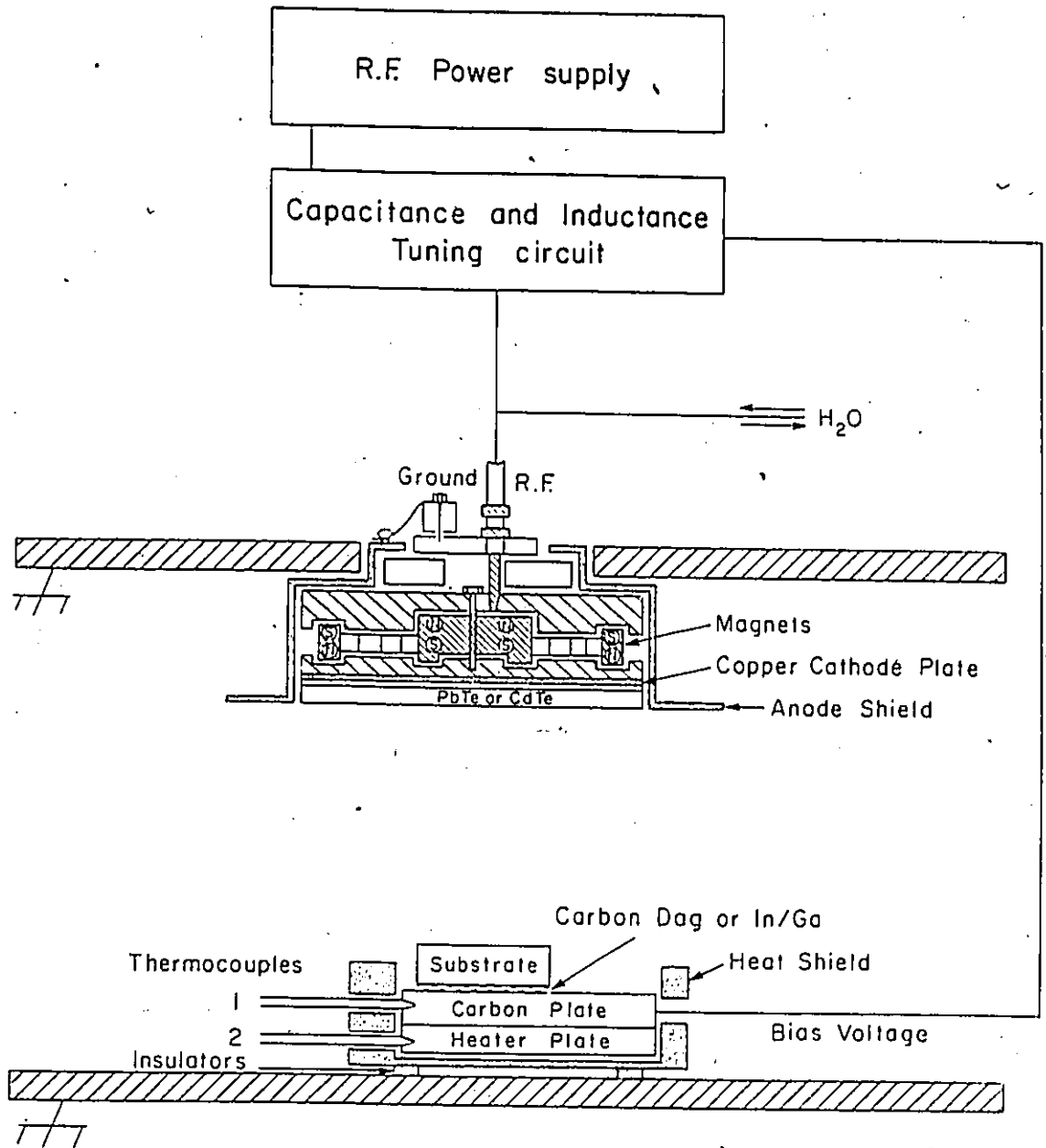


Figure 2.2: Schematic of a magnetron cathode.

suitable vacuum (at least 4×10^{-7} torr for film deposition), which often required an overnight pumpdown with heating of the substrates to the desired temperature.

On the following day, the base pressure, the substrate temperature, and the RGA (residual gas analyser) trace were recorded. Then, Ar was introduced and the pressure was adjusted to 3.5 mtorr or the desired value. The flow-rate was generally kept between 80 and 100 SCCM. The next step consisted of turning on the power supply, adjusting the shutters for the pre-sputtering mode, selecting the various targets to be sputtered with the individual select on/off knobs and tuning the network to the power supply for minimum reflected power.

Next, the high voltage section of the power supply was turned on and the power was increased to the desired value. The glow start button was pushed until a plasma was generated in the chamber. Finally, a fine tune, if necessary, adjusted our parameters and set the reflected power to its minimum. The target was first pre-sputtered for 10-15 minutes at 100 W for CdTe and 50 W for PbTe to clean the target surface while protecting the substrates with a shutter. Then, the shutters are removed and film deposition started at the desired pressure, power, target voltage, and substrate bias by readjusting the tuning parameter, if necessary.

The film thickness was determined at the end of the run by measuring the thickness of the film on a glass slide. A scratch was made on the glass, and the thickness of the step was measured using a Dektak II-A stylus. Alternately, an Inficon quartz crystal thickness and rate monitor was used for in-situ thickness measurements during deposition, particularly when

conducting emission spectroscopy studies.

2.3 Plasma emission spectroscopy

The arrangement for emission spectroscopy is shown schematically in fig. 2.3. Spectroscopy was carried out through a large quartz side window by means of a PT Analytical PSS-100 computer-run spectrometer, which scanned the range of 200-800 nm with a resolution of 0.1 nm. The grating was blazed at 250 nm.

To improve the light-gathering capability of the apparatus for measurements of intensity versus rf power, gas pressure, and bias voltage, a large portion of the discharge was exposed directly to the monochromator using suitable masks. Emission intensities were determined near the cathode by means of a vertical mask exposing a 1×12 cm portion of the discharge just below the cathode. The discharge near the substrate was studied using a mask exposing a region 0.75×3 cm immediately above the substrate. The rf power was determined, as is usual, between the rf supply and the tuning circuit, while the total gas pressure was measured using the capacitance manometer.

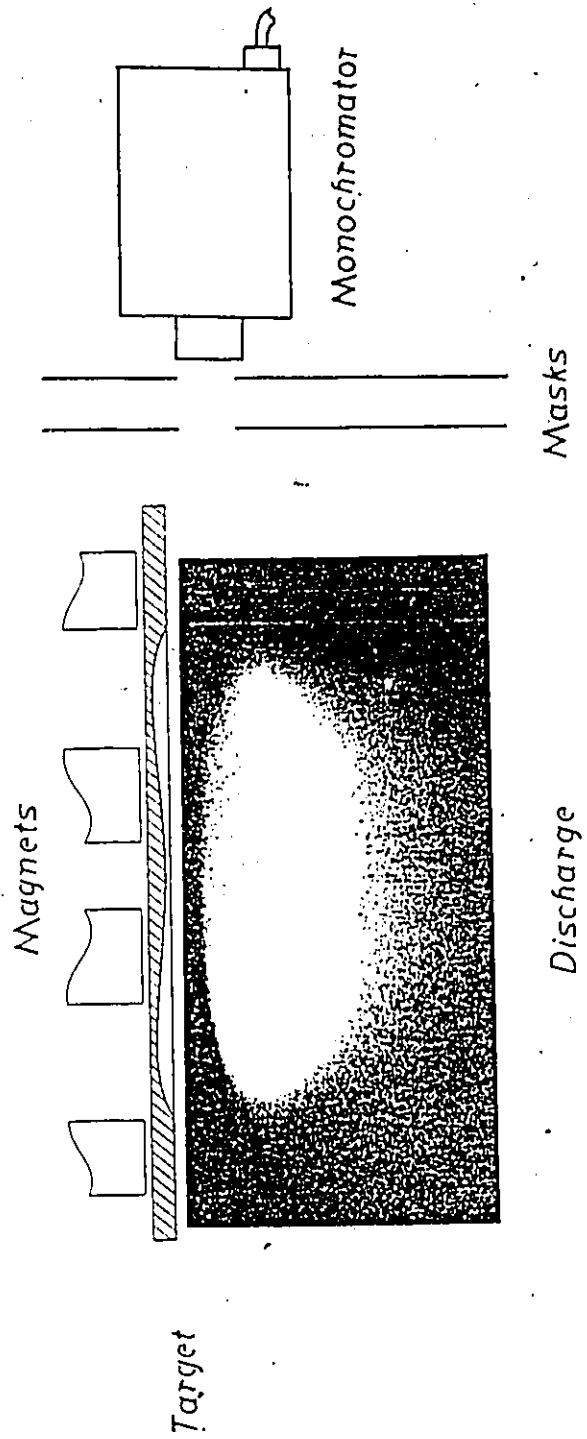


Figure 2.3: Schematic of the emission spectroscopy arrangement.

2.4 Structural characterization of CdTe

The films were structurally characterized principally by x-ray diffraction. The Phillips x-ray diffractometer is provided with several units controlled by a PW 1710 diffraction control unit (fig. 2.4). The PW 1710 provides four major functions:

- Control of the x-ray diffractometer.
- Measurement and processing of x-ray intensities.
- Control of peripherals such as VDU's and/or computers.
- Execution of commands and user-made programs.

The system comprises two modules: The control module which houses the electronics and the power module which houses the power supply circuitry. Moreover, the PW 1710 has its own front panel mounted alphanumeric keyboard and display plus extra command keys and system status indicators. In addition, it controls the PW 1820 vertical goniometer, the PW 1771 radiation shield as well as the PW 8203 A one line recorder.

First, a film was loaded by inserting it into a sample holder. The generator was then set at a voltage of 35 KV and a current of 20 mA and the shutter was opened. The first scan consisted of a preliminary search for diffraction peaks at a quite high speed. Next, every single peak was more carefully considered, by scanning at a low speed. This allowed us to choose

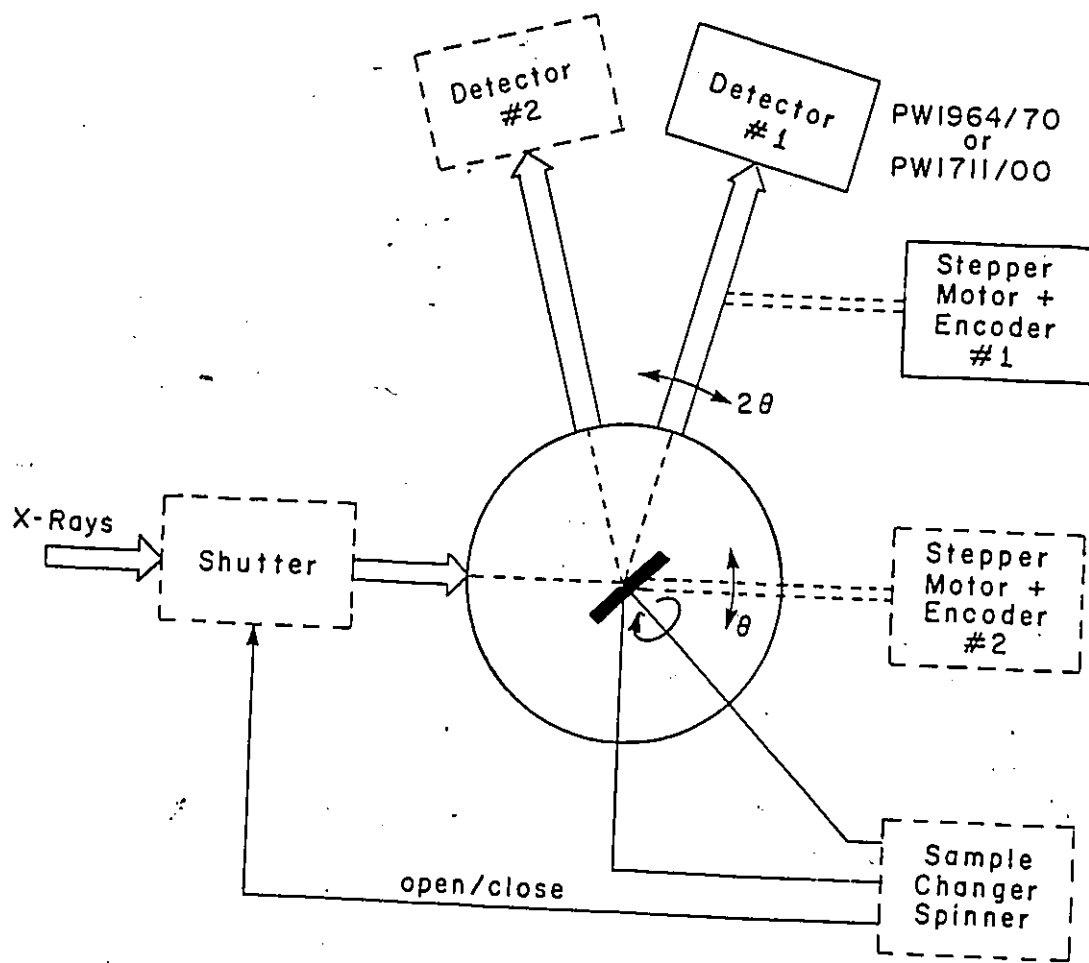


Figure 2.4: Schematic diagram of the x-ray diffractometer.

the proper scale for the final step. A final scan was, therefore, performed and the different peaks as a function of 2θ were recorded on a chart paper.

Diffraction of coherent radiation by the three-dimensional array of atoms in a crystal is governed by Bragg's law, which states that the incident beam is reflected by a set of lattice planes (hkl) if

$$2d \sin \theta = n\lambda \quad (2.1)$$

where d is the interplanar spacing, θ is the angle between the incident (or reflected) beam and the planes (hkl) and λ the wavelength of the diffracted radiation.

The X-ray technique is based on monochromatic radiation. The main radiation source in our case was the copper $K\alpha_1$, $K\alpha_2$, and $K\beta$ radiation. However, a tungsten $L\alpha_1$ and $L\alpha_2$ radiation was recognized to cause the appearance of one of the very weak peaks. The observed 2θ values corresponding to the different peaks in the recorded scan were compared with the 2θ values expected for different hkl planes for the substrate and the film material from the known crystallographic structures and lattice parameters. For cubic crystals,

$$d = \frac{a}{(\sqrt{h^2 + k^2 + l^2})} \quad (2.2)$$

where a is the lattice parameter.

2.5 Photoluminescence spectroscopy

Photoluminescence studies were conducted using a Fourier transform spectrometer (FTS). The major components of our PL apparatus (fig. 2.5) are: (i) a source (Ar ion laser) to excite the PL, (ii) a cryostat to cool the sample, and (iii) a spectrometer to analyze the PL spectrum. The Ar ion (Ar^{2+}) laser line was at 514.5 nm (2.410 eV) and the nonlaser plasma emission was removed from the laser beam with a Brewster angle prism disperser and a Schott BG 38 glass filter. Without the laser prefilter, strong plasma lines were observed via scattering in the 1.25-1.8 μm range. Laser power at the sample compartment was measured with an Eppley thermopile radiometer. Some of the samples were clamped in vacuum on the cold finger of a Janis Supertran continuous flow cryostat with CaF_2 windows on the room-temperature shroud. The cryostat's base sample temperature was below 5 K, as verified from the temperature dependence of the PL of an InP standard sample. Below 80 K, the measurement of temperature was done with a germanium resistance thermometer. Other samples were glued on the sample holder of a *varitemp*-type cryostat and immersed in liquid helium at 4.2 K.

Fourier transform spectroscopy (FTS) is the dominant spectrophotometric technique in the infrared. This instrument is a form of Michelson interferometer and its mode of operation is made clear in fig. 2.5. A beam of mixed radiations from the source S_0 traverses the sample S_a and is collimated. The parallel beam is directed at an angle of 45 degrees onto a

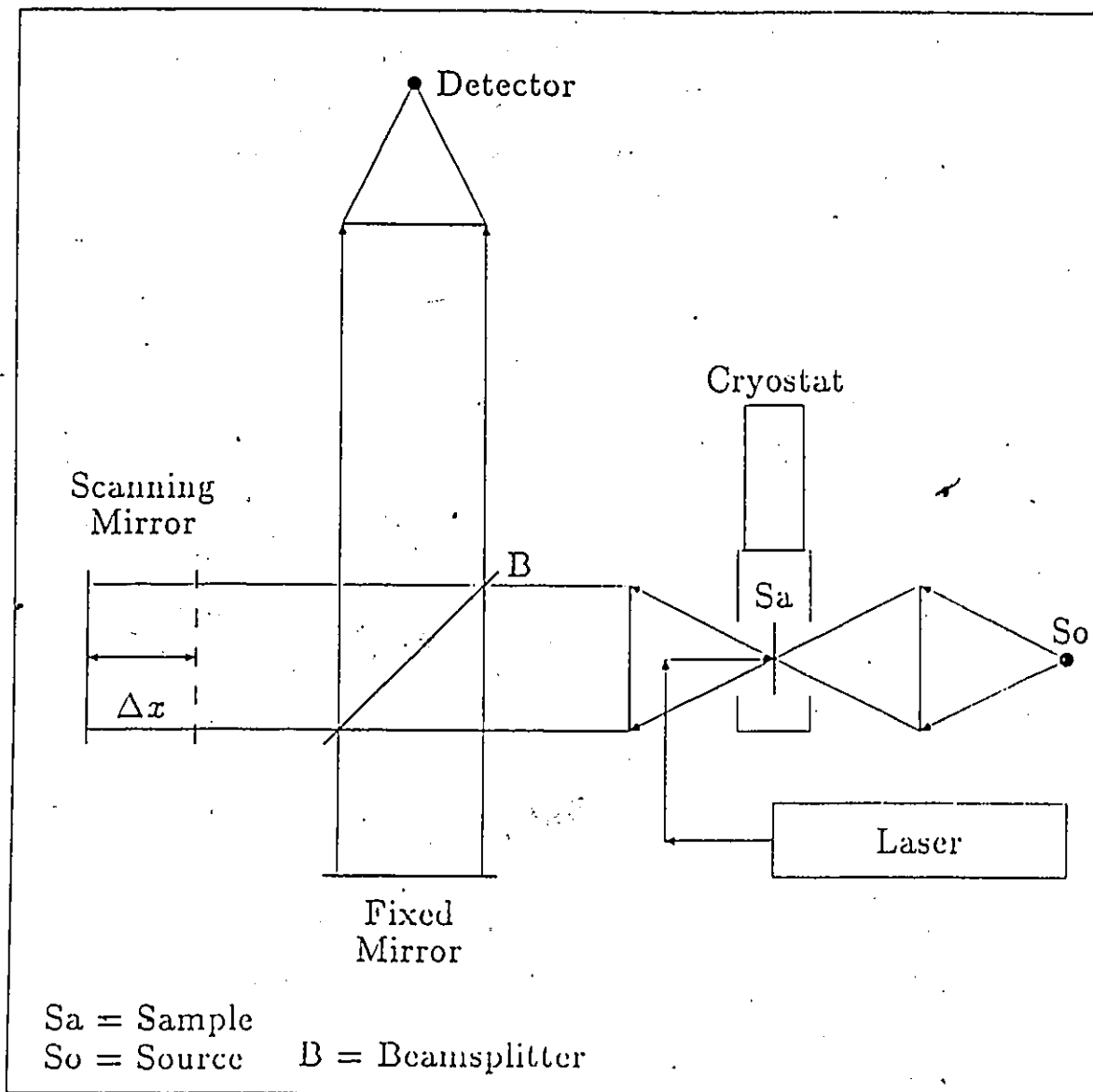


Figure 2.5: Components of a Fourier transform photoluminescence apparatus.

beamsplitter B. Part of the radiation is reflected and the remainder transmitted: the transmitted part falls at normal incidence on a plane mirror, capable of movement along a line perpendicular to its surface, and is returned to be partially reflected by B and finally to form, with the help of a condensing system, a reduced image of the entrance aperture on the detector. That part of the original parallel beam reflected by the beamsplitter falls at normal incidence on a fixed plane mirror, is returned to B and after transmission is also condensed onto the detector. Since the two parts of the original beam follow different paths, there is in general, for a particular wavelength λ , a phase displacement between them equal to $2\pi x/\lambda$, where the path difference x and λ are both measured in cm. Replacing $1/\lambda$ by wavenumber σ (waves per cm), the phase difference becomes $2\pi\sigma x$; when x is zero (ZPD) all frequencies are in phase and the amplified and rectified signal from the detector is at a maximum. As the path difference is steadily increased from zero by movement of the plane mirror, detector output falls to a minimum and thereafter passes through a succession of maxima and minima with a tendency for the fluctuations to diminish. The resulting curve is known as an interferogram and it can be shown that a power spectrum can be derived from it by performing a Fourier transformation, and for this purpose a high speed digital computer is usually employed. If one spectrum is obtained with the sample and another one without the sample, the ratio of the two spectra gives a transmittance spectrum, similar to that obtainable with any other spectrometer. Clearly, when using a digital computer it is not possible to utilize every point of the interferogram and in practice the output from the detector is measured only at uniform incre-

ments of path difference, Δx .

The interferometer has a number of advantages over the conventional spectrometer. Most important, there is a large energy gain, particularly at high resolution, since instead of passing radiation through a narrow slit, as in prism or grating spectrometer, quite a large circular entrance aperture may be used, and this feature is very welcome at long wavelengths where the energy from available sources is low.

FT-IR spectrometers are routinely used for the measurement of transmittance (τ) and reflectance (ρ). More recently, other types of sampling including photoacoustics, diffuse reflectance, photothermal ionization, photoconductivity, Raman and PL have been combined with FTS. In our investigation, the spectrometer used for analysing the PL was a Bomem DA3.02 FT infrared spectrophotometer. The sample cryostat was centered vertically at the normal absorbance focus position in the sample chamber and the PL was collected, collimated, directed *backwards* through the interferometer, filtered, and focused on the detector and at the normal source position. Thus, the PL arrangement required minimal modification to the instrument. Spurious effects due to air absorptions coincident in frequency with the luminescence were avoided by evacuating the spectrometer to a pressure of 0.1 torr. FTS is relatively insensitive to the scattering and defocusing of the incident laser and to the amplitude fluctuations in the emission due to turbulence that occurs when the sample is surrounded with liquid helium. In fact, FT instruments can tolerate a sample area several millimetres in diameter and maintain a resolution of 0.1 meV or better. Also, the FT process removes amplitude fluctuations because they are outside the

FT filter bandwidth.

The detector used was a North coast 817 S germanium PIN photodiode. Its time constant limited the scanning speed of our interferometer to a maximum of 0.05 cm/s. One problem with this detector was its sensitivity to charged particle events caused by cosmic rays. At the output of the detector preamplifier, these events produced large spikes which were removed electronically. The spectral results were checked with the noisier, but wider band, InSb detector to be sure that no large features at lower energy had been overlooked. A Schott RG-850 glass filter in front of the detector removed the laser stray light from the collected radiation. Otherwise, the FT spectrometer would have redistributed the exciting line's photon noise over the whole spectrum, thus swamping the luminescence.

Photoluminescence spectra of magnetron sputter deposited epitaxial (100) CdTe ranging from 1.8 to 14 μm grown on freshly cleaved (100) KBr substrate were recorded at 4.2 K and at an incident excitation power of 100 mW. On some selected samples, detailed measurements of the temperature dependence (4.2-80 K) and the excitation power dependence (10-200 mW) of the photoluminescence spectra were also carried out.

Chapter 3

Emission spectroscopy results and discussion

3.1 Introduction

CdTe and PbTe are excellent candidates for potential use in alloy (because of the wide difference in their bandgap) or multilayer structures (close match in lattice parameters). Our group has recently begun to explore the magnetron discharge as a means of preparing such structures. It would, therefore, be particularly useful if such discharge parameters as the cathode ion current, the sputtered atom density, and the electron energy, which have a large influence on the way films are deposited, could be related to such system operating parameters as the gas pressure and power input.

Emission spectroscopy, the study of the spectral dependence of the intensity of light given off by atoms excited to emitting states by, for instance, inelastic electron-neutral collisions, is one way in which the relationships between system operating parameters and discharge parameters may be explored and in turn correlated to compositional properties of the above structures.

In two recent papers [43,44] an emission spectroscopy study has been made of an rf magnetron discharge used to sputter-deposit CdTe in Ar. In such a discharge one may write the intensity of, for instance, a Cd line as

$$I_{Cd} = K_{Cd} \times N_{Cd} \times \eta_{Cd} \quad (3.1)$$

where K_{Cd} is a constant, N_{Cd} is the local density of Cd atoms, and η_{Cd} is the probability of exciting a Cd atom to the emitting state. It is a function of the energy distribution of the electrons and the cross-section for excitation of a Cd atom from its ground state to the emitting state in question and is equal to P_i of equation 1.12. It was found that at normal sputtering pressures ($p \approx 1$ Pa) the ratio η_{Cd}/η_{Ar} was insensitive to the rf power, so that, the ratio I_{Cd}/I_{Ar} was proportional to N_{Cd}/N_{Ar} as the rf power was varied. Thus, Cd intensities were simply related to Cd densities. On the other hand, when the gas pressure was varied, such a relationship was not obeyed. The relationship of the sputtered atom density to the Ar-normalized intensity as the power is varied has also been observed by Pech et al. [45] for a dc magnetron discharge.

In the present work, a study is made of a discharge used to sputter deposit PbTe in Ar so as to prepare for co-deposition or sequential deposi-

tion of CdTe and PbTe in a multi-gun magnetron system, using emission spectroscopy as a probe for process control and analysis. The principal Pb and Te lines in the discharge are identified, and their dependence on rf power determined over a wide range of pressures to look for a relationship between the Pb atomic density and the Ar-normalized Pb intensities. The pressure dependence of the principal lines is determined at constant power. Finally, some preliminary studies are made of the variation of line intensities just above the substrate with bias voltage on the substrate, an important film growth parameter.

The sputtering chamber and the emission spectrometer have been previously described in chapter 2. It was found that when the rf power fed to the cathode was increased past 100 W or so, the discharge occasionally changed from its normal configuration, a half-toroid positioned just inside the outer ring of magnets [44], to an intensely luminous spot discharge which moved over the target on a circle of 7 cm diameter with a period of approximately a second. This circle was just within the outer ring of magnets and centered on the region of the highest sputter removal rate. This discharge resulted in fine near-circular erosion channels in the cathode. The likelihood for its occurrence increased with power, but was not very sensitive to pressure. Since the sputter rate of a magnetron discharge also increases with power but is relatively insensitive to pressure and the sputter deposition rate of PbTe is unusually high in the present system, approximately 12.5 Å/s at 50 W rf power, we would tentatively attribute the occurrence of this localized discharge to unusually high sputtered atom fluxes near the target. This spot discharge was not studied in the present

work, but, by forcing us to operate at relatively low levels, adversely affected the accuracy of some of the results described below.

Emission intensities were determined near the cathode and near the substrate as a function of rf power and pressure by means of vertical masks as described earlier in chapter 2. The power dependence of the deposition rate was measured using a quartz thickness monitor.

The resolving power of the spectrometer, 0.1 nm, was such that a dozen or so Pb I lines could be discerned. Those at 261.4, 280.2, 283.3, 363.8, 368.3, and 405.8 nm were particularly strong. As in the case of the CdTe discharge, Te I lines at 214.3, 225.9, and 238.6 nm were resolved but were relatively weak and broad; in this paper, the attention will focus on the Pb lines. A number of strong Ar I lines could readily be observed.

3.2 Results

The dependence of the main Pb, Te and Ar emission lines intensities on rf power was determined both near the cathode and near the anode, placed 5 cm below the cathode, at gas pressures of 0.068 Pa, 0.53 Pa, and 5.3 Pa. Some data representative of intensities measured near the target are given in figures 3.1 and 3.2. The emission intensities of the sputtered species vary superlinearly with power, while the Ar intensities vary sublinearly with power. This was also observed with the CdTe discharge (figs. 3.3, 3.4). This behaviour is to be attributed to the fact that the sputtered atom density increases with power, while the Ar pressure does not. Fig-

ures 3.1 and 3.2, which are log-log plots, indicate that the data are well represented by $I \propto W^n$. The straight lines drawn through the data satisfy this relationship, with n determined by a least mean squares deviation fit. Values for n were determined for five lines of both Pb and Ar near the cathode and near the substrate at the three pressures mentioned above and are given in table 3.1.

At the lowest pressures and near the cathode a number of new lines appeared at wavelengths between 450 and 475 nm. Their emergence with increasing pressure is shown by the spectra of figs. 3.5 and 3.6 which unambiguously identified them as Ar^+ lines [46]. Their power dependence at 0.07 Pa was very similar to that of the neutral Ar lines (fig. 3.1; table 3.1). These Ar^+ lines were not observed near the substrate at low gas pressures. All these observations also apply to the CdTe discharge, except that the power dependence of the Ar^+ lines was not examined for that discharge.

The intensities of the main Pb, Te, and Ar emission lines near the target were measured while the gas pressure was varied at a constant rf power level of 50 W (figs. 3.7, 3.8). The sputtered species intensities are relatively insensitive to pressure for pressures below 0.5 Pa, and increase more rapidly with pressure at higher pressures. The pressure dependence of the Ar lines is quite different. Again, the Ar^+ intensities decrease rapidly with increasing pressure.

The data of fig. 3.7 are similar to the data obtained for the CdTe discharge (fig. 3.9), in that $I(p)$ curves change slope near 0.5 Pa, at which pressure the electron-neutral collision frequency is near the rf frequency [47] if collective effects may be ignored. These curves differ from the CdTe

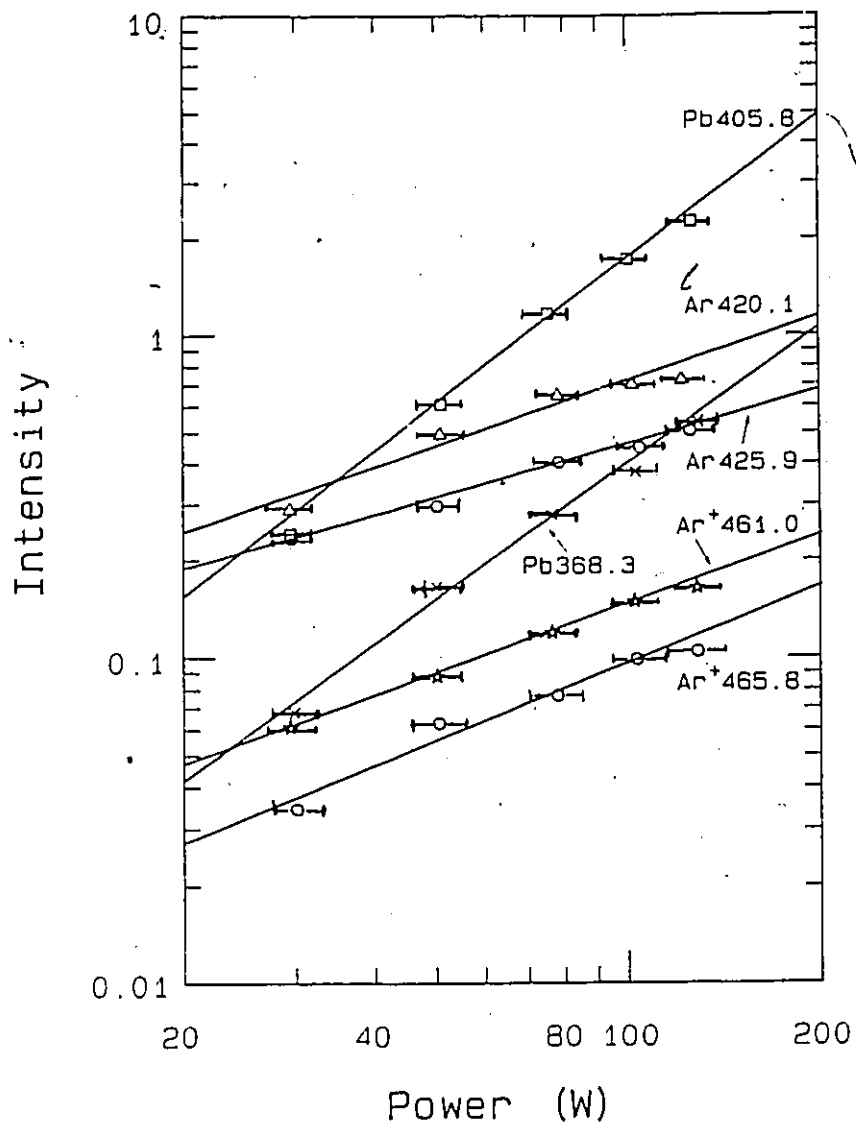


Figure 3.1: The power dependence of some Pb, Ar, and Ar⁺ emission intensities at a gas pressure of 0.068 Pa.

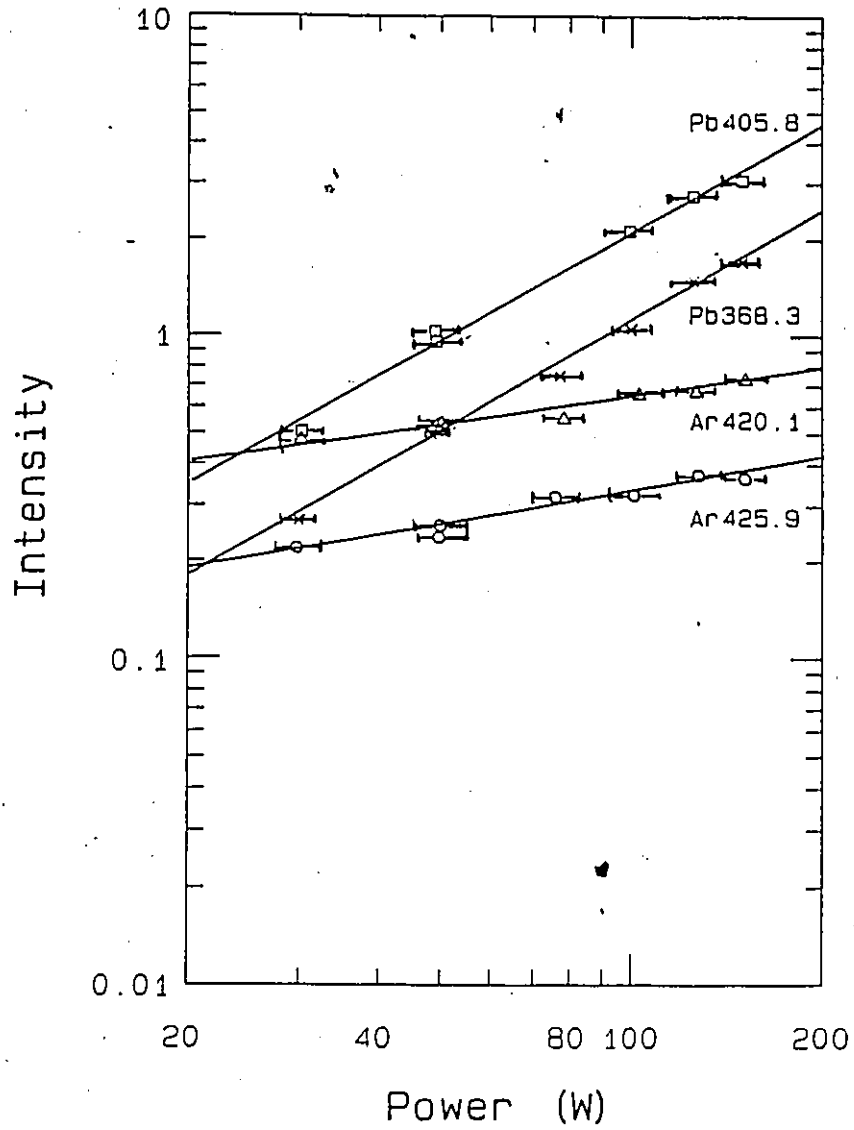


Figure 3.2: The power dependence of intense Pb and Ar lines at a pressure of 5.3 Pa.

Pressure (Pa)	Negative Glow			Positive Column			Deposition Rate
	Pb	Ar	Ar ⁺	n(Pb)-n(Ar)	Pb	Ar	
0.060	1.55±.13	0.61±.03	0.70±.08	0.94	1.48±.13	0.56±.16	0.92
0.53	1.51±.09	0.41±.05		1.1	1.46±.07	0.42±.07	1.0
5.3	1.09±.07	0.34±.03		0.75	1.40±.14	0.96±.05	0.44

Table 3.1: The function W^n , where W is the rf power, was fit to the data for emission intensities and deposition rate versus power. The error limits for the intensity n values represent the scatter in the separate values for the various Pb and Ar emission lines. The uncertainty limits for the rate are due to the scatter in the original data.

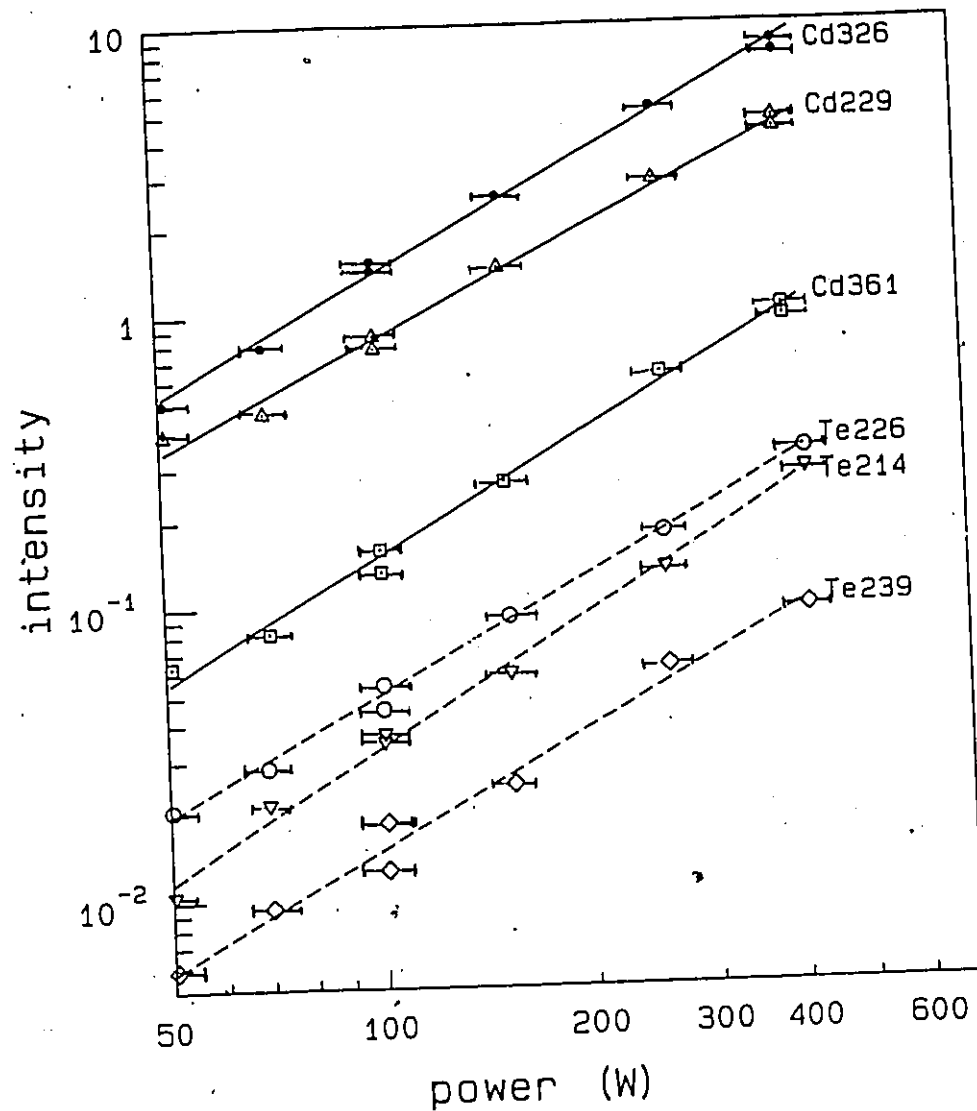


Figure 3.3: The intensity of strong Cd and Te atomic lines for the negative glow, in relative units, as a function of rf power. The pressure was 0.5 Pa.

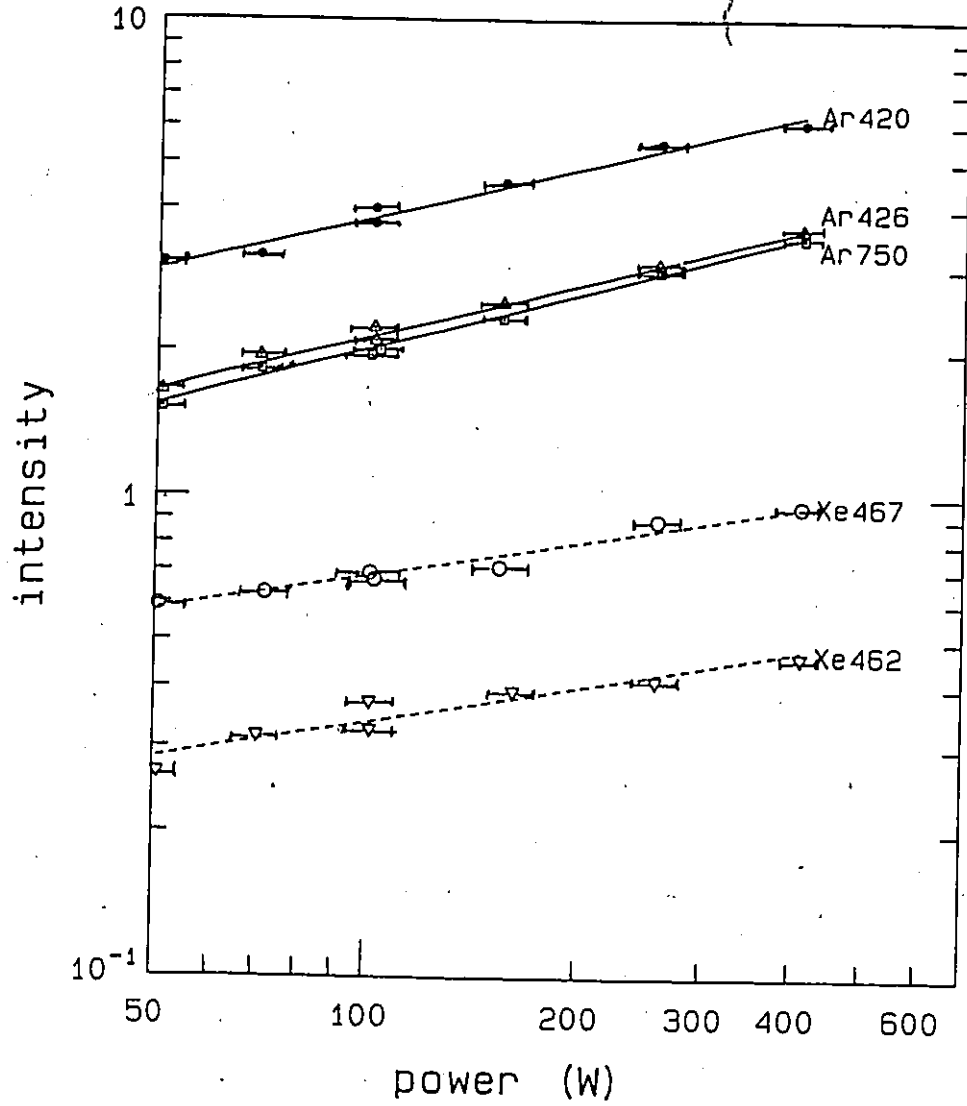


Figure 3.4: The intensity of some Ar and Xe atomic lines for the negative glow as a function of rf power; the total pressure was 0.5 Pa.

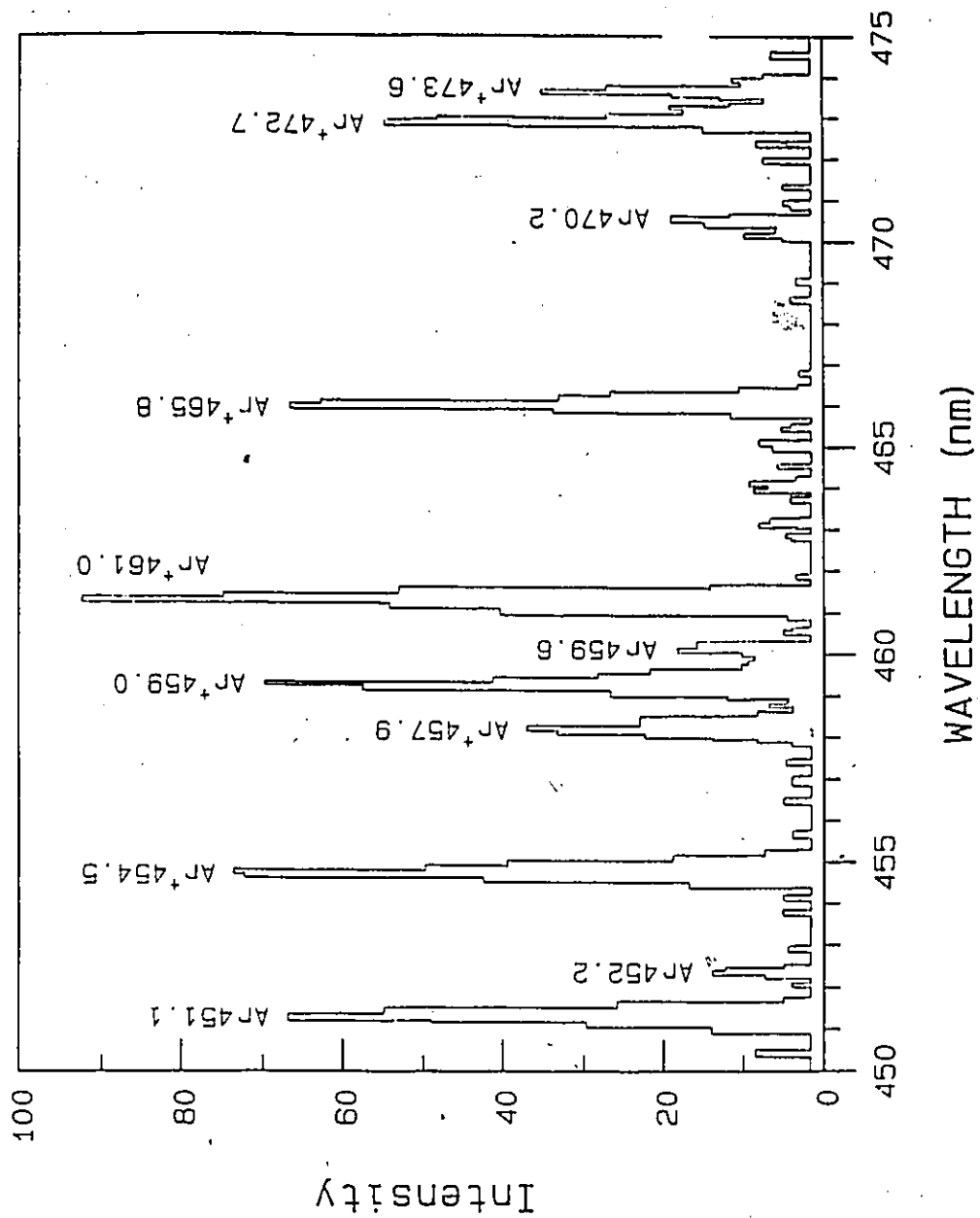


Figure 3.5: Part of the spectrum observed near the target at 50 W, 0.068 Pa. The smaller peaks are largely noise.

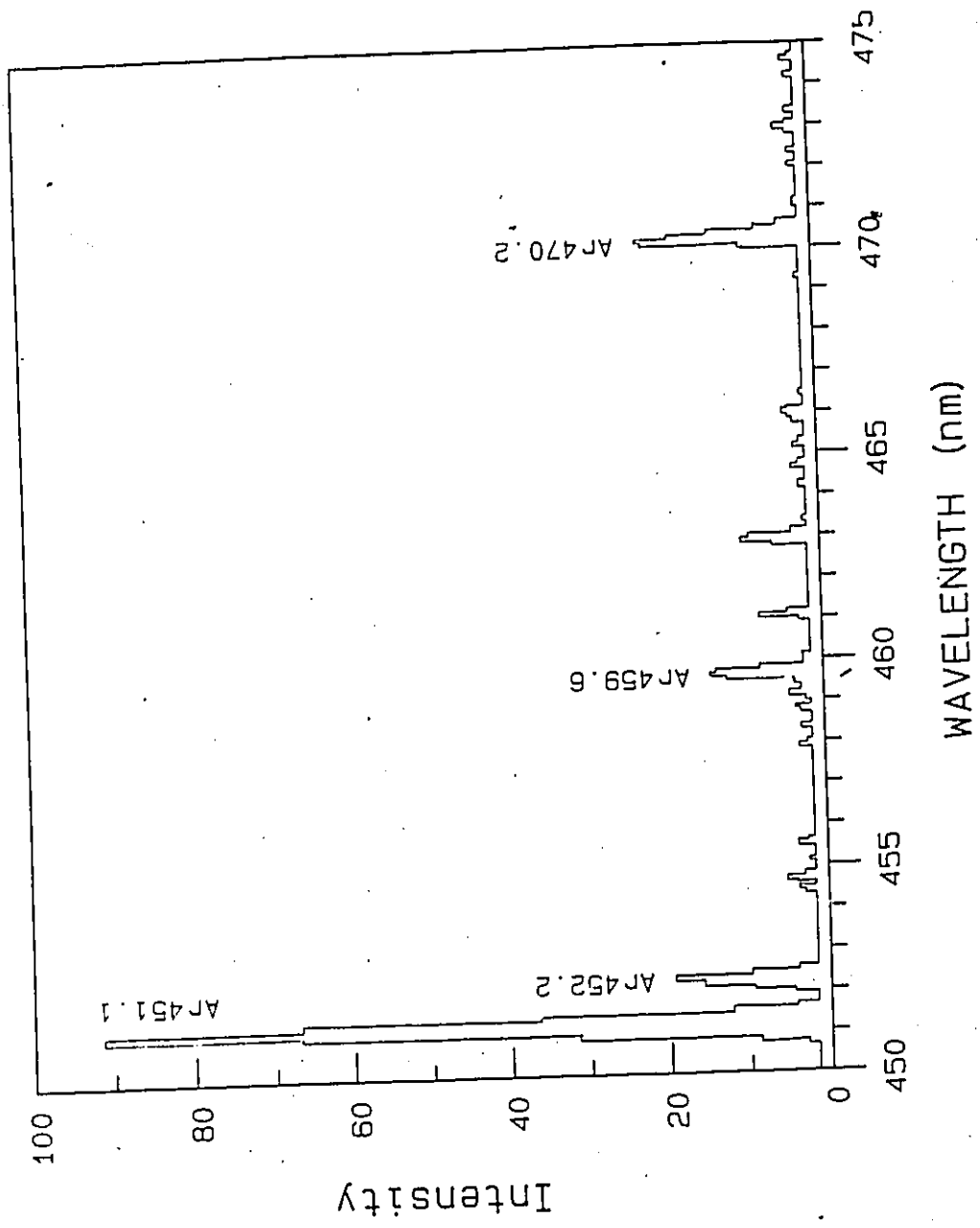


Figure 3.6: Part of the spectrum measured near the target at 50 W, 0.5 Pa. The intensities are in relative units, which differ from those of fig. 3.5.

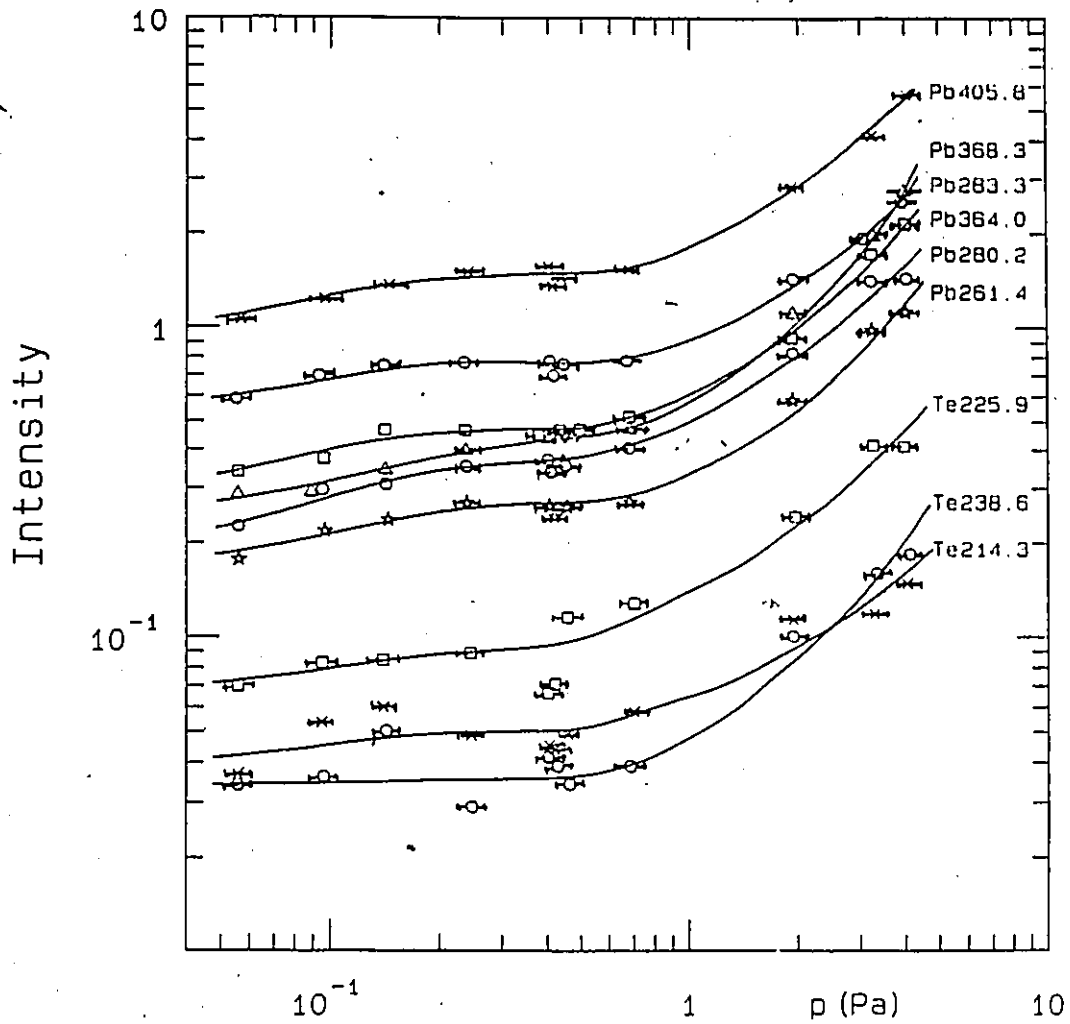


Figure 3.7: Pb and Te emission intensities as a function of gas pressure at 50 W rf power.

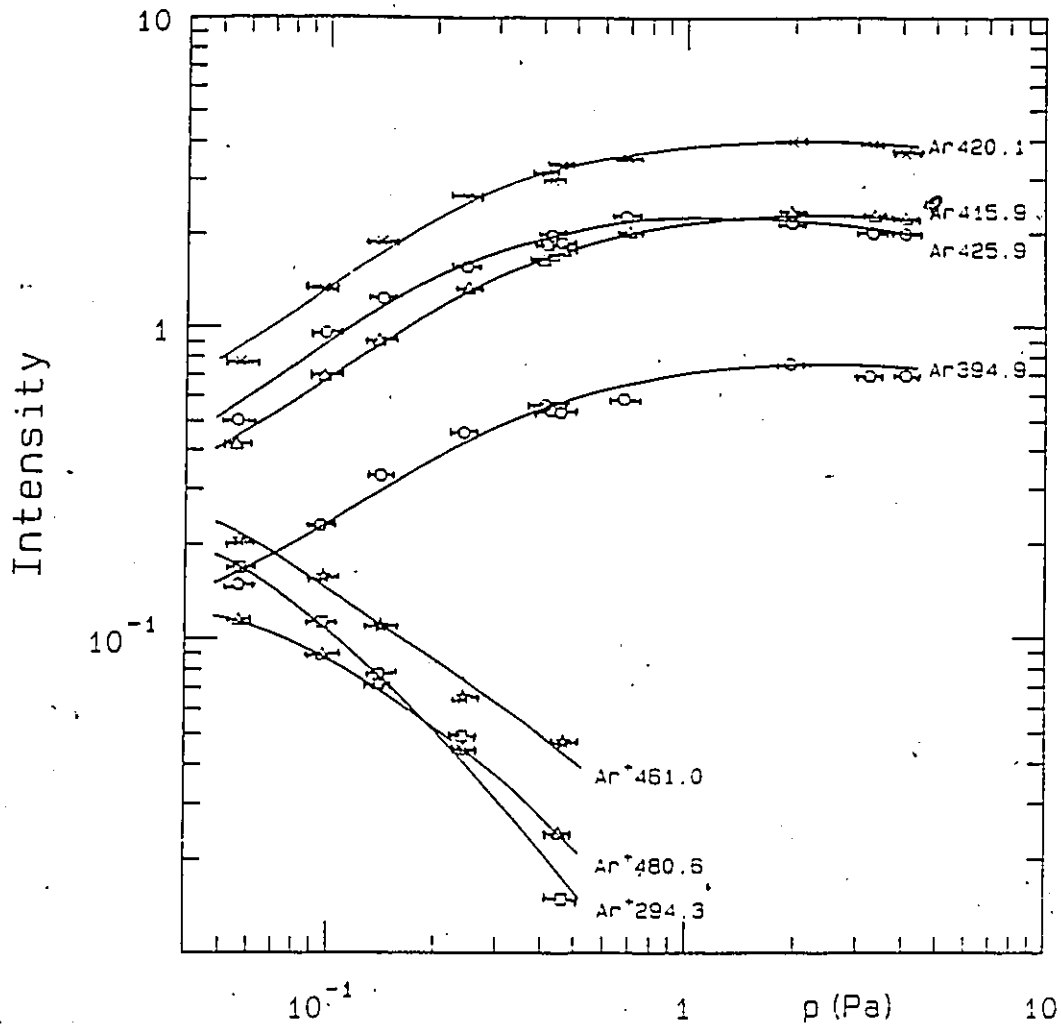


Figure 3.8: Emission intensities for neutral and singly-ionized Ar as a function of gas pressure at 50 W.

curves in that there is less line-to-line variation, even among the Te lines, which are common to the two cases. The Ar curves do not show the downturn at high pressures observed in the CdTe discharge (fig. 3.10); possibly because the present data were obtained on a new target which had not as yet been eroded.

The intensities were also measured as a function of gas pressure while the rf power was adjusted so as to keep the target self-bias voltage V_{SB} constant. For $V_{SB} = -90V$, which at most pressures corresponds to rf power levels near 50 W, the intensities for the sputtered species were less sensitive to gas pressure than for constant power conditions, except for a sharp drop in intensity at low pressures, just above extinction, where V_{SB} rises sharply with pressure [44,46]. There, the power had to be reduced to keep V_{SB} constant, with a consequent drop in intensities.

The deposition rate was determined as a function of rf power between 40 W and 125 W for various gas pressures. It also was found to vary as W^n , with $n \approx 1$ and increasing only slightly with pressure as the latter increased by nearly two orders of magnitude (table 3.1).

Emission intensities near the target and the substrate were also examined while a bias voltage was applied to the substrate. By adjusting the total power and the tuning capacitors between the two electrodes (target and substrate) and their common power source, the substrate self-bias voltage V'_{SB} could be varied while keeping either the target power or the target voltage V_{SB} constant. The results were rather complex and difficult to interpret, so not all the data are shown here. Generally, the Ar intensities increased faster with substrate bias than did the sputtered atom intensi-

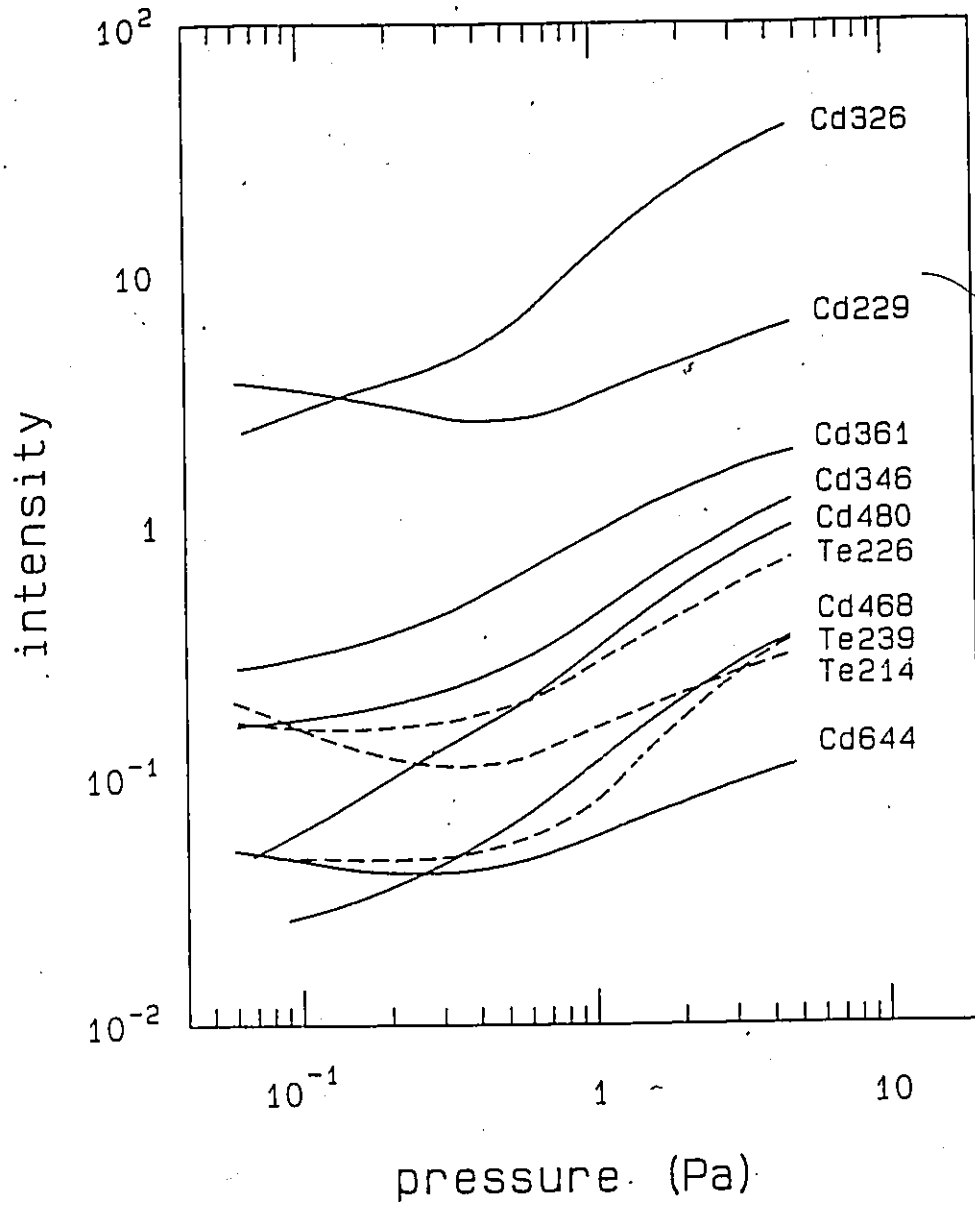


Figure 3.9: Intensities for some Cd and Te lines observed in the negative glow as a function of the total gas pressure. For the sake of clarity, data points are not shown. The rf power level was 100 W.

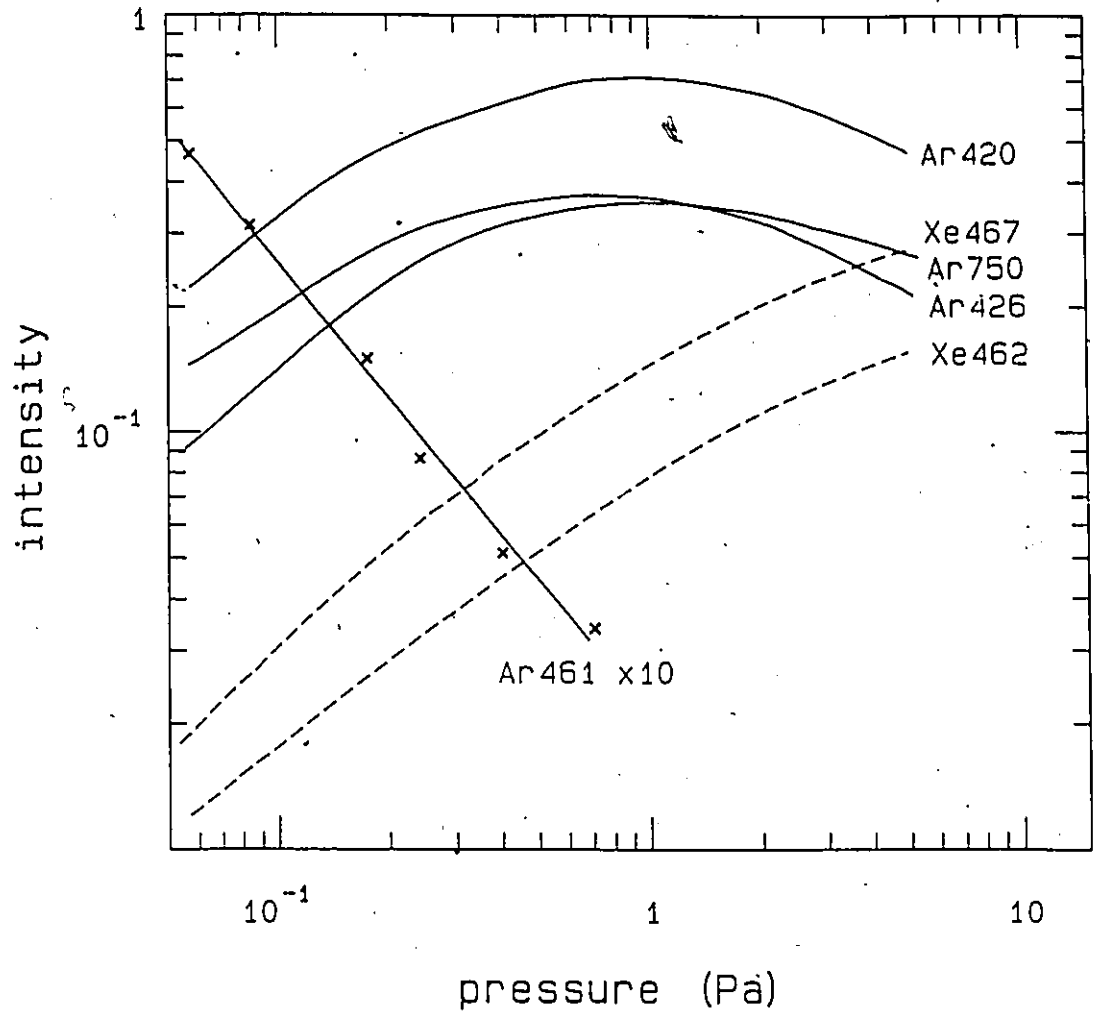


Figure 3.10: The variation of strong Ar and Xe lines in the negative glow with the total gas pressure. The rf power was 100 W.

ties. In fig. 3.11 is shown some Pb and Ar intensities at the substrate as a function of V'_{SB} at $V_{SB} = -90V$. Under these conditions, the Ar intensities increased much faster than those of Pb; the difference is approximately a factor of three. No evidence for Ar^+ lines was observed, even at the highest substrate voltages. The variation of I_{Pb} and I_{Ar} with V'_{SB} near the target was similar to that of fig. 3.11, except that the increase with V'_{SB} was not as marked.

3.3 Discussion

From eq. 3.1 applied to the present discharge it follows that

$$\frac{I_{Pb}}{I_{Ar}} = \frac{K_{Pb} N_{Pb} \eta_{Pb}}{K_{Ar} N_{Ar} \eta_{Ar}} \quad (3.2)$$

As stated in section 3.1, $\eta_{Pb} = \int n_e(E) \sigma_{Pb}(E) dE$. If the electron temperature, which is a measure of the average electron kinetic energy in a Maxwell-Boltzmann distribution represented by $n_e(E)$, and hence η_{Pb}/η_{Ar} are not sensitive to such a system operating parameter as the rf power or gas pressure, then as that parameter varies the sputtered atom density N_{Pb} is linearly related to the ratio I_{Pb}/I_{Ar} . It has been noted above that for the CdTe discharge such a relationship was found to be valid for changes in rf power, but not for pressure changes.

Consider first the present data obtained for varying rf power levels. It follows from table 3.1 that in both the negative glow and in the positive column, at pressures as high as 0.5 Pa, the power dependence of the left-

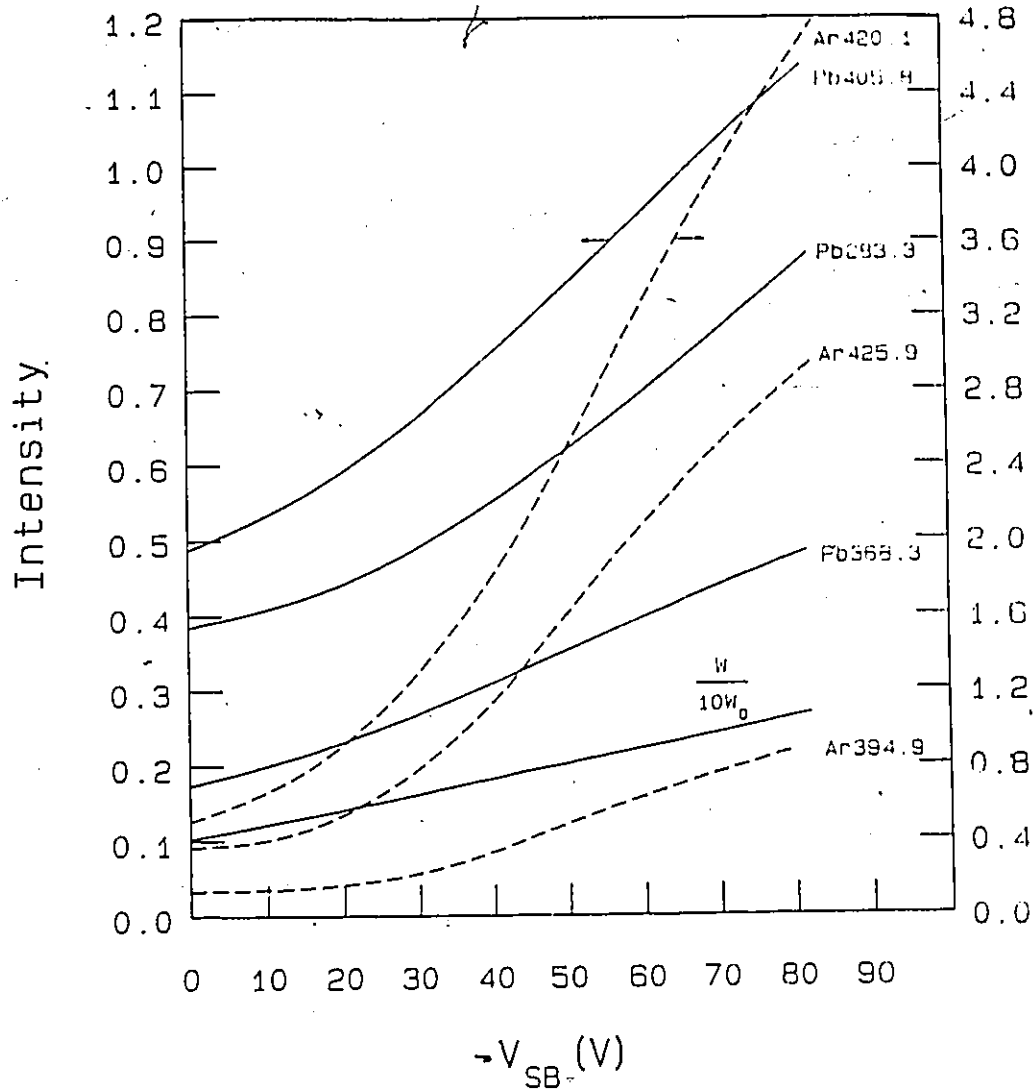


Figure 3.11: Some emission intensities near the substrate for varying self-bias voltage on the substrate. The target self-bias voltage was -90 V, and the gas pressure was 0.5 Pa. The power W required to achieve these conditions is given normalised on its value at $V'_{SB} = 0V$ (left axis).

hand side of the above equation varies approximately linearly with power. At the target, the peak of the energy distribution of the sputtered atoms is insensitive to the energy of the incident Ar ions and to the rf power level. At low pressures, transport of these atoms to the substrate will be by drift, so that the power dependence of N_{Pb} will be equal to that of the sputtering rate, which, again from table 3.1, is close to linear. It follows that at these pressures the power dependence of η_{Pb}/η_{Ar} will be relatively weak; the electron temperature is not sensitive to power.

As the pressure increases the sputtered atoms begin to collide more frequently with gas atoms, their initial energies are reduced, and their movement to the substrate becomes diffusive. A recent experimental study of a magnetron discharge [48] suggests that energy loss of the sputtered atoms becomes serious at a distance of approximately 5 mean free paths. At 0.7 Pa, the mean free path of Pb atoms in Ar is of the order of 1 cm, while the target to substrate distance in the present apparatus is 5 cm, so that the power dependence of N_{Pb} may be approximated by that of the deposition rate at pressures up to 0.7 Pa, but not at higher pressures. Indeed, table 3.1 shows that at 5 Pa the power dependence of the deposition rate is quite different from that of I_{Pb}/I_{Ar} . At this pressure the transport of Pb atoms to the substrate will be diffusive, and the deposition rate is proportional not to N_{Pb} near the substrate, but to the spatial gradient of this quantity. No conclusion can therefore be reached regarding the power dependence of the electron temperature on rf power at these higher pressures, and N_{Pb} need not be simply related to I_{Pb}/I_{Ar} .

For the CdTe discharge further evidence for the validity of the

actinometry approximation ($N_x \propto I_x/I_{Ar}$) as the power was varied, was obtained from a plot of n against the energy of the Cd emitting states, which varied from 3.8 eV to 8.1 eV. It was found that n was insensitive to this energy, which implied that the electron temperature was insensitive to power variations. In the present instance the variation in the energy of the emitting states of Pb is rather less [49], from 4.37 eV (the lines at for instance 283.3, 364.0 and 405.8 nm) to 5.7 eV (261.4 nm), so that such arguments are not conclusive.

In the previous analysis of the CdTe discharge an observed near square-root dependence of I_{Ar} on W and a linear dependence of I_{Ar} on W/V_{SB} was shown to indicate that Ar atoms in this discharge at 0.5 Pa are excited to short-lived, emitting states by single electron-atom collisions. The assumption of the predominance of such collisions is basic to eq. 3.2 above. In the present case, at both the 0.07 Pa and 0.5 Pa, n for I_{Ar} is less than 0.5 and plots of I_{Ar} against W/V_{SB} are linear, so that the same conclusion is suggested. At 5 Pa, however, n for I_{Ar} as measured near the substrate is close to unity (table 3.1) and plots of I_{Ar} intensities against W/V_{SB} are no longer clearly linear. Thus, at these high pressures metastable Ar ions may be influencing the optical properties of the discharge. A more detailed study of the spectra and sputtered atom transport at such pressures is therefore required.

Consider now the pressure dependence of the emission intensities and the ratio η_{Pb}/η_{Ar} . For reasons given above, one may expect that the ratio of N_{Pb} to the sputtering rate will be insensitive to pressure for pressures from 0.07 Pa to 0.5 Pa. The latter was found to change by only 10% or so

over this pressure range, so N_{Pb} may be taken to be pressure independent. The pressure dependencies of both I_{Pb} and I_{Ar} are not line sensitive (fig. 3.7, 3.8); inserting typical values of these quantities into equation (3.2), one finds η_{Pb}/η_{Ar} to increase by a factor of approximately four as the pressure increases from 0.07 Pa to 0.5 Pa. Since η is an integral of the product of the electron energy distribution and the relevant cross-section, this implies a decrease in electron temperature as the pressure increases. Additional evidence for such behaviour is provided by the sharp decrease in the ratio of Ar^+ intensities to neutral Ar intensities as the pressure is increased (fig. 3.8). Thus, η_{Pb}/η_{Ar} is pressure sensitive and the pressure dependence of N_{Pb} differs from that of I_{Pb}/I_{Ar} .

In the previous CdTe studies, a corresponding conclusion was reached, based in part on the large line-to-line variations in the pressure dependencies of I_{Cd} and I_{Te} . Such a variation is not observed with I_{Pb} and I_{Te} in the present case. This must be due in part to the smaller range of Pb excited state energies which has been noted above.

Finally, we turn to the intensities observed for varying substrate self-bias voltage V_{sb} . As a rule, when films are grown for varying V'_{sb} , a phenomenological approach is used, in that a series of films is grown for varying ratios of V'_{sb} to target voltage V_{sb} , and relationships are sought between this ratio and the properties of the film deposited. Little is known about the intrinsic parameters of that portion of the discharge adjacent to the substrate and their effect on film growth.

Fig. 3.11 indicates that for constant V_{sb} and 0.5 Pa, the Ar intensities rise much faster with V'_{sb} than do the Pb intensities. This would appear

to indicate that the electron temperature near the substrate increases with substrate power, which is quite different from the behaviour observed at this pressure with power applied only to the magnetron target. Such a shift of the electron distribution to higher energies would increase the Ar^+ density and thus influence film growth, which is quite sensitive to the bombardment of such ions.

These spectra are however difficult to interpret. It has been mentioned that also near the target, the Pb intensities were observed to increase with V'_{sb} . Energetic electrons will be produced near the substrate, and, not being confined by a magnetic field, will excite Pb atoms and produce Ar ions in the negative glow. The latter will influence the sputter removal rate even though V_{sb} is kept constant. Both effects should increase I_{Pb} , so that, again, one would conclude the observed increase of I_{Ar}/I_{Pb} with V'_{sb} signals a rise in electron temperature.

The complexity of this situation and the importance of V'_{sb} to film growth call for a more detailed study. In such work, the power applied to the target substrate should be monitored separately, resputtering at the substrate should be accounted for, and the use of more direct probes for the atomic densities and the electron temperatures should be considered.

3.4 Summary

An rf magnetron discharge used to sputter deposit PbTe in Ar has been studied using emission spectroscopy. A number of intense Pb I and Ar I

lines are identified, and their dependence on rf power and gas pressure determined.

From pressures near 0.07 Pa, which is close to the extinction pressure, up to 5.3 Pa, the stronger Pb and Ar line intensities, both near the target and near the substrate, vary with rf power (W) as W^n . The values of n are not line sensitive, and, in averaged form, are given in table 3.1.

The deposition rate at these pressures also varies as W^n . For pressures up to and including 0.5 Pa, which is a common sputtering pressure, it follows from an identification of the power dependence of this rate with that of the sputtered atom density N_{Pb} that the latter is given by the ratio I_{Pb}/I_{Ar} . Thus, the electron temperature is independent of rf power at these pressures. For higher pressures, the Pb atoms become strongly scattered by the Ar atoms, and their transport becomes diffusive; no conclusions on the dependence of the electron temperature on rf power can be reached.


It is seen from the dependence of I_{Ar} on W and on W/V_{SB} that below 0.5 Pa the excitation of Ar atoms occurs by single electron-Ar scattering events. At higher pressures, the influence of metastable Ar atoms could not be ruled out.

From the pressure dependencies of the Pb emission intensities and of the deposition rate, it is deduced that the electron temperature is pressure sensitive, so that N_{Pb} is not proportional to I_{Pb}/I_{Ar} while the pressure is varied.

The Pb and Ar line intensities near the substrate were determined for constant target self-bias voltage and increasing substrate voltage. The Ar intensities were observed to increase much faster than the Pb intensities

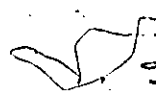


(fig. 3.11). This suggests that near the substrate, the electron energies and hence the number of Ar ions bombarding the substrate are very sensitive to the substrate voltage, but further work is required to study this important matter.



Chapter 4

Photoluminescence spectroscopy of epitaxial CdTe films

4.1 Photoluminescence in CdTe

Photoluminescence measurements (referred to as PL in this thesis) in II-VI compounds [50] can provide valuable information concerning the type and distribution of defects and impurities in a crystal and, hence, can be an important indicator of crystal quality. However, the interpretation of PL data in the II-VI compounds is not straightforward because of the variety of defects introduced by deviation from stoichiometry and their interaction

with one another and with foreign atoms. In order to interpret the PL spectra we will first mention briefly the salient characteristics of the various radiative transitions in CdTe described in section 1.7:

1. Band to band transition: For CdTe, the band to band line broadens and shifts to lower energy with increasing temperature [51]. In contrast, the peak position shifts to higher energies as the excitation intensity increases. This is due to the fact that states deeper in the band become filled, permitting emission at higher photon energies [40].
2. Exciton transitions: Since the exciton binding energy is much smaller than the band gap, the temperature dependence of the exciton emission follows the temperature dependence of the band gap [52]. With increasing temperature, excitons are difficult to observe by conventional measurements because of phonon broadening and screening by an increased free carrier density and lattice defects [52].
3. Donor-acceptor (D-A) transition [52]: (i) The emission line shifts to higher energies as the excitation intensity increases because of the saturation of the long-distance pairs with higher r values [53], the energy transition between an acceptor level and a donor level being given by eq. 1.16. (ii) Appreciable narrowing of the emission band occurs with increasing intensity. (iii) The band shifts towards higher energies as the donor concentration increases. (iv) The band intensity rapidly decreases as the temperature increases (from 25 to 35 K). (v)

A shift of the peak to higher energies occurs over the same temperature range as in (iv). This shift can be quite small for direct-gap semiconductors and for undoped materials.

However, conditions (ii) and (v) are not always fulfilled for D-A transitions. Kaminskii and Pokrovskii [54] examined this effect for double-doped Si. They noted that the form of the temperature dependence of $h\nu$ depends on whether E_a and E_d are comparable or are widely different. Thus for Si:Sb,B where $(E_d)_{Sb} = 36meV$, $(E_a)_B = 44meV$, the D-A spectral peaks narrowed and shifted to lower energy between 4.2 K and 30 K. In contrast, a broadening and shift to higher energy occurred between 4.2 K and 37 K for Si:Sb,Ga where $(E_a)_{Ga} = 65meV$.

4. Conduction band-acceptor (C.B.-A) or donor-valence band (D-V.B.) transition: Some of the above characteristics, 3(ii) and 3(iv) for instance, are common with a C.B.-A or a D-V.B. transition. For example, a shift of the line to higher energies is observed for these transitions as the excitation is increased, driving the quasi-fermi level for electrons deeper in the C.B., and the quasi-fermi level for holes deeper in the V.B. [40]. For a band to defect level transition, the peak position should follow almost the same trend as the band gap. However, at finite temperatures, emission-peak energy variation for a C.B.-A transition in GaAs as the temperature increases differs slightly from the band-gap variation determined by Sturge [55]. Also, the peak should broaden with increasing excitation intensity for a band to de-

fect center transition because of the effect on the quasi-fermi levels for holes or for electrons.

In this chapter, we present the results of the photoluminescence spectroscopy studies on a series of epitaxial rf magnetron sputter-deposited CdTe layers of varying thicknesses (up to $14 \mu m$) grown on freshly cleaved (100) KBr substrates in the deposition system described in chapter 2. These set of CdTe samples were grown at a substrate temperature of 325 degrees Celsius, an Ar pressure of 3.5 mtorr and an rf power of 50 W. No bias substrate was applied. The growth rate under the above conditions was $\approx 5.5 \text{ \AA/s}$.

Photoluminescence spectroscopy was carried out in the system described in section 2.5. On selected samples, detailed measurements of the temperature and excitation intensity dependence of the PL spectra were performed. For comparison, the PL spectra were also recorded for a CdTe bulk single crystal from II-VI Inc., a bulk polycrystalline CdTe wafer from II-VI Inc., a piece of the hot-pressed CdTe sputtering target, and a bulk single crystal CdTe wafer from Cominco.

4.2 Results

4.2.1 Structural properties of CdTe

Only the (200), (400) and (600) reflections were observed in the x-ray diffractometer scan of the CdTe layers, which indicated that the films had the same orientation as the (100) KBr substrate. Large area electron channeling patterns observed in the scanning electron microscope [56] confirmed the films to be monocrystalline over the entire area. A typical x-ray diffractometer scan for a CdTe layer is shown in fig. 4.1. Shown in the figure are the (200) and (400) reflections for the CdTe layer as well as the KBr substrate. It should be noted that while the $Cu_{K\alpha_1}$ and $Cu_{K\alpha_2}$ peaks for the (400) plane are well resolved for KBr, they are not for the CdTe layer. The peak width is generally used as an indicator of crystal structural quality. To compare the crystalline quality of the CdTe layers as a function of thickness, we used a computer fitting program to deconvolute the CdTe (400) peak as a sum of two Gaussians. The criterion is to minimize the sum of the squares of the errors. Two Gaussian curves were obtained from this deconvolution as illustrated in fig. 4.2 for sample HM29. These curves are due to the diffraction of the $K\alpha_1$ and $K\alpha_2$ radiation by the (400) CdTe plane and were quite broad. Fig. 4.3 shows the FWHM (full width at half maximum) of the (400) $K\alpha_1$ line (as determined from the fitting program) as a function of the CdTe layer thickness. The FWHM value decreased exponentially with increasing thickness.

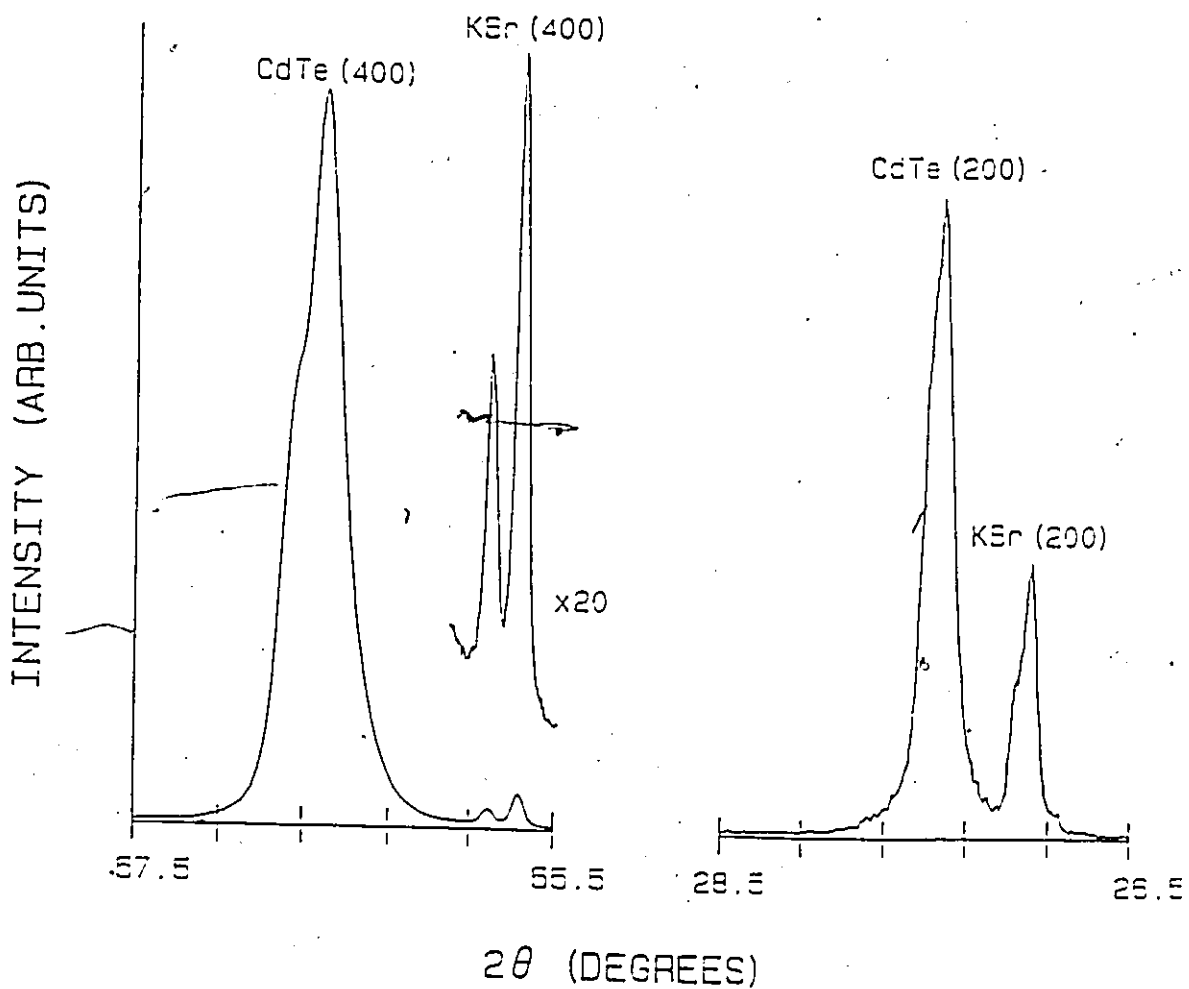


Figure 4.1: X-ray diffractometer scan of (200) and (400) reflections for (100)-oriented CdTe films grown on (100)-oriented KBr substrates. The corresponding reflections from the KBr substrate are also shown for comparison.

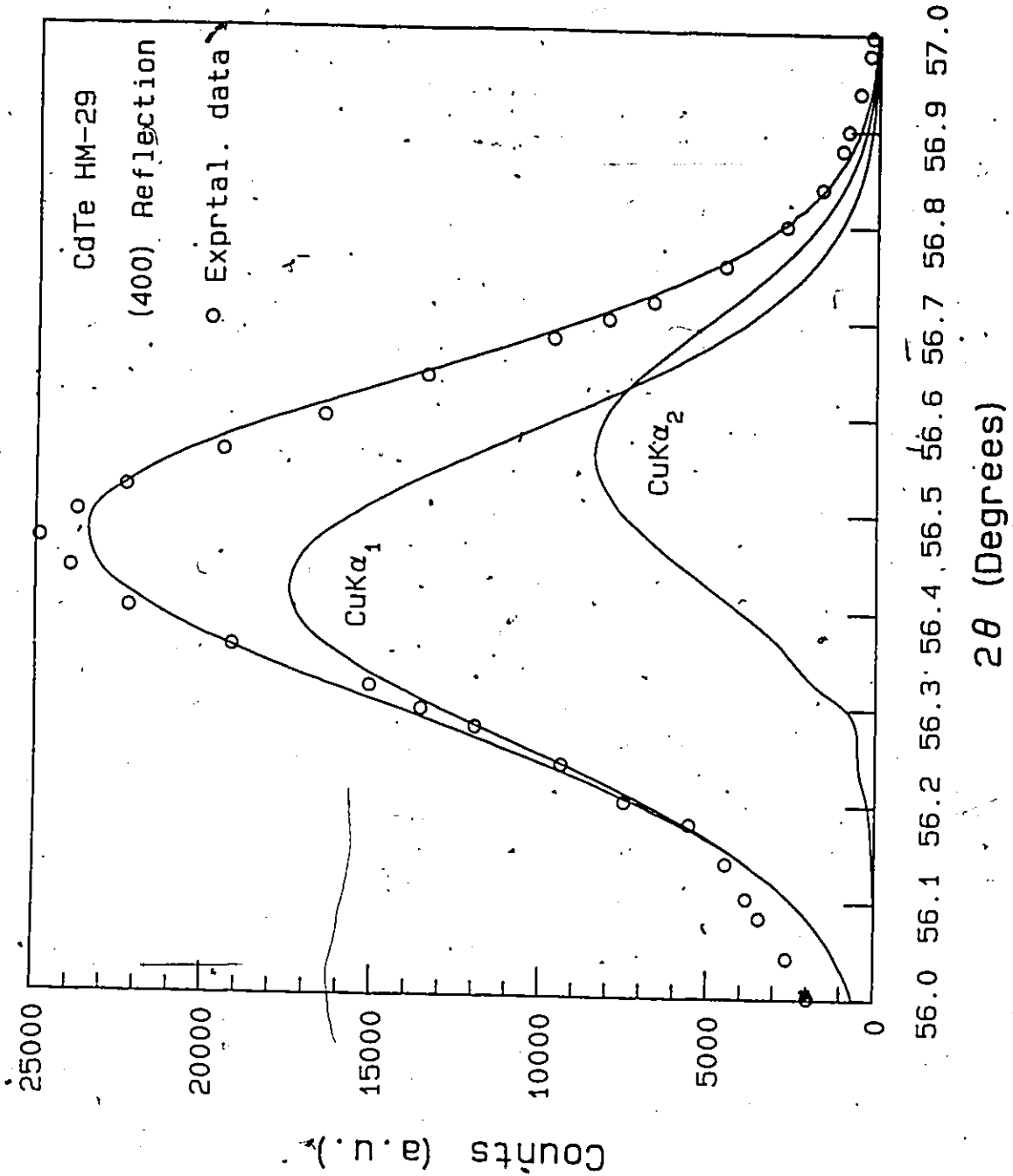


Figure 4.2: Deconvolution of the experimental (400) x-ray reflection peak for CdTe (sample HM29) grown on KBr (100) into two Gaussian peaks corresponding to $K\alpha_1$ and $K\alpha_2$ reflections.

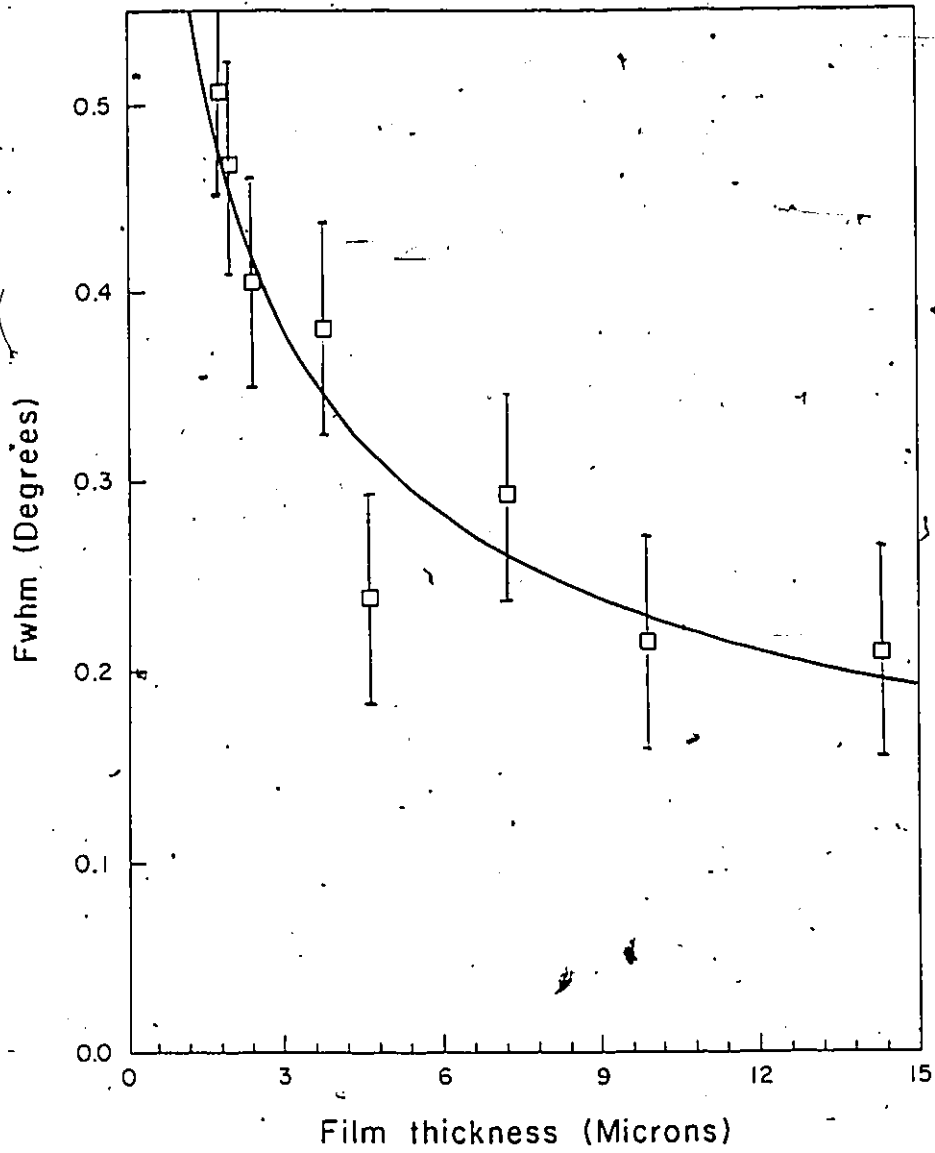


Figure 4.3: Thickness dependence of the FWHM of the (400) $K\alpha_1$ x-ray reflection for CdTe sputter-deposited layers.

4.2.2 PL spectra

PL spectra recorded at 4.2 K and at a laser excitation power of 100 mW were pretty much the same for the different film samples. A typical spectra is shown in fig. 4.4. The essential features are two broad bands centered at 1.00 eV and 1.42 eV. The latter peak has been reported by many workers [57]. However, this is the first time that a band centered at 1.0 eV has been reported in epitaxial CdTe layers. The only other report of PL bands in the 0.8-1.2 eV range is a very recent study on chemically etched bulk single crystal CdTe [58]. A fine structure was seen on the 1.00 eV broad band for two of our samples (HM32 and HM27). For HM32 these peaks were located at 0.81, 0.84, 0.86, 0.88, 0.90, 0.92, 0.94, 0.96, 0.98, 1.00, 1.03, 1.05, 1.07, and 1.09 eV whereas for HM27 these peaks were at 0.89, 0.92, 0.95, 0.97, and 1.00 eV. These peaks were power and temperature independent. No band edge peak nor excitonic peak were seen in the sputter-deposited films.

PL spectra for a CdTe bulk single crystal from II-VI Inc., a bulk polycrystalline CdTe wafer from II-VI Inc., a piece of the hot-pressed CdTe sputtering target, and a bulk-single crystal CdTe wafer from Cominco are shown in figs. 4.5-4.8. For all these samples, the band edge peak at 1.59 eV and excitonic peaks at 1.52, 1.54, 1.55, 1.57, and 1.59 eV were observed and were quite strong. The 1.42 eV peak was observed for the polycrystalline CdTe sample and the hot-pressed CdTe sputtering target, but not for the single crystal samples from II-VI Inc. and Cominco. No band in the 0.7-1.2 eV range was observed.

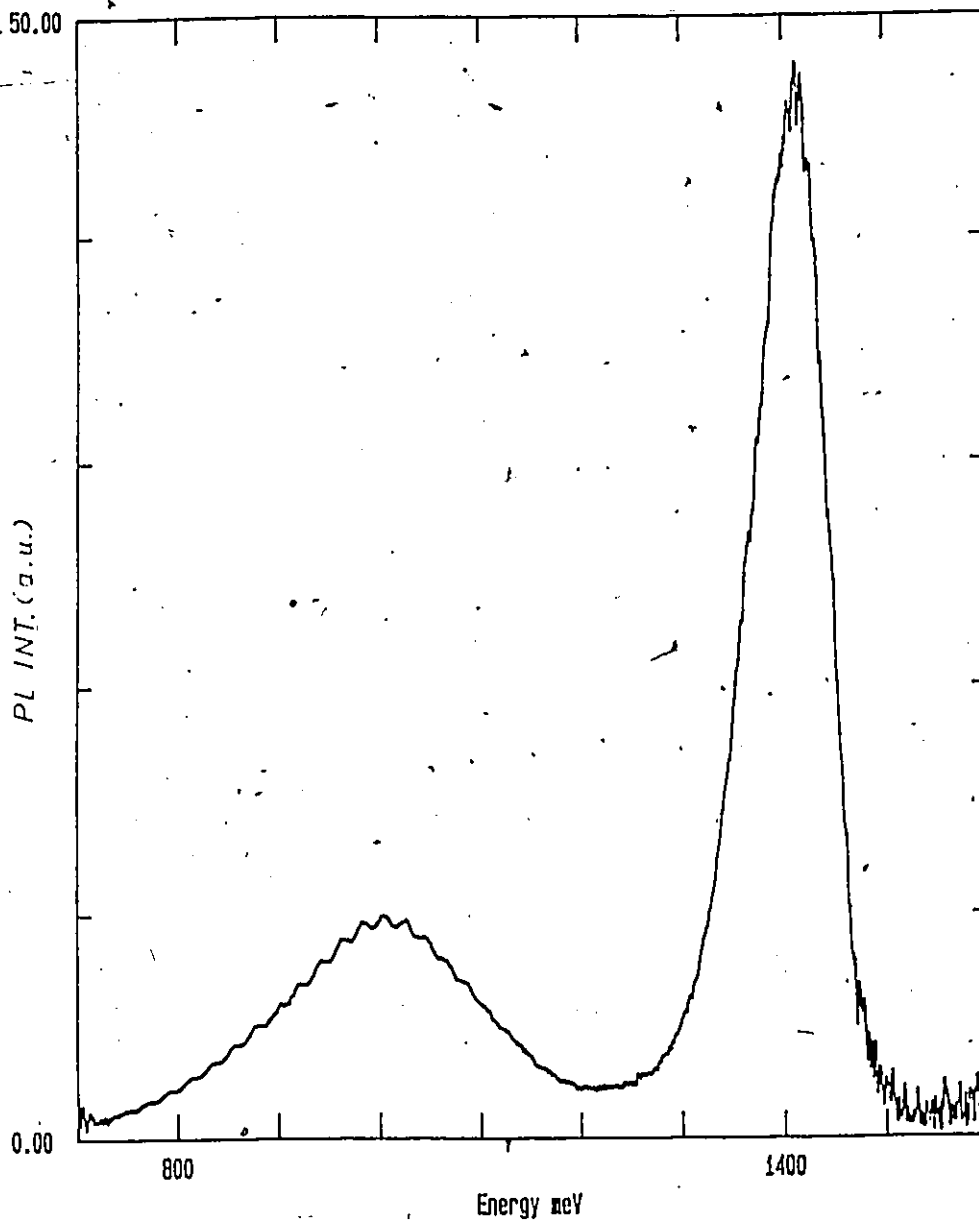


Figure 4.4: PL spectra at 4.2 K for a (100) oriented CdTe epilayer (HM32). The laser power was 100 mW.

However, after mechanically polishing the bulk samples and recording their PL spectra, a broad band in the 0.7-1.2 eV range emerged in addition to the peaks at 1.42 eV and the band edge peaks for all the samples. Fig. 4.9 is a PL spectra for the single-crystal from II-VI Inc. after polishing.

The 1.00 eV peak was deconvoluted using a computer least-square fitting program. We ended up with two Gaussians at 0.80 eV and 1.00 eV. For the lines at 0.80, 1.00, and 1.42 eV, the peak position, the height, and the FWHM were determined (directly from the computer plot for the peak at 1.42 eV and from the fitting program for the peaks at 0.80 eV and 1.00 eV). The experimental error on the peak position was 4 meV while it was double that for the FWHM. The FWHM of the 1.42 eV band agreed well with the FWHM reported in the literature [51].

4.2.3 Variation of PL with thickness

The three peak intensities were plotted against film thickness and were randomly scattered. The same conclusion was reached regarding the peak position. However, as shown in fig. 4.10, the FWHM of the 1.42 eV line decreased with thickness in a manner similar to that of the FWHM of the (400) x-ray diffraction peak. Both FWHM were plotted against each other and the result is shown in fig. 4.11.

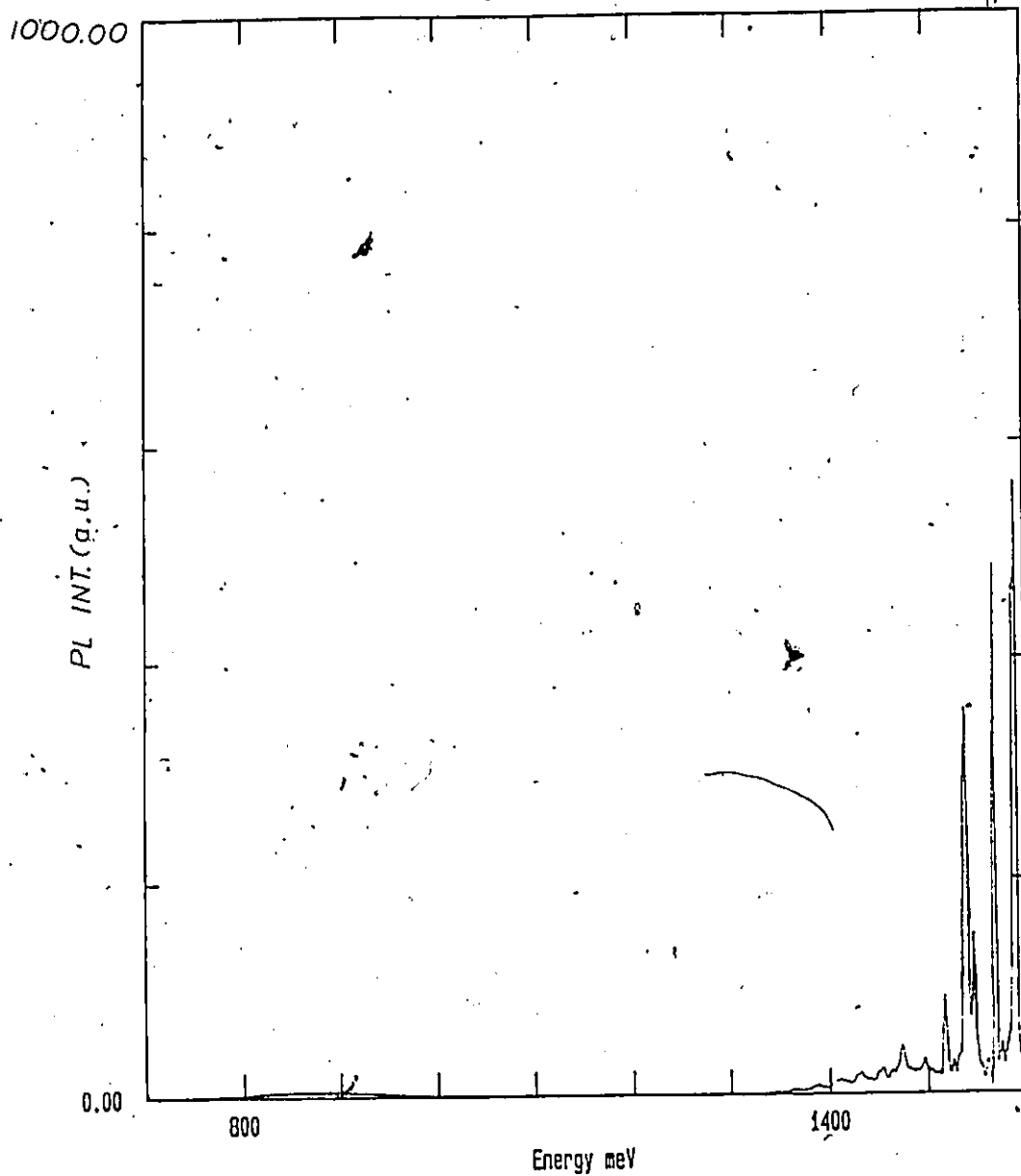


Figure 4.5: PL spectra at 4.2 K for a CdTe bulk single crystal from II-VI Inc.. The laser power was 100 mW.

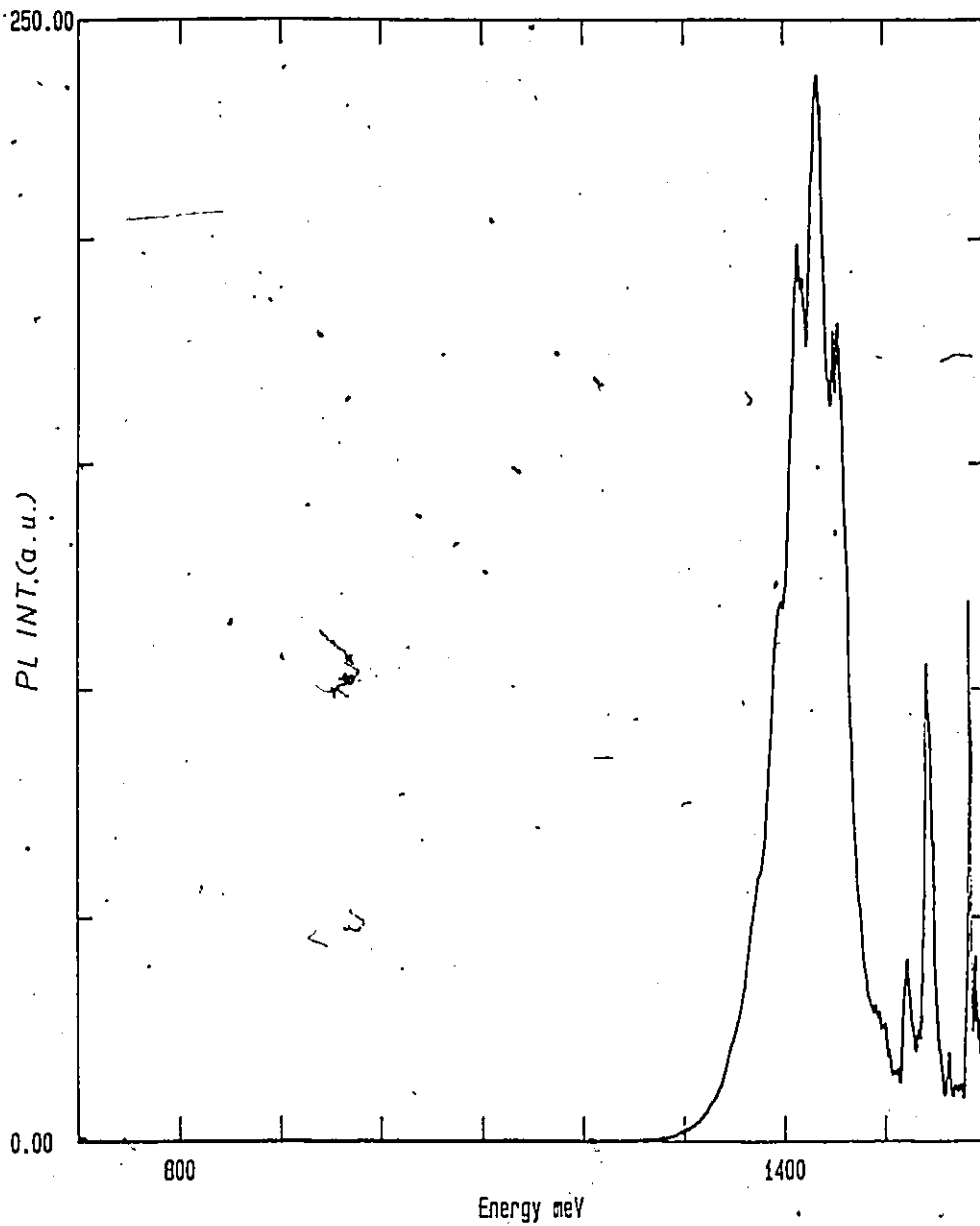


Figure 4.6: PL spectra at 4.2 K for a bulk polycrystalline CdTe wafer from II-VI Inc.. The laser power was 100 mW.

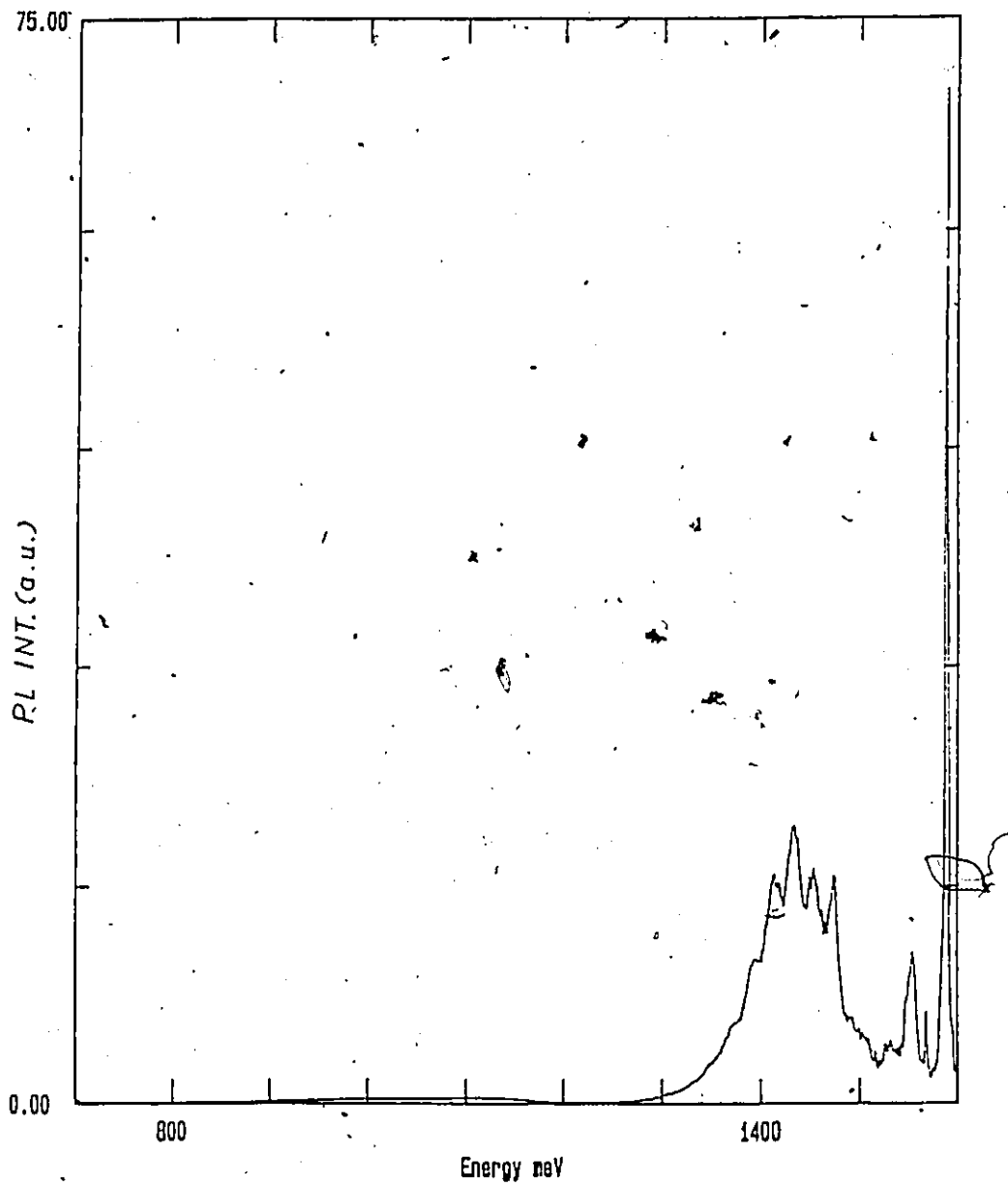


Figure 4.7: PL spectra at 4.2 K for the hot-pressed CdTe sputtering target. The laser power was 100 mW.

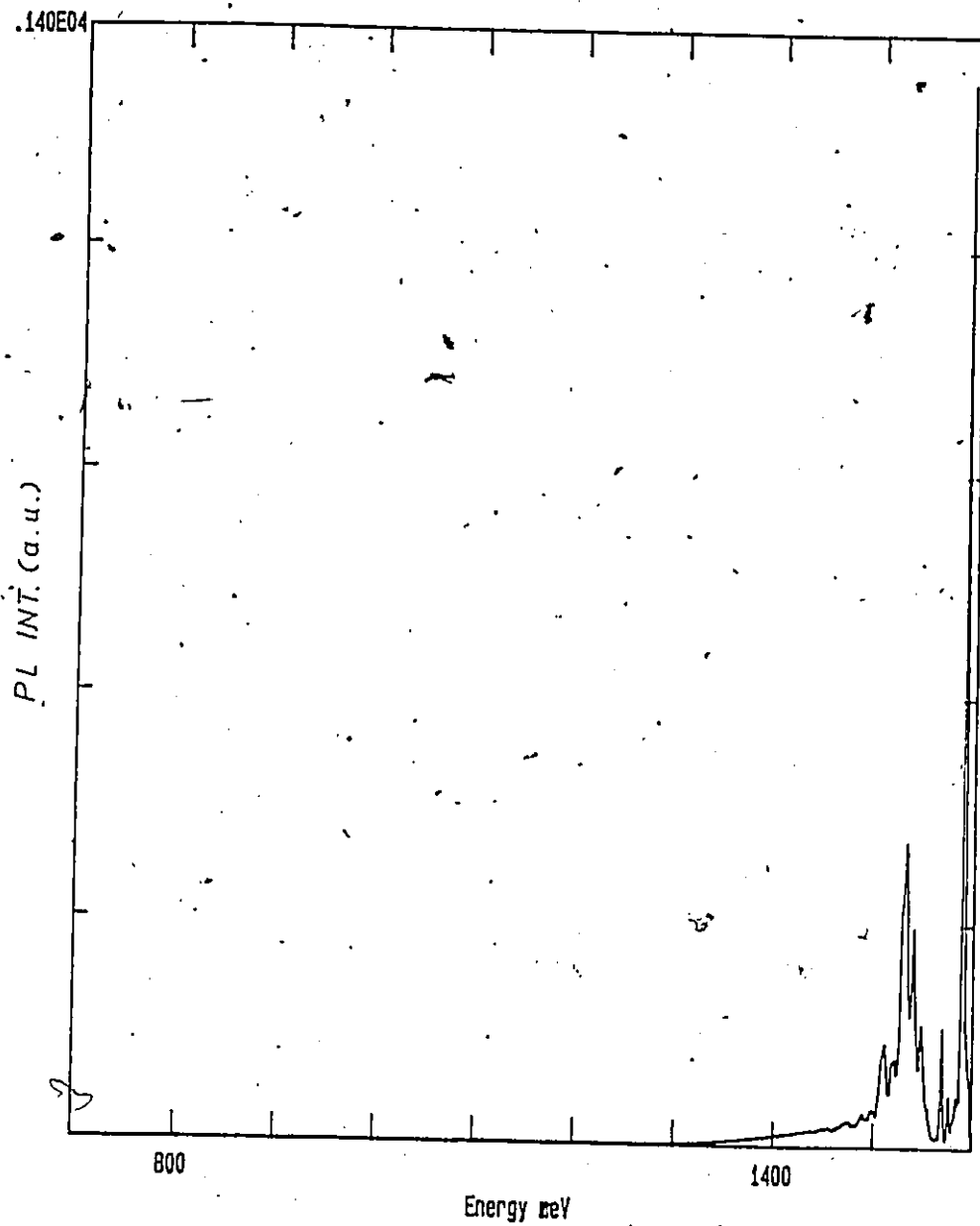


Figure 4.8: PL spectra at 4.2 K for a bulk single crystal CdTe wafer from Cominco. The laser power was 100 mW.

2

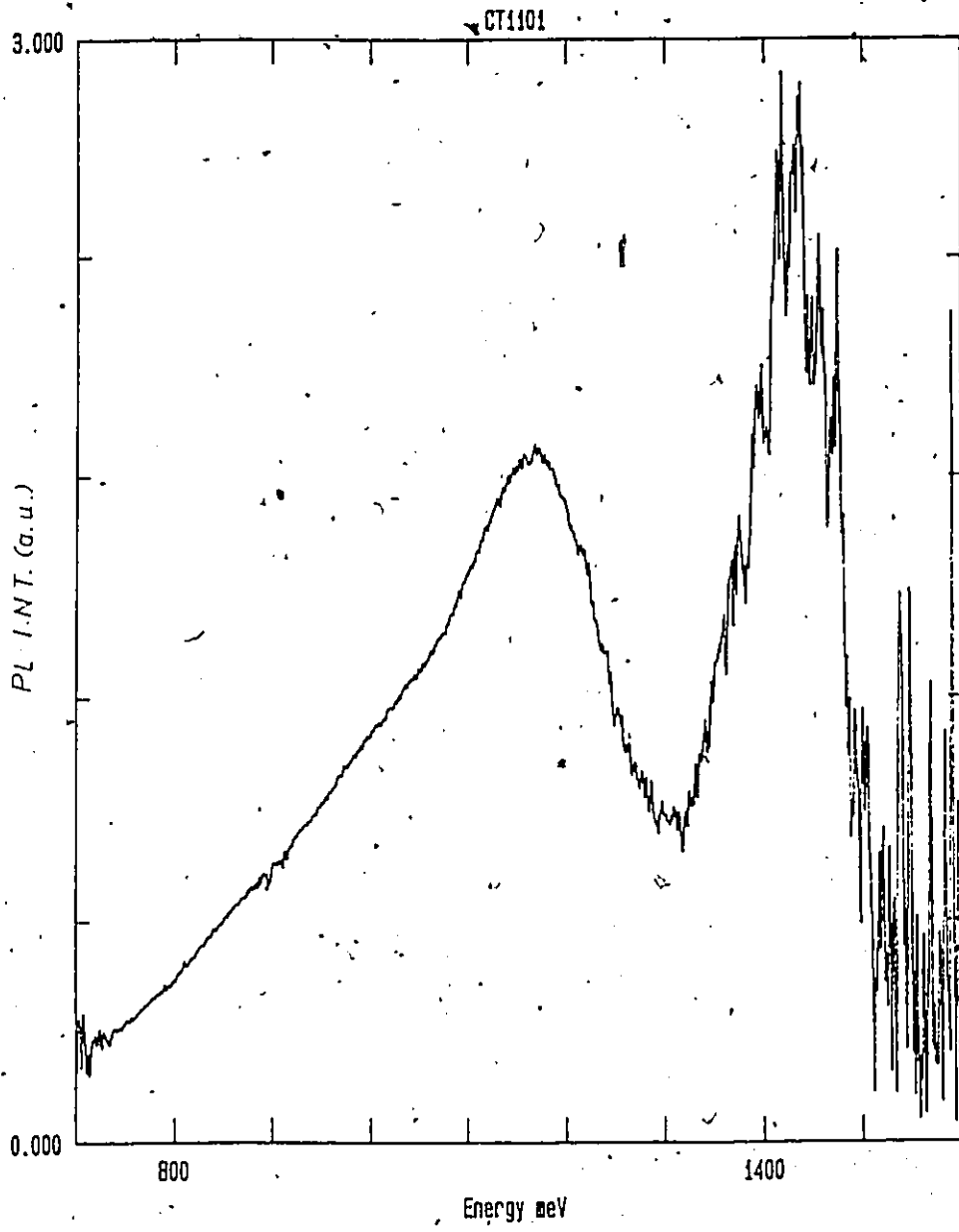


Figure 4.9: PL spectra at 4.2 K for a CdTe bulk single crystal from II-VI Inc. after mechanical polishing. The laser power was 100 mW.

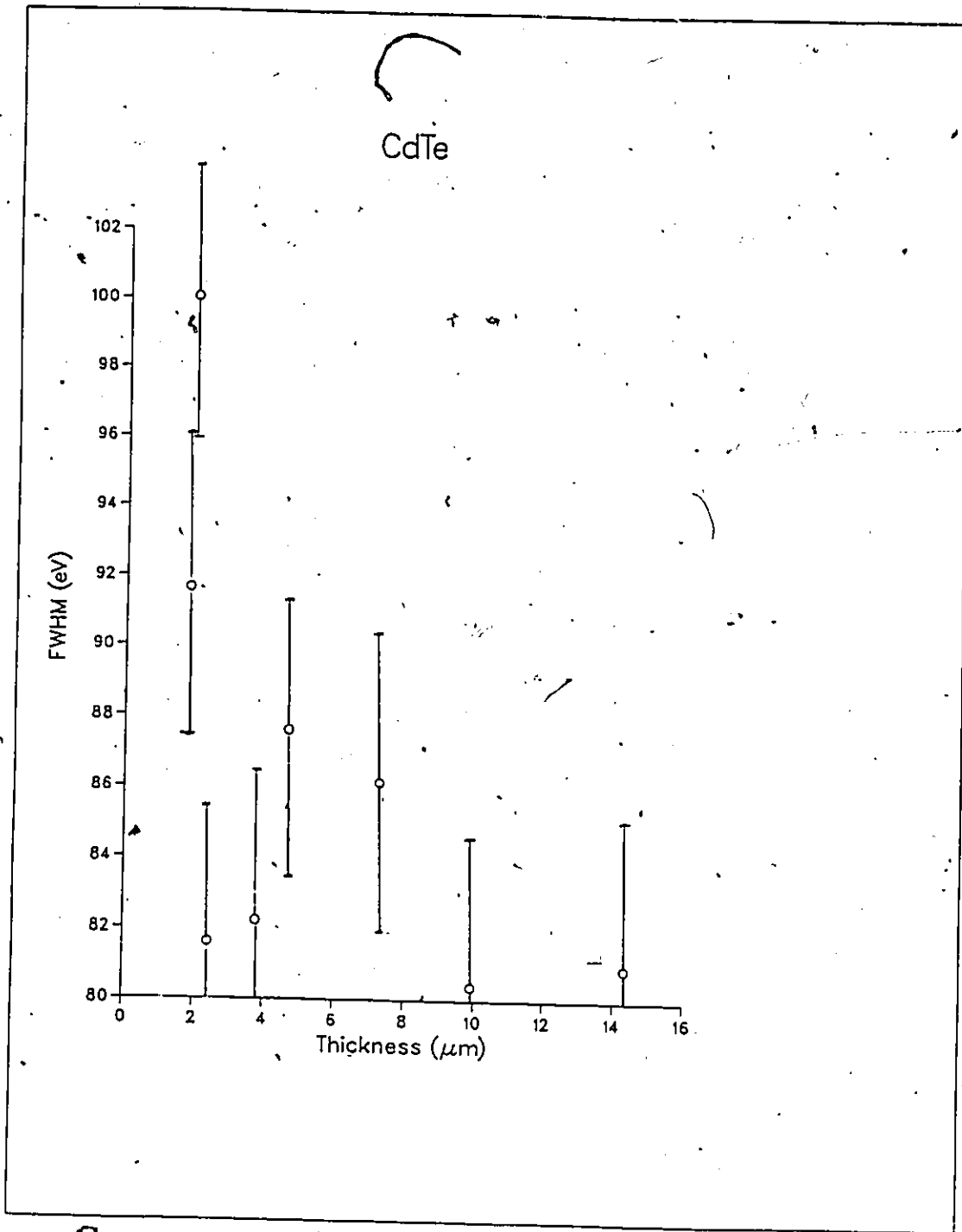


Figure 4.10: Thickness dependence of the FWHM of the 1.42 eV line for CdTe sputter-deposited layers.

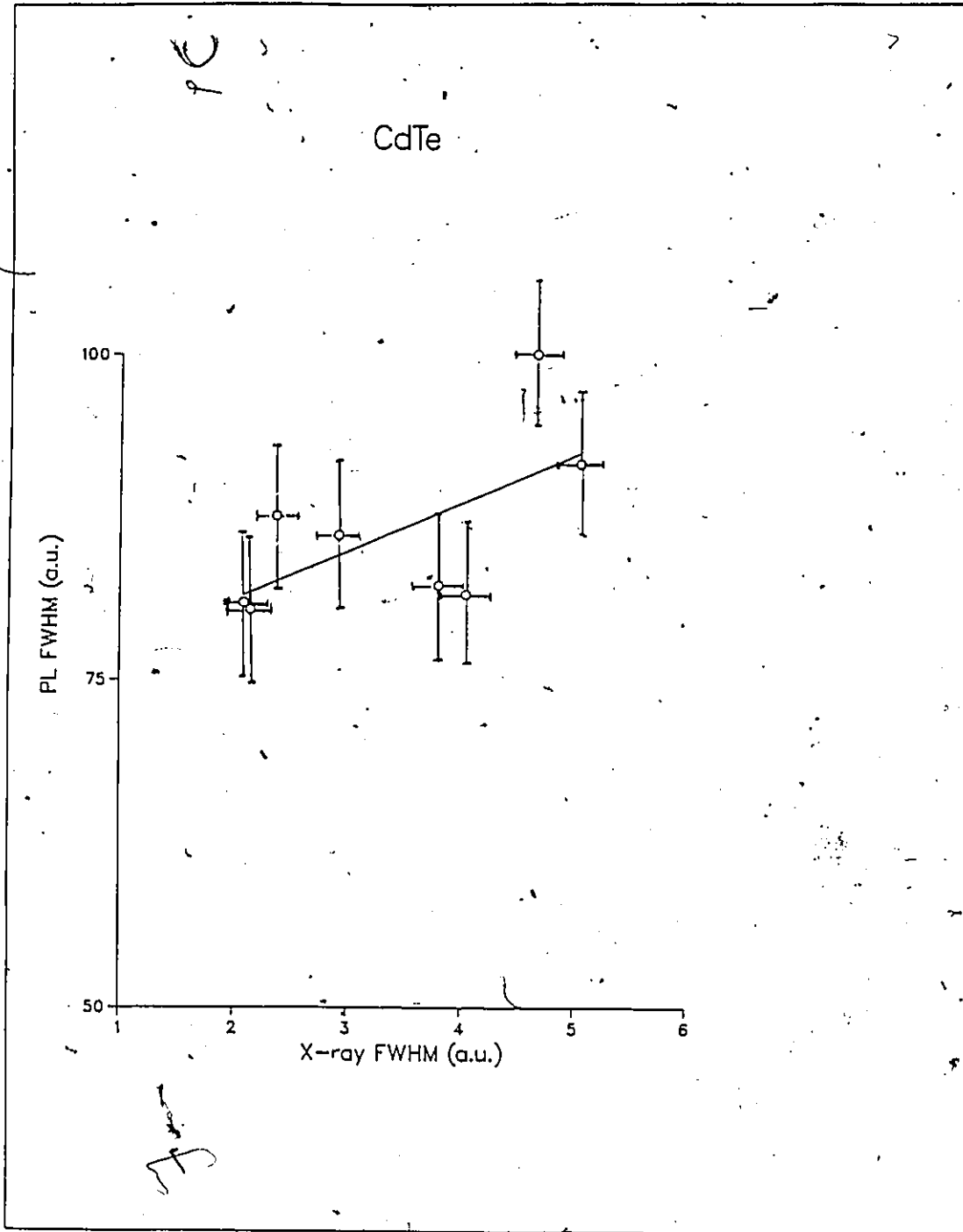


Figure 4.11: FWHM of the 1.42 eV PL line for CdTe sputter-deposited samples as a function of the corresponding FWHM of the (400) x-ray diffraction peak.

4.2.4 Variation of PL with laser power

The excitation intensity dependence of the PL spectra was studied for sample HM32. The laser power was varied up to 200 mW, while the film was held at liquid helium temperature. The general shape of the spectra did not change with incident power. As shown in fig. 4.12, the peak height of the 1.42 eV line had a linear variation with power, whereas the two other lines had a sublinear dependence on power ($I \propto W^{0.75}$). The three lines shifted slightly to higher energies with increasing laser power (fig. 4.13). However, their FWHM did not show any appreciable shift (fig. 4.14) although the 1.00 eV and 0.80 eV lines showed a tendency to decrease with power within the experimental error.

4.2.5 Variation of PL with temperature

The temperature dependence of the PL spectra for the same sample (HM32) was measured from liquid helium temperature up to 80 K at a constant laser power of 100 W. The peak intensity of the 1.00 eV and 1.42 eV lines decreased appreciably over this temperature range (fig. 4.15). For the 0.80 eV band, a slight decrease was noticed at higher temperatures. The peak position of the 0.8 eV line increased to higher energies with increasing temperature (fig. 4.16). In contrast, no shift was observed within the experimental error for the other lines, although a trend towards lower energies was observed for the 1.42 eV peak. The FWHM increased steadily

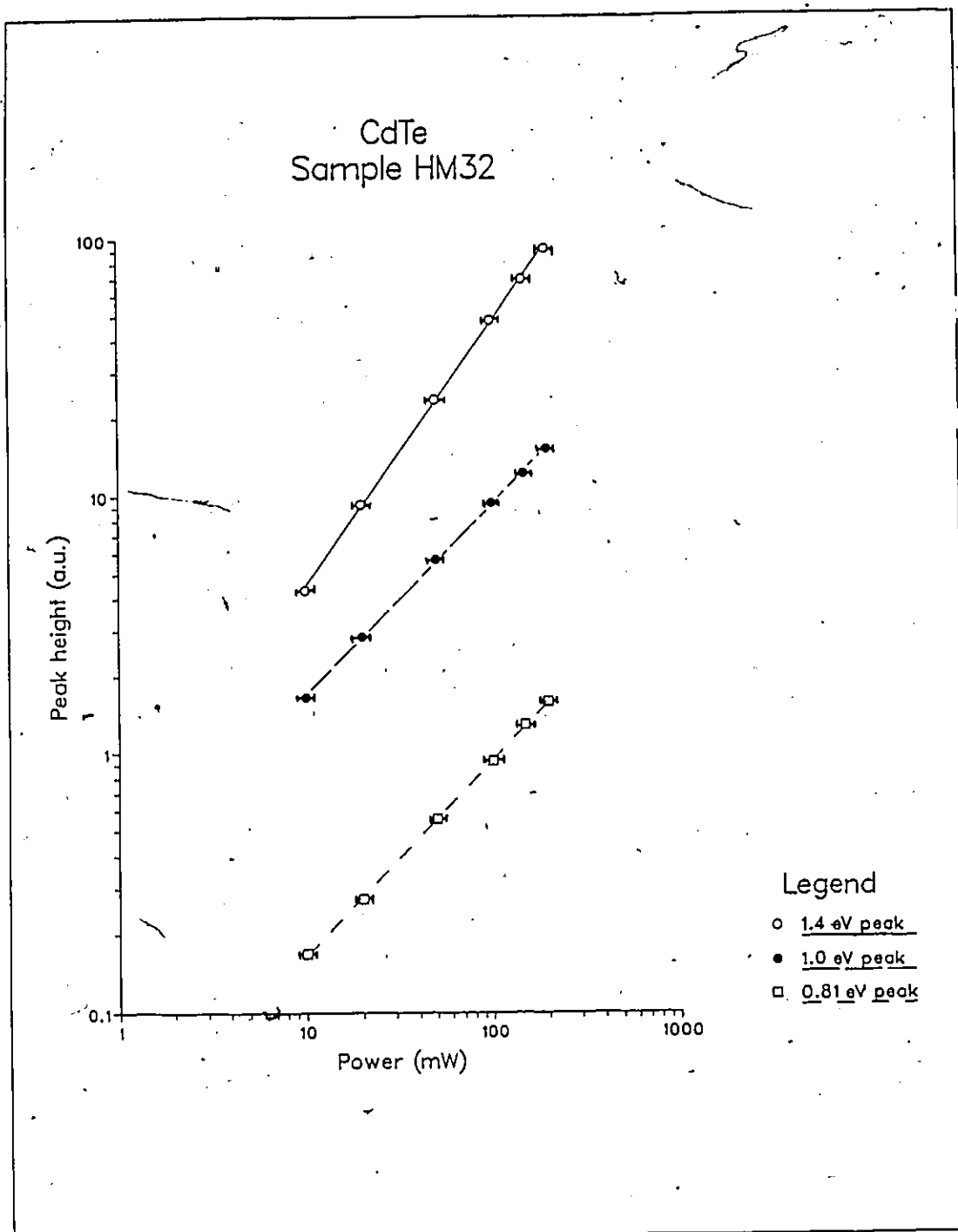


Figure 4.12: Injection level dependence of the PL band emission intensities for CdTe (sample HM32) at 4.2 K.

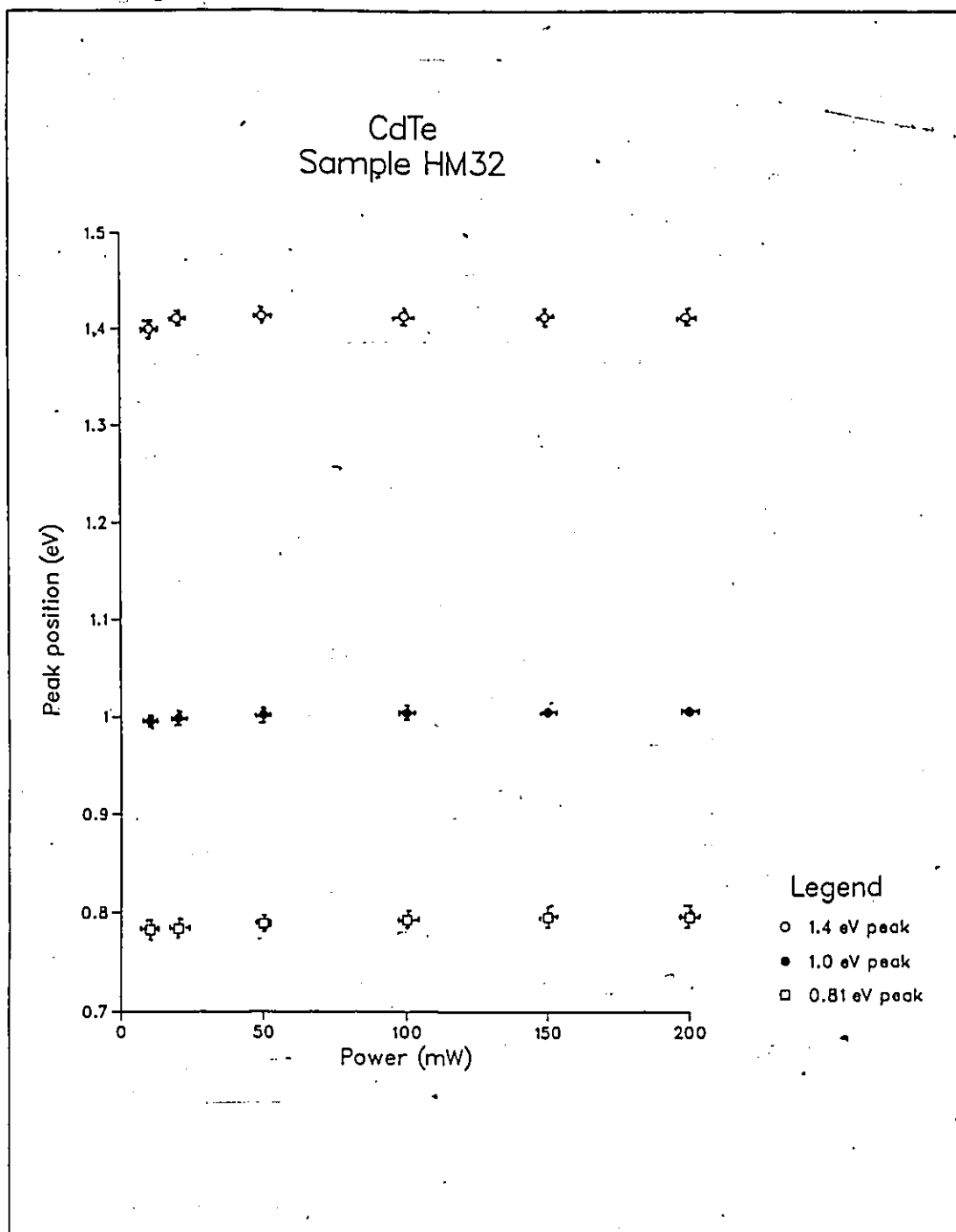


Figure 4.13: Injection level dependence of the peak position of the different PL bands for CdTe (sample HM32) at 4.2 K.

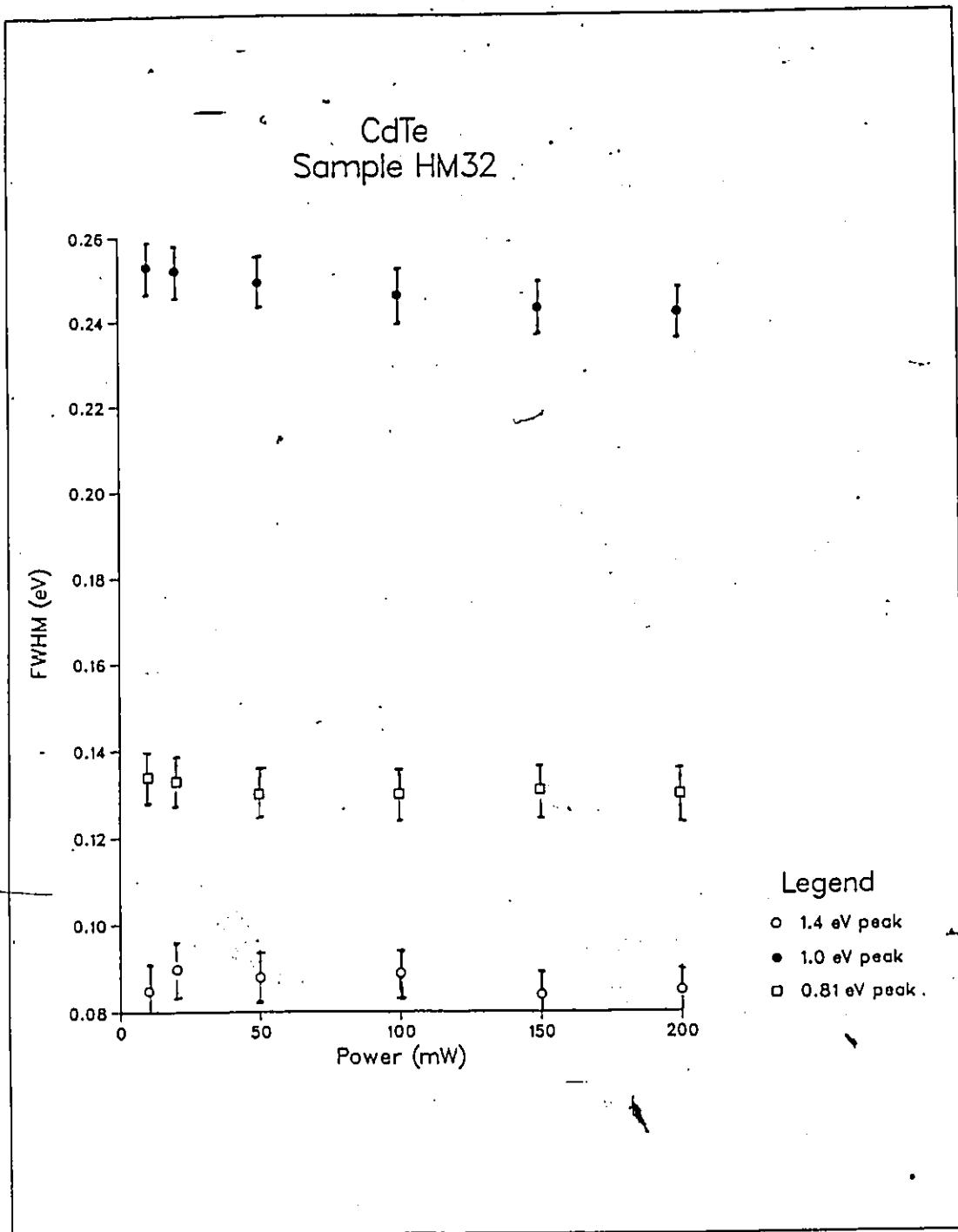


Figure 4.14: Injection level dependence of the FWHM of the different PL bands for CdTe (sample HM32) at 4.2 K.

for the 0.8 eV peak, decreased for the 1.0 eV peak and remained constant for the 1.42 eV peak (fig. 4.17). It should be noted that in this part, the experimental point at 4.2 K was taken from the power dependence run. A larger error is therefore expected for this point as a result of the slightly different experimental conditions. Fig. 4.18 is a graph of the peak height of the 1.0 eV line versus the peak height of the 0.8 eV line for different powers and temperatures.

4.3 Discussion

A decrease of the FWHM of the x-ray diffraction peak with increasing thickness similar to fig. 4.3 has been observed by other workers for heteroepitaxial growth for both CdTe [59] as well as other semiconductors [60]. This behaviour is attributed to the presence of defects at the substrate/layer interface (due to lattice mismatch) whose density decreases towards the surface of the growing film. Hence, thicker films have a much lower density of defects at the surface and consequently exhibit better crystal quality as evidenced by a narrower FWHM of the x-ray diffraction peaks.

The photoluminescence spectra of CdTe is quite complicated. First, numerous defect centers have been reported whose origin is still controversial. As an illustration, D. Verity et al. [61] from deep level transient spectroscopy (DLTS) studies observed nine different electron traps between 0.22 and 0.89 eV in two of their thin film samples. Takebe et al. [62] have tabulated the levels that have been reported by various workers using dif-

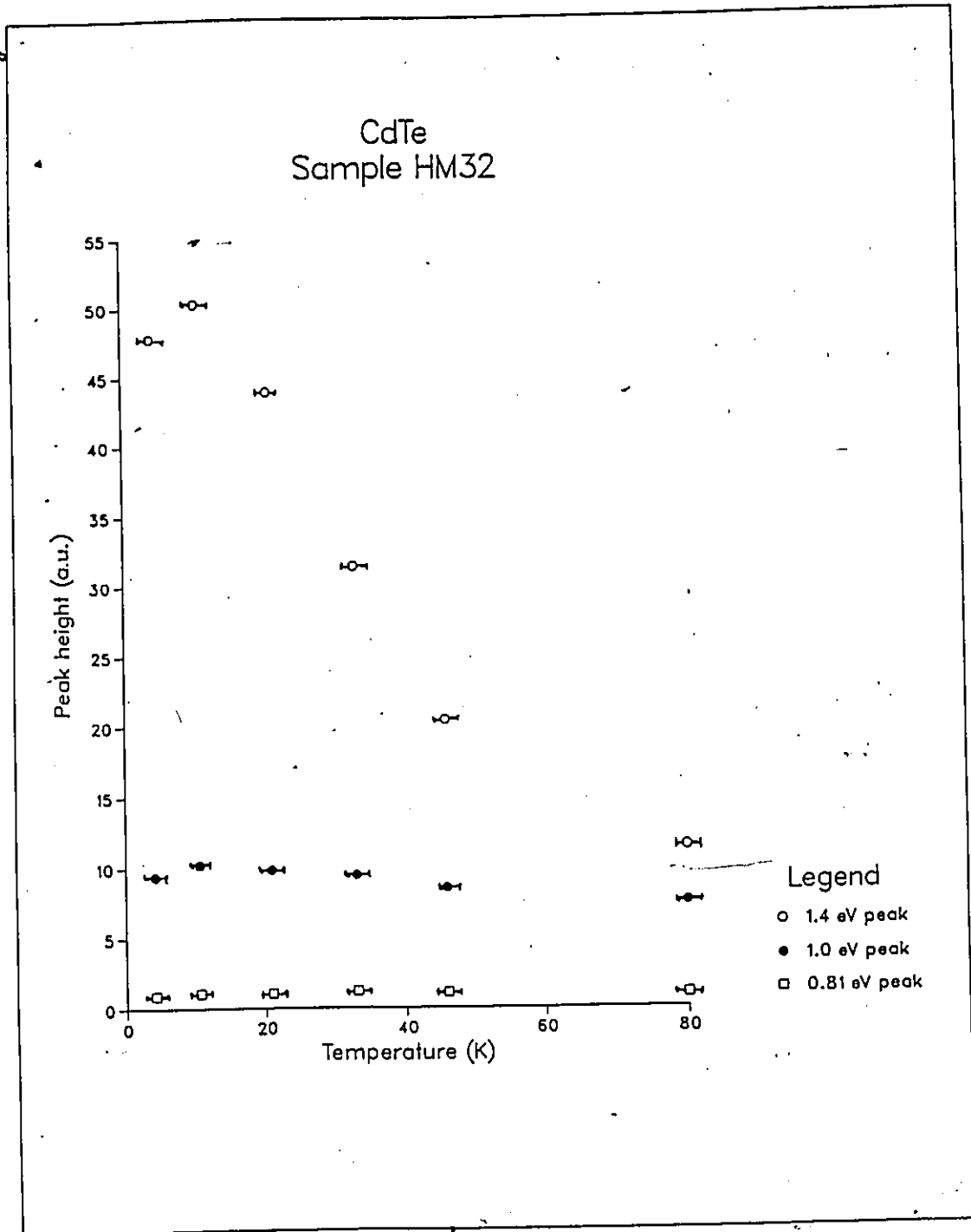


Figure 4.15: Temperature dependence of the PL band emission intensities for CdTe (sample HM32) at 100 mW.

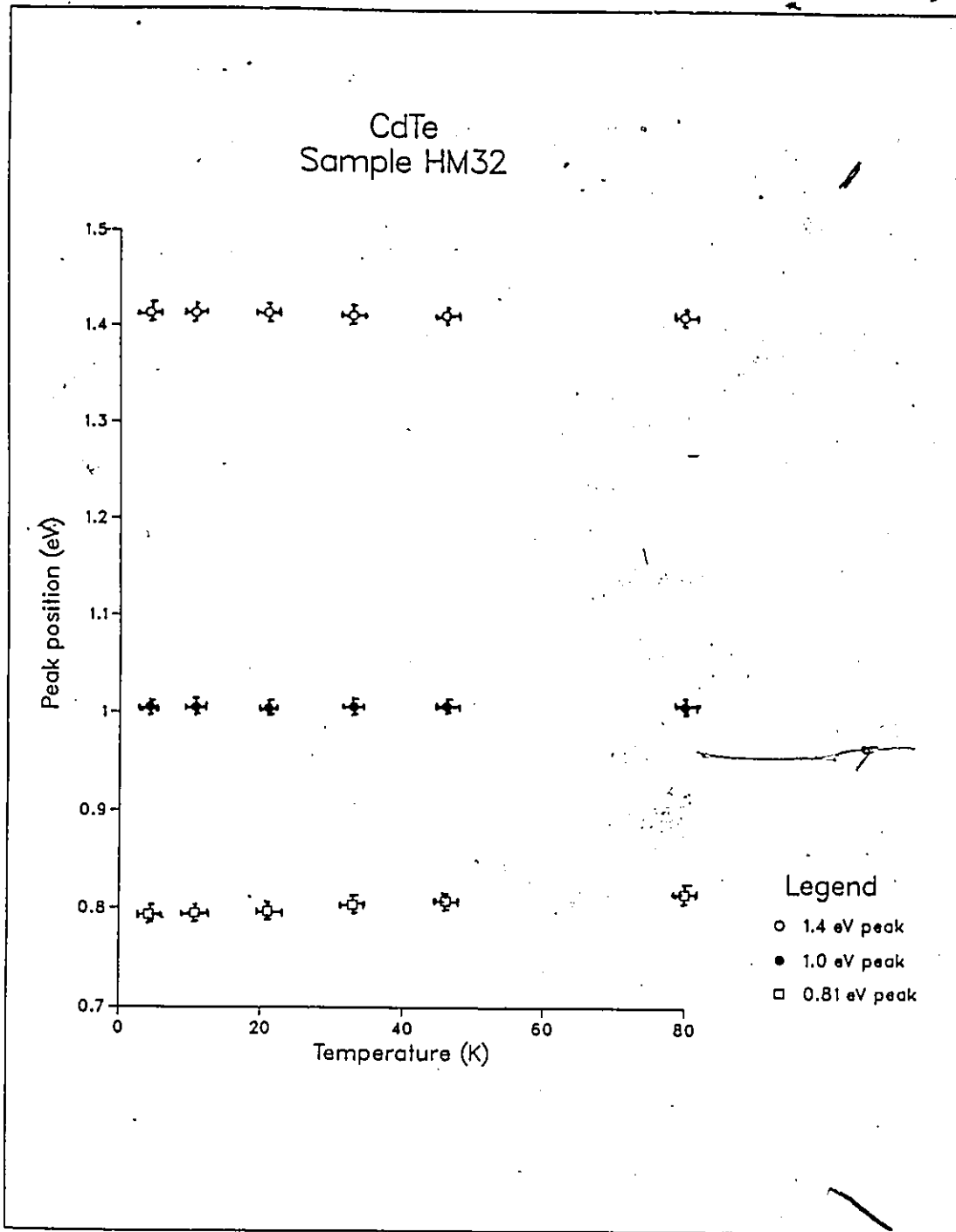


Figure 4.16: Temperature dependence of the peak position of the different PL bands for CdTe (sample HM32) at 100mW.

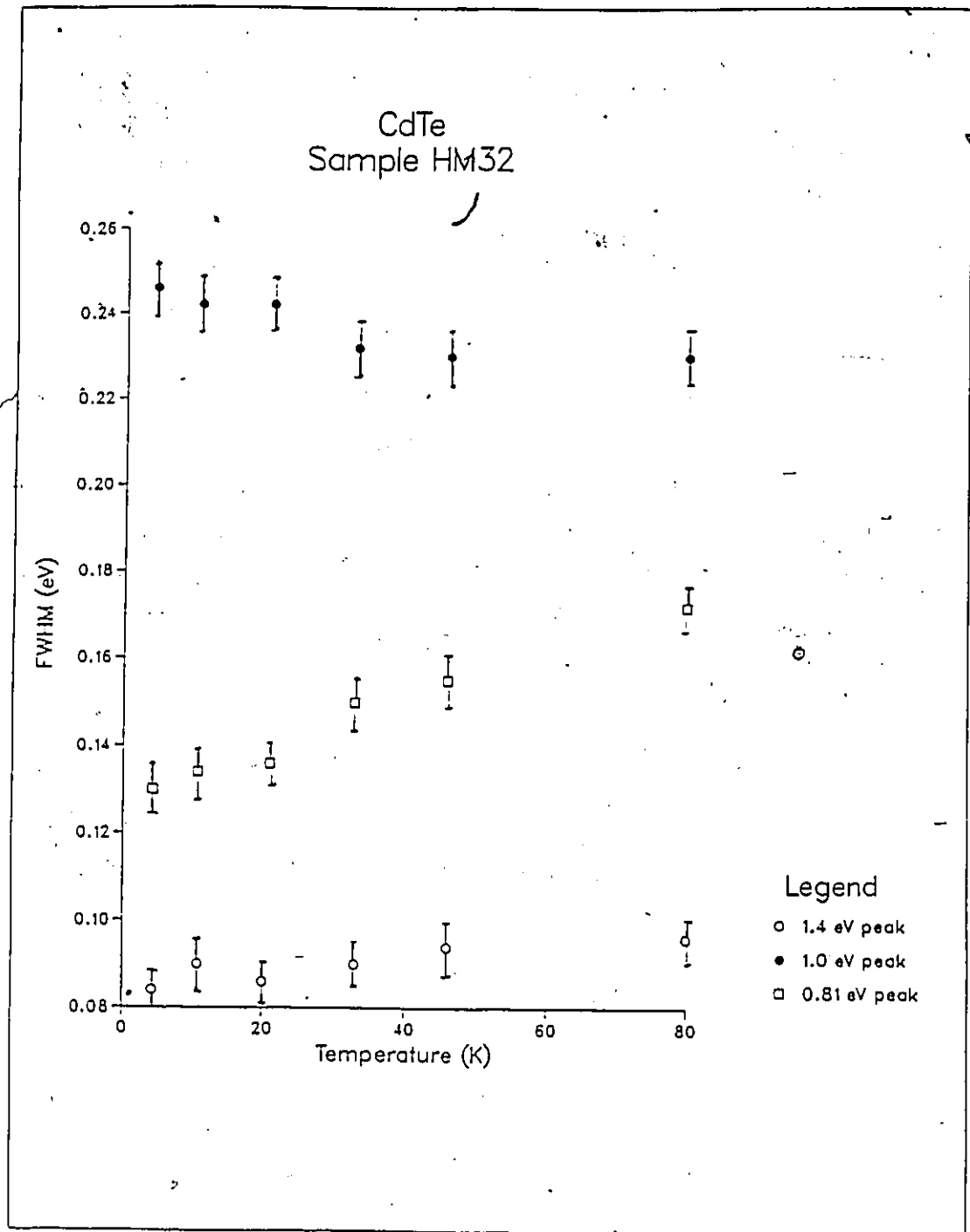


Figure 4.17: Temperature dependence of the FWHM of the different PL bands for CdTe (sample HM32) at 100 mW.

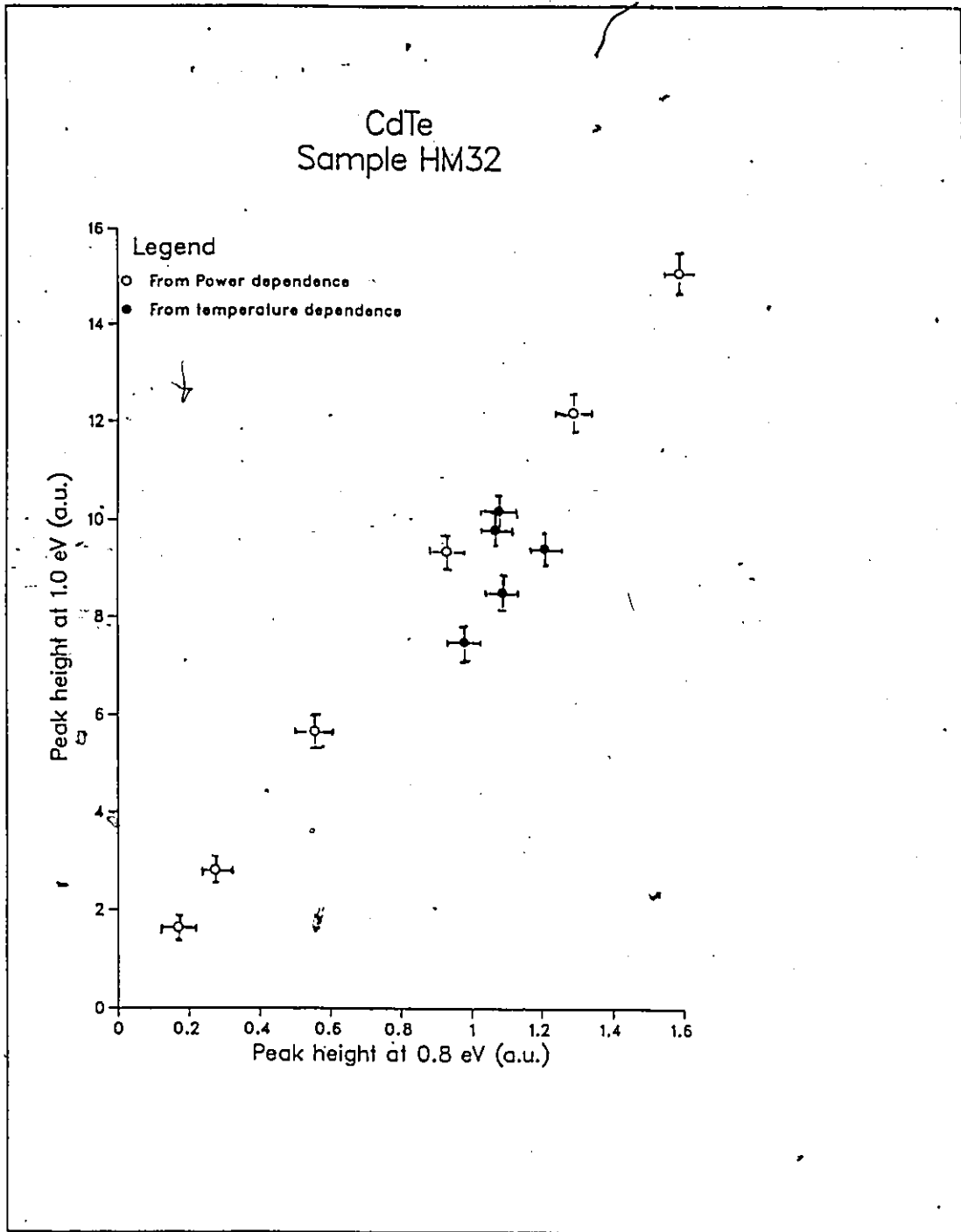


Figure 4.18: Peak intensity of the 1.0 eV line as a function of the peak intensity of the 0.8 eV line at different temperatures and laser power for CdTe (sample HM32).

ferent experimental techniques. Photoluminescence is even more complex to understand for such a semiconductor for two reasons: (i) the absolute values of defect levels or their concentrations cannot be obtained and (ii) non-radiative centers cannot be detected.

The presence of such a huge number of defect levels is a result of the open zinc blende structure of CdTe which can lodge interstitial atoms. As a matter of fact, a high concentration of native defects for zinc blende structures is more probable for II-VI compounds than for III-V ones because of the significant ionic contribution in their bonding (CdTe is 72 % ionic). The nature of the binding has a large effect on the electrical and optical properties of a material. Ionic bonding requires alternating positive and negative charges whereas covalent bonding requires a tetrahedral relationship between the atoms. Moreover, the atomic spacing in CdTe is larger than for any other tetrahedral structures while its cohesive strength is smaller. Correspondingly, the concentration of vacancies is larger and the energy of vacancy formation smaller.

The 1.42 eV band, termed the defect band, has been observed by many workers [51,57,63,64,65]. It is thought to arise due to the presence of structural defects in the samples which give rise to levels in the gap. Some authors have suggested that this band is a D-A transition [63,66,67] while others [68,69] have proposed a C.B.-A transition to account for this emission.

The ratio of the band edge peak to the defect peak at 1.42 eV is usually taken as a measure of crystal quality. The absence of the 1.42 eV band for the single crystal samples confirms their high quality. For the

same reason, the presence of the 1.42 eV peak is expected for the polycrystalline and the hot-pressed bulk samples. For our films, the absence of a band edge peak and the presence of the 1.42 eV peak suggests that they are of a poorer quality than even the bulk polycrystalline and hot-pressed samples. However, this inference is erroneous for reasons discussed later in connection with the presence of the 0.8 and 1.0 eV bands. The similarity in the sample thickness dependence of the FWHM of the 1.42 eV band (fig. 4.10) and the thickness variation of the FWHM of the (400) diffraction peak (fig. 4.3) and the strong correlation between the two FWHM values (fig. 4.11) confirms that the origin of the 1.42 eV PL band is defect related. This hypothesis is further reinforced by the observation of the 1.42 eV band in the single crystal bulk sample after mechanical polishing (fig. 4.9) which induces surface damage and creates structural defects at the surface. Leopold et al. [70] have also observed a correlation between the intensity of a defect-related PL band at 1.474 eV and the x-ray diffraction peak widths for (100) and (111) oriented MBE (molecular beam epitaxy) grown CdTe layers on GaAs.

From fig. 4.13, it appears that the 1.42 eV band is injection level dependent and moves towards higher energy with increasing injection level. Other workers [51] have observed a similar behaviour. Peak shifts with excitation level as large as the one noticed for the 1.42 eV band is taken to suggest that this emission band is caused by donor-acceptor pair recombination [71]. Large peak shifts have been observed in ZnSe (18 meV/decade), and strongly compensated GaAs (15 meV/decade). However, the FWHM of this band did not seem to be affected by the excitation intensity (fig.

4.14) and any variation did not exceed the experimental error. Norris [51] observed a broadening of 3 meV with excitation intensity which is below the resolution of our set-up.

The decrease in luminescence intensity (fig. 4.15) with increasing temperature can be explained in terms of thermally activated diffusion to non-radiative centers [64]. This behaviour is common to both D-A and C.B.-A transitions. The 1.42 eV band broadens (fig. 4.17) with increasing temperature. A trend towards lower energy for the peak position is observed with increasing temperature although it is within the experimental error (fig. 4.16). However, the peak position of the 1.42 eV band does not track the peak position of the edge emission band with increasing temperature; instead it shifts with temperature at a lesser rate. Similar results have been reported by Norris [51]. From the above, it is clear that an unambiguous identification for the type of transition responsible for the 1.42 eV emission in our samples is not possible at this stage. Measurements such as deep level transient spectroscopy and/or photoconductivity studies are necessary to resolve this question.

The PL bands at 1.0 and 0.8 eV have not been reported before except recently by Sobiesierski et al. [58] on bulk CdTe. Other workers [72] have observed a deep level located at 0.746 eV by means of PL on MBE grown CdTe. It was observed in both the best quality CdTe grown at high substrate temperatures as well as in the CdTe grown at low substrate temperatures. This suggests that the deep level responsible for the 0.746 eV band is not defect related. In some of the bulk material samples, for instance the polycrystalline sample (fig. 4.6) and the hot-pressed target

(fig. 4.7), the PL spectra showed a band at 1.42 eV but did not show any evidence of bands at lower energies. This too clearly indicates that the levels which are responsible for the 1.42 eV emission and the 0.8 and 1.0 eV emissions do not share a common origin. Further evidence for this picture is the observation that while the FWHM of the 1.42 eV peak decreased with increasing thickness of the film no such behaviour was observed for the two other peaks. From fig. 4.18, the 0.8 and the 1.0 eV bands are clearly related which suggests that they have the same origin. A possible explanation is that the 1.42 eV peak is due to structural defects whereas the 1.0 eV and the 0.8 eV lines are due to levels in the gap which result from deviation from stoichiometry. Deviation from stoichiometry at the surface resulting from mechanical polishing could also explain the appearance of the 0.8 eV and 1.0 eV bands in the PL spectra of the single crystal and polycrystalline bulk samples after polishing. Sobiesierski et al. [58] have also shown for chemically etched bulk CdTe that the bands at 0.875 eV and 1.125 eV observed by them result from deviation from stoichiometry.

The same sublinear power dependence of the 0.8 and 1.0 eV emission line intensities suggests that these transitions have a common final state which is saturating. This level must be a deep level, probably the one usually seen in the 0.6-0.7 eV range and which has been attributed to a second doubly charged acceptor complex as a result of Cd vacancies (V_{Cd}^{2-}) [62,73,74,75,76]. These levels lying close to the midgap are very important recombination centers which reduce considerably the near band-gap radiative transition or even quench it. In most cases, recombination through imperfection dominates for low-carrier densities, and direct recombination

becomes important only for high-carrier densities.

For the 0.8 eV band, conditions 3(i) to 3(v) seem to be fulfilled (figs. 4.13-4.16). A narrowing of the emission line is observed with increasing excitation intensity but is not appreciable. Also, a slight shift towards lower energies is noticed only when the temperature exceeds 50 K. This band is tentatively proposed as being a donor-acceptor transition involving two widely different activation energies E_a and E_d . For the 1.0 eV band, conditions for a C.B.-A or D-V.B. transition are fulfilled except that the emission band becomes narrower with increasing laser intensity. It should be noted that in this part of the investigation any conclusion for small peak shifts would be erroneous because the error is larger than that for the 1.42 eV band (experimental error plus fitting error).

The fine structure at 1.00 eV seen on two of our samples (HM32 and HM27) could be a priori either an interference pattern or phonon replicas. We first thought of the latter because the energy difference between any two successive peaks was 21.36 meV for HM32 and was power and temperature independent, a behaviour expected for phonon replicas. Moreover, 21 meV corresponds to LO-phonons in CdTe. Further, optical constants are relatively independent of temperature in CdTe. In a like manner, ω_{LO} should be nearly constant with temperature by the Lyddan-Sachs-Teller relation [57].

However, this hypothesis was ruled out because (i) the peak position of these lines did not shift to higher energies when the excitation power was varied up to 200 mW, (ii) the peak positions did not shift to lower energy with increasing temperature and (iii) the peaks were located at 29.18 meV

intervals for HM27.

The interference equation is

$$nd = \frac{\lambda_1 \lambda_2}{2\Delta\lambda_{1,2}} \quad (4.1)$$

where λ_1 and λ_2 are the wavelengths of two successive peaks, $\Delta\lambda_{1,2}$ the difference between them, n the refractive index and d the thickness of the film. We found $nd = 29.62\mu m$ for HM32 (for which $d = 9.92\mu m$) and $nd = 21.36\mu m$ for HM27 (for which $d = 7.25\mu m$). This suggests that $n = 2.99$ for HM32 and $n = 2.95$ for HM27. The small difference between the two values is of course due to the errors introduced by the thickness measurement, the errors on the wavelengths and mainly the error on $\Delta\lambda_{1,2}$ (the error on $\Delta\lambda_{1,2}$ was expected to be about 10% while it is relatively negligible for the other terms).

4.4 Conclusion

From the PL study on sputter-deposited CdTe films reported in this thesis, three bands are observed at 0.80, 1.00, and 1.42 eV. This is the first time that the 0.80 and 1.00 eV lines have been seen in epitaxial layers. From a systematic study of the injection level dependence and temperature dependence of these lines, the former is attributed to a band to defect level transition whereas the latter is tentatively attributed to a donor-acceptor transition. These bands seem to quench band to band and excitonic peaks

which are therefore not observed in our films. The 0.8 and 1.0 eV bands are tentatively attributed to levels resulting from deviation from stoichiometry while the origin of the 1.42 eV emission is confirmed to be due to structural defects.

Chapter 5

Scope of future work

From the present work on emission spectroscopy of PbTe sputter discharge in Ar and previous work by our group on a CdTe sputter discharge in Ar, it has been shown that the sputtered atom density N_{Pb} (N_{Te} , N_{Cd}) and, hence, the rate of deposition, is proportional to I_{Pb}/I_{Ar} (I_{Te}/I_{Ar} , I_{Cd}/I_{Ar}) as the rf power is varied at pressures ≈ 0.5 Pa which is a typical sputtering pressure. ~~As a~~ result, emission spectroscopy can be utilized as a non-invasive probe for monitoring deposition rate and for process control at the above mentioned pressure. However, the substrate bias dependence of the emission lines was rather difficult to interpret. The complexity and the importance of the substrate bias voltage to film growth call for a more detailed study. In such work, the power applied to the target substrate should be monitored separately, resputtering at the substrate should be accounted for, and the use of more direct probes for the atomic densities

and electron temperatures should be considered.

Plasma emission spectroscopy studies should be extended to a multi-target discharge such as in the case of CdTe and PbTe co-sputtering which is being used presently by our group to deposit $Cd_xPb_{1-x}Te$ alloy films. Such studies are needed to evaluate emission spectroscopy as an in-situ probe for compositional analysis of the alloy films.

With reference to photoluminescence studies on CdTe, our attempts to understand the mechanism responsible for the 1.42 eV line were inconclusive because the measured injection level dependence and temperature dependence did not clearly indicate whether the transition originated from a band state or was from a donor to acceptor state. Complementary measurements such as DLTS (deep level transient spectroscopy) and photoconductivity measurements are needed to locate the levels present in the gap and unambiguously determine the levels associated with the different transitions of 1.42 eV, 1.00 eV, and 0.80 eV.

Bibliography

- [1] C. Kittel, *Introduction to Solid State Physics*, Wiley, New York (1967).
- [2] R. A. Smith, *Semiconductors*, University press, Cambridge (1961).
- [3] A. J. Dekker, *Solid State Physics*, Prentice hall, New Jersey (1965).
- [4] P. Emtage, *J. Appl. Phys.* 33, 1950 (1962).
- [5] J..M. Borrego, S. K. Ghandi, and D. A. Page, *Proc. 17th IEEE Photo-voltaic Specialists Conference*, Kissimmee (1984), IEEE Press (1984), p. 223.
- [6] S. R. Das, K. Rajan, P. van der Meer, and J. G. Cook, *Can. J. Phys.* 65, 864 (1987).
- [7] S. R. Das, K. Rajan, and J. G. Cook, paper presented at the *14th Int. Conf. on Metallurgical Coatings*, San Diego, CA, 1987.
- [8] S. R. Das, W. Boland, and J. G. Cook, to be presented at the *Int. Conf. Metallurgical Coatings*, San Diego, CA, April (1989).

- [9] F. W. Aston, *Proc. Roy. Soc. A* 79, 80 (1907).
- [10] W. R. Larsen, C. W. Wilmsenand, and P. W. Chan, *J. Appl. Phys.* 44, 2153 (1973).
- [11] E. W. McDaniel, "*Collision Phenomena in ionized gases*", J. Wiley, New York (1964).
- [12] W. D. Westwood, "*AVS short course on sputtering*", Bell-Northern Research Ottawa, Canada, K1Y 4H7.
- [13] W. D. Davis and T. A. Vanderslice, *Phys. Rev.* 131, 219 (1963).
- [14] J. M. Schroerer, R. N. Rhodin, and R. C. Bradley, *Surf. Sci.* 34, 571 (1973).
- [15] W. C. Kreye, *J. Appl. Phys.* 35, 3575 (1964).
- [16] R. V. Stuart and G. K. Wehner, *J. Appl. Phys.* 35, 1819 (1964).
- [17] G. K. Cowell and H. P. Smith, *J. Appl. Phys.* 43, 412 (1972).
- [18] J. W. Coburn, *Rev. Sci. Inst.* 41, 1219 (1970).
- [19] J. W. Coburn and E. Kay, *Appl. Phys. Lett.* 18, 435 (1971).
- [20] J. W. Coburn and E. Kay, *J. Vac. Sci. Technol.* 8, 738 (1971).
- [21] J. W. Coburn and E. Kay, *Solid. St. Tech.* 12, 49 (1971).
- [22] I. Brodie, L. T. Lamont, and D. O. Myers, *J. Vac. Sci. Technol.* 6, 124 (1969).

- [23] K. L. Chopra, *Thin film phenomena*, McGraw Hill, New York, 1969.
- [24] B. Lewis and D. S. Campbell, *J. Vac. Sci. Technol.* 4, 209 (1967).
- [25] B. N. Chapman, *J. Vac. Sci. Technol.* 11, 106 (1974).
- [26] B. Swaroop and I. Adler, *J. Vac. Sci. Technol.* 11, 503 (1973).
- [27] J. M. Seeman, *Vacuum* 17, 129 (1967).
- [28] O. Christensen, *Solid St. Technol.* 13, 12 (1970).
- [29] J. W. Coburn and E. Kay, *J. Appl. Phys.* 18, 1554 (1974).
- [30] A. I. Morozov and S. V. Lebedev, *Reviews of Plasma Physics* 8 (Consultant Bureau, New York, 1980), p. 301.
- [31] A. V. Hippel, *Ann. Phys. (Leipz)* 80, 672 (1926).
- [32] R. V. Stuart and G. K. Wehner, *Phys. Rev. Lett.* 4, 409 (1960).
- [33] R. V. Stuart and G. K. Wehner, *J. Appl. Phys.* 33, 2345 (1962).
- [34] C. Kreye, *J. Appl. Phys.* 34, 2897 (1963).
- [35] E. Sawatzky and E. Kay, *Rev. Sci. Instrum.* 37, 1324 (1966).
- [36] J. E. Greene and J. M. Whelan, *J. Appl. Phys.* 44, 2509 (1973).
- [37] J. E. Greene and F. Sequeda-Osorio, *J. Vac. Sci. Technol.* 10, 1144 (1973).
- [38] W. R. Harshbarger, R. A. Porter, T. A. Miller, and P. Norton, *Appl. Spectrosc.* 31, 201 (1977).

- [39] J. W. Coburn and M. Chen, *J. Appl. Phys.* 51, 3134 (1980).
- [40] J. I. Pankove, *Optical processes in semiconductors*, Dover, New York (1975).
- [41] W. D. Lawson, S. Nielsen, and A. S. Young, *Solid State Phys.: Electron. Telecommun. Proc. Int. Conf.* 2, 830 (1960).
- [42] M. G. Williams, R. D. Tomlinson, and M. J. Hampshire, *Solid State Commun.* 7, 1831 (1969).
- [43] J. G. Cook and S. R. Das, *J. Appl. Phys.* 65, 1846 (1989).
- [44] J. G. Cook and S. R. Das, *Chemtronics* 3, 166 (1988).
- [45] T. Pech, J. P. Charberie, and A. Ricard, in *Proceedings of the 6^{ème} Colloque international sur les Plasmas et la pulvérisation Cathodique* (Soc. Franç. du Vide, Paris, 1987), p. 224.
- [46] A. R. Striganov and N. S. Sventitskii, *Tables of Spectral Lines of Neutral and Ionized Atoms*, (IFI/Plenum, N.Y.1968).
- [47] S. Maniv, *J. Appl. Phys.* 63, 1022 (1988).
- [48] L. T. Ball, I. S. Falconer, D. R. McKenzie, and J. M. Smelt, *J. Appl. Phys.* 59, 720 (1986).
- [49] W. F. Meggers, C. H. Cordiss, and B.F. Scribner, *Tables of Spectral-Line Intensities, Part I* (NBS monograph 32(I), U.S. Gov. Washington, 1961).

- [50] R. E. Halsted in *Physics and chemistry of II-VI compounds*, edited by M. Aven and J. S. Prener (North-Holland, Amsterdam, 1967), p.385; D. Curie and J. S. Prener, *ibid*, p.435.
- [51] C. B. Noris, *J. Appl. Phys.* 51, 6342 (1980).
- [52] *Semiconductors and Semimetals* (Edited by R. K. Willardson and A. C. Beer), vol.8. Academic press, New York (1972).
- [53] K. Maeda, *J. Phys. Chem. Solids* 26, 595 (1965).
- [54] A. S. Kaminskii and Y. E. Pokrovskii, *Soviet. Phys. Semicond.* 3, 1496 (1970).
- [55] M. D. Sturge, *Phys. Rev.* 129, 768 (1962).
- [56] S. R. Das and J. G. Cook, *Thin solid films* 163, 409 (1988).
- [57] K. Zanio, *Semiconductors and Semimetals* (Edited by R. K. Willardson and A. C. Beer), vol. 13. Academic Press, New York (1978).
- [58] Z. Sobiesierski, I. M. Dharmadassa, and R. H. Williams, *Appl. Phys. Lett.* 53, 2623 (1988).
- [59] G. R. Woolhouse, T. J. Magee, H. A. Kawayoshi, C. S. H. Leung, and R. D. Ormond, *J. Vac. Sci. Technol. A* 3, 83 (1985).
- [60] T. Sudersena Rao, C. Halpin, J. B. Webb, J. P. Noad, and K. Rajan, *Thin solid films* 163, 399 (1988).

- [61] D. Verity, F. J. Bryant, C. G. Scott, and D. Shaw, *Journal of Crystal Growth* 59, 234 (1982).
- [62] T. Takebe, T. Hirata, J. Saraie, and H. Matsunami, *J. Phys. Chem Solids* 43, 5 (1982).
- [63] N. Matsumara, T. Ohshima, J. Saraie, and Y. Yodogawa, *Journal of crystal growth* 71, 361 (1985).
- [64] B. J. Feldman, J. L. Boone, and T. Van Doren, *Appl. Phys. Lett.* 38, 703 (1981).
- [65] N. C. Giles-Taylor, R. N. Bicknell, D. K. Blanks, T. H. Myers, and J. F. Schetzina, *J. Vac. Sci. Technol. A* 3, 76 (1985).
- [66] K. Sugiyama, *Thin Solid Films* 115, 97 (1984).
- [67] J. E. Espinosa, J. M. Gracia, H. Navarro, A. Zehe, and R. Triboulet, *Journal of luminescence* 28, 163 (1983).
- [68] F. J. Bryant and D. H. J. Totterdel, *Phys. Status Solidi A* 10, K75 (1972).
- [69] N. V. Agrinskaya, E. N. Arkadéva, and O. A. Matveev, *Sov. Phys. Semicond.* 5, 767 (1971).
- [70] D. J. Leopold, J. M. Ballingall, and M. L. Wroge, *Appl. Phys. Lett.* 49, 1473 (1986).
- [71] K. Kaneko and M. Ayabe, *J. Appl. Phys.* 51, 6337 (1980).

- [72] H.-X. Han, B. J. Feldman, M. L. Wroge, D. J. Leopold, and J. M. Ballingall, *J. Appl. Phys.* 61, 2670 (1987).
- [73] C. Scharager, J. C. Muller, R. Stuck, and P. Siffer, *Phys. Status Solidi (a)* 31, 247 (1975).
- [74] A. M. Mancini, C. Manfredotti, C. de Blasi, G. Micoccio, and A. Tepore, *Rev. Phys. Appl.* 12, 255 (1977).
- [75] C. Canali, M.-A. Nicolet, and J. M. Mayer, *Solid St. Electron.* 18, 871 (1975).
- [76] B. Rabin, H. Tabatabai, and P. Siffert, *Phys. Status Solidi (a)* 49, 577 (1978).